ZERO-SHOT WHOLE-BODY HUMANOID CONTROL VIA BEHAVIORAL FOUNDATION MODELS

Anonymous authors
Paper under double-blind review

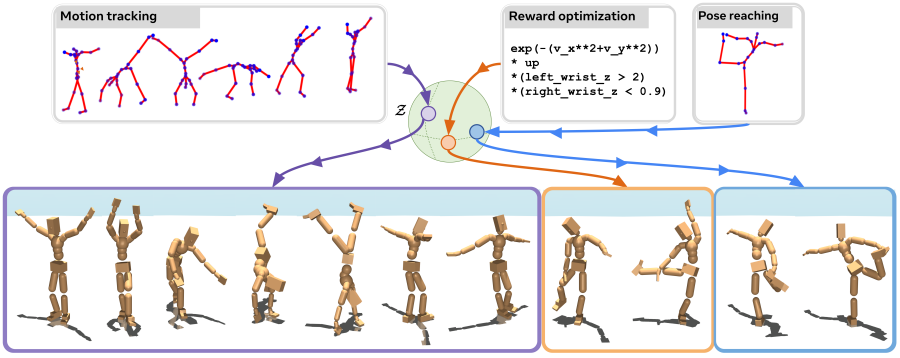

Figure 1: With FB-CPR we pre-train the first behavioral foundation model for humanoid that can solve tracking, goal-reaching, and reward optimization tasks in a zero-shot fashion.

ABSTRACT

Unsupervised reinforcement learning (RL) aims at pre-training models that can solve a wide range of downstream tasks in complex environments. Despite recent advancements, existing approaches suffer from several limitations: they may require running an RL process on each task to achieve a satisfactory performance, they may need access to datasets with good coverage or well-curated task-specific samples, or they may pre-train policies with unsupervised losses that are poorly correlated with the downstream tasks of interest. In this paper, we introduce FB-CPR, which regularizes unsupervised zero-shot RL based on the forward-backward (FB) method towards imitating trajectories from unlabeled behaviors. The resulting models learn *useful* policies imitating the behaviors in the dataset, while retaining zero-shot generalization capabilities. We demonstrate the effectiveness of FB-CPR in a challenging humanoid control problem. Training FB-CPR online with observation-only motion capture datasets, we obtain the first humanoid behavioral foundation model that can be prompted to solve a variety of whole-body tasks, including motion tracking, goal reaching, and reward optimization. The resulting model is capable of expressing human-like behaviors and it achieves competitive performance with task-specific methods while outperforming state-of-the-art unsupervised RL and model-based baselines.

1 INTRODUCTION

Foundation models pre-trained on vast amounts of unlabeled data have emerged as the state-of-the-art approach for developing AI systems that can be applied to a wide range of use cases and solve complex tasks by responding to specific prompts (e.g., Anil et al., 2023; OpenAI et al., 2024; Dubey et al., 2024). A natural step forward is to extend this approach beyond language and visual domains, towards *behavioral* foundation models (BFMs) for agents interacting with dynamic environments through actions. In this paper, we aim to develop BFMs for humanoid agents and we focus on whole-body control from proprioceptive observations, a long-standing challenge due to the high-dimensionality and intrinsic instability of the system (Peng et al., 2021; Won et al., 2022; Luo et al., 2024a). Our goal is to learn BFMs that can express a diverse range of behaviors in response to various prompts, including behaviors to imitate, goals to achieve, or rewards to optimize. By doing so,

we could significantly simplify the creation of general-purpose humanoid agents for robotics (Cheng et al., 2024), virtual avatars, and non-player characters (Kwiatkowski et al., 2022).

While recent advancements in unsupervised reinforcement learning (RL) have demonstrated the potential of pre-trained models to solve a wide range of downstream tasks, several limitations still exist. Pre-trained policies or representations (e.g., Eysenbach et al., 2019; Schwarzer et al., 2021) still require training an RL agent to solve any given downstream task. Unsupervised zero-shot RL algorithms (e.g., Touati et al., 2023; Frans et al., 2024) aim to address this limitation by pre-training policies that are directly *promptable* (e.g., by rewards or goals) without requiring additional samples and compute. However, these algorithms rely on **1)** access to large and diverse datasets of transitions collected through some *unsupervised exploration* strategy, and **2)** optimize *unsupervised losses* that aim at learning as many and diverse policies as possible, but provide limited inductive bias on which ones to favor. As a result, zero-shot RL performs well in simple environments (e.g., low-dimensional continuous control problems), while struggle in complex scenarios with high-dimensional control and unstable dynamics, where unsupervised exploration is unlikely to yield useful samples and unsupervised learning may lead to policies that are not well aligned with the tasks of interest.

An alternative approach is to train sequence models (e.g., transformer- or diffusion-based) from large demonstration datasets to clone or imitate existing behaviors and rely on their generalization capabilities and prompt conditioning to obtain different behaviors (e.g., Schmidhuber, 2019; Chen et al., 2021; Wu et al., 2023). This approach is particularly effective when high-quality task-oriented data are available, but it tends to generate models that are limited to reproducing the policies demonstrated in the training datasets and struggle to generalize to unseen tasks (Brandfonbrener et al., 2022). Recently, several methods (e.g., Peng et al., 2022; Gehring et al., 2023; Luo et al., 2024b) integrate demonstrations into an RL routine to learn "regularized" policies that preserve RL generalization capabilities while avoiding the issues related to complete unsupervised learning. While the resulting policies can serve as *behavior priors*, a full hierarchical RL process is often needed to solve any specific downstream task. See App. A for a full review of other related works.

In this paper, we aim at leveraging an unlabled dataset of trajectories to ground zero-shot RL algorithms towards BFMs that not only express *useful* behaviors but also retain the capability of solving a wide range of tasks in a *zero-shot fashion*. Our main contributions in this direction are:

- We introduce FB-CPR(Forward-Backward representations with Conditional Policy Regularization) a novel online unsupervised RL algorithm that grounds the unsupervised policy learning of forward-backward (FB) representations (Touati & Ollivier, 2021) towards imitating observation-only unlabeled behaviors. The key technical novelty of FB-CPR is to leverage the FB representation to embed the unlabeled trajectories to the same latent space used to represent policies and use a latent-conditional discriminator to encourage policies to "cover" the states in the dataset.

- We demonstrate the effectiveness of FB-CPR by training a behavioral foundation model for whole-body control of a humanoid that can be prompted to solve a wide range of different tasks (i.e., motion tracking, goal reaching, reward optimization) in zero-shot. In particular, we consider a humanoid agent based on SMPL (Loper et al., 2015), a widely used skeleton in the virtual character animation community for its expressiveness and human-like structure, and we use the AMASS dataset (Mahmood et al., 2019), a large collection of uncurated motion capture data, for regularization. Through an extensive quantitative and qualitative evaluation, we show that our model expresses behaviors that are "natural", while being competitive with ad-hoc methods trained for specific tasks, and it outperforms unsupervised RL as well as model-based baselines.

2 Preliminaries

We consider a reward-free discounted Markov decision process $\mathcal{M} = (S, A, P, \mu, \gamma)$, where S and A are the state and action space respectively, P is the transition kernel, where $P(\mathrm{d}s'|s, a)$ denotes the probability measure over next states when executing action a from state s, μ is a distribution over initial states, and $\gamma \in [0, 1)$ is a discount factor. A policy π is the probability measure $\pi(\mathrm{d}a|s)$ that maps each state to a distribution over actions. We denote $\Pr(\cdot|s_0, a_0, \pi)$ and $\mathbb{E}[\cdot|s_0, a_0, \pi]$ the probability and expectation operators under state-action sequences $(s_t, a_t)_{t\geq 0}$ starting at (s_0, a_0) and following policy π with $s_t \sim P(\mathrm{d}s_t|s_{t-1}, a_{t-1})$ and $a_t \sim \pi(\mathrm{d}a_t|s_t)$.

Successor measures for zero-shot RL. For any policy π, its *successor measure* (Dayan, 1993; Blier et al., 2021) is the (discounted) distribution of future states obtained by taking action a in state s and following policy π thereafter. Formally, this is defined as

$$M^\pi(X|s,a) := \sum_{t=0}^{\infty} \gamma^t \Pr(s_{t+1} \in X \mid s, a, \pi) \qquad \forall X \subset S, \tag{1}$$

and it satisfies a measure-valued Bellman equation (Blier et al., 2021),

$$M^\pi(X|s,a) = P(X \mid s,a) + \gamma \mathbb{E}_{s' \sim P(\cdot|s,a), a' \sim \pi(\cdot|s')} \Big[M^\pi(X|s',a') \Big], \quad X \subset S. \tag{2}$$

We also define $\rho^\pi(X) := (1-\gamma)\mathbb{E}_{s\sim\mu, a\sim\pi(\cdot|s)}\big[M^\pi(X|s,a)\big]$ as the stationary discounted distribution of π. Given M^π, the action-value function of π for any reward function $r : S \to \mathbb{R}$ is

$$Q_r^\pi(s,a) := \mathbb{E}\Big[\sum_{t=0}^{\infty} \gamma^t r(s_{t+1}) \mid s, a, \pi\Big] = \int_{s' \in S} M^\pi(\mathrm{d}s'|s,a) r(s'). \tag{3}$$

The previous expression conveniently separates the value function into two terms: 1) the successor measure that models the evolution of the policy in the environment, and 2) the reward function that captures task-relevant information. This factorization suggests that learning the successor measure for π allows for the evaluation of Q_r^π on any reward without further training, i.e., zero-shot policy evaluation. Remarkably, using a low-rank decomposition of the successor measure gives rise to the *Forward-Backward (FB)* representation (Blier et al., 2021; Touati & Ollivier, 2021) enabling not only zero-shot policy evaluation but also the ability to perform zero-shot policy optimization.

Forward-Backward (FB) representations. The FB representation aims to learn a finite-rank approximation to the successor measure as $M^\pi(X|s,a) \approx \int_{s' \in X} F^\pi(s,a)^\top B(s') \rho(\mathrm{d}s')$, where ρ is the a state distribution, while $F^\pi : S \times A \to \mathbb{R}^d$ and $B : S \to \mathbb{R}^d$ are the *forward* and *backward* embedding, respectively. With this decomposition, for any given reward function r, the action-value function can be expressed as $Q_r^\pi(s,a) = F^\pi(s,a)^\top z$, where $z = \mathbb{E}_{s\sim\rho}[B(s)r(s)]$ is the mapping of the reward onto the backward embedding B. An extension of this approach to multiple policies is proposed by Touati & Ollivier (2021), where both F and π are parameterized by the same task encoding vector z. This results in the following unsupervised learning criteria for pre-training:

$$\begin{cases} M^{\pi_z}(X|s,a) \approx \int_{s' \in X} F(s,a,z)^\top B(s')\, \rho(\mathrm{d}s'), & \forall s \in S,\ a \in A, X \subset S, z \in Z \\ \pi_z(s) = \arg\max_a F(s,a,z)^\top z, & \forall (s,a) \in S \times A,\ z \in Z, \end{cases} \tag{4}$$

where $Z \subseteq \mathbb{R}^d$ (e.g., the unit hypersphere of radius $\sqrt{d}$). Given the policies (π_z), F and B are trained to minimize the temporal difference loss derived as the Bellman residual of Eq. 2

$$\begin{aligned} \mathscr{L}_{\mathrm{FB}}(F,B) = \mathbb{E}_{\substack{z\sim\nu, (s,a,s')\sim\rho, \\ s^+\sim\rho, a'\sim\pi_z(s')}} \Big[\big(F(s,a,z)^\top B(s^+) - \gamma \overline{F}(s',a',z)^\top \overline{B}(s^+) \big)^2 \Big] \\ - 2\mathbb{E}_{z\sim\nu,(s,a,s')\sim\rho}\big[F(s,a,z)^\top B(s')\big], \end{aligned} \tag{5}$$

where ν is a distribution over Z, and $\overline{F}, \overline{B}$ denotes stop-gradient. In continuous action spaces, the $\arg\max$ in Eq. 4 is approximated by training an actor network to minimize

$$\mathscr{L}_{\mathrm{actor}}(\pi) = -\mathbb{E}_{z\sim\nu, s\sim\rho, a\sim\pi_z(s)} \Big[F(s,a,z)^\top z \Big]. \tag{6}$$

In practice, FB models have been trained offline (Touati et al., 2023; Pirotta et al., 2024), where ρ is a distribution over an offline dataset of transitions collected by unsupervised exploration.

Zero-shot inference. Pre-trained FB models can be used to solve different tasks in zero-shot fashion, i.e., without performing additional task-specific learning, planning, or fine-tuning. Given a dataset of reward samples $\{(s_i, r_i)\}_{i=1}^n$, a reward-maximizing policy π_{z_r} is inferred by computing $z_r = \frac{1}{n}\sum_{i=1}^n r(s_i)B(s_i)$[1]. Similarly, we can solve zero-shot goal-reaching problems for any state $s \in S$ by executing the policy π_{z_s} where $z_s = B(s)$. Finally, Pirotta et al. (2024) showed that FB models can be used to implement different imitation learning criteria. In particular, we recall the *empirical reward via FB* approach where, given a demonstration [2] $\tau = (s_1, \ldots, s_n)$ from an expert policy, the zero-shot inference returns $z_\tau = \mathrm{ER}_{\mathrm{FB}}(\tau) = \frac{1}{n}\sum_{i=1}^n B(s_i)$.

[1] The inferred latent z can also be safely normalized since optimal policies are invariant to reward scaling.

[2] While the original method is defined for multiple trajectories, here we report the single-trajectory case for notation convenience and to match the way we will use it later.

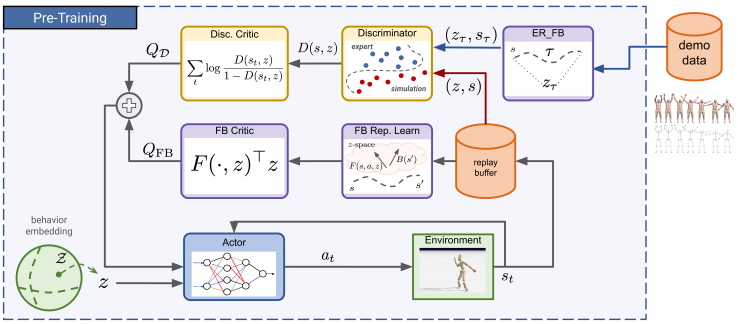

Figure 2: Illustration of the main components of FB-CPR: the discriminator is trained to estimate the ratio between the latent-state distribution induced by policies (π_z) and the unlabeled behavior dataset $\mathcal{M}$, where trajectories are embedded through $\mathrm{ER}_{\mathrm{FB}}$. The policies are trained with a regularized loss combining a policy improvement objective based on the FB action value function and a critic trained on the discriminator. Finally, the learned policies are rolled out to collect samples that are stored into the replay buffer $\mathcal{D}_{\mathrm{online}}$.

In the limit of d and full coverage of ρ, FB can learn optimal policies for any reward function and solve any imitation learning problem (Touati & Ollivier, 2021). However, when d is finite, FB training has a limited inductive bias on which policies to favor, except for the low-rank dynamics assumption, and when the dataset has poor coverage, it cannot reliably optimize policies using offline learning. In this case, FB models tend to *collapse* to few policies with poor downstream performance on tasks of interest (see experiments on walker in App. E).

3 FB WITH CONDITIONAL POLICY REGULARIZATION

At pre-training, the agent has access to a *dataset of unlabeled behaviors* $\mathcal{M} = \{\tau\}$, which contains observation-only trajectories $\tau = (s_1, \ldots, s_{\ell(\tau)})$[3] where states are drawn from a generic distribution $\rho^\tau(X), X \subseteq \mathcal{S}$. Furthermore, the agent can directly interact with the environment from initial states $s_0 \sim \mu$ and we denote by $\mathcal{D}_{\mathrm{online}}$ the associated replay buffer of (unsupervised) transitions.

FB with conditional policy regularization. We now describe how we steer the unsupervised training of FB towards capturing the diverse behaviors represented in $\mathcal{M}$. We first outline our formalization of the problem, followed by a detailed discussion of the design choices that enable the development of a scalable and effective algorithm.

In FB, we pretrain a continuous set of latent-conditioned policies $\pi(\mathrm{d}a|s,z)$, where z is drawn from a distribution ν defined over the latent space Z. The space of behaviors represented by FB can be compactly represented by the joint space (s,z) where $z \sim \nu$ and $s \sim \rho^{\pi_z}$. We denote by $p_\pi(s,z) = \nu(z)\rho^{\pi_z}(s)$ the joint distribution induced by FB over this space. We summarize the behaviors represented in the unlabeled dataset in a similar way by assuming that each trajectory can be produced by some FB policy π_z. Since the dataset only contains states with no latent variables, for each trajectory τ we must infer a latent z such that the policy π_z would visit the same states as τ. Pirotta et al. (2024) proposed several methods for inferring such latent variables from a single trajectory using an FB model. Among these, we choose to encode trajectories using $\mathrm{ER}_{\mathrm{FB}}$, a simple yet empirically effective method, and represent each trajectory τ in the dataset as $\{(s, z = \mathrm{ER}_{\mathrm{FB}}(\tau))\}_{s\sim\rho^\tau}$. We assume a uniform distribution over $\tau \in \mathcal{M}$ and denote by $p_{\mathcal{M}}(s,z)$ the joint distribution of the dataset induced by this process.

To ensure that FB policies encode similar behaviors to the ones represented in the dataset, we regularize the unsupervised training of the FB actor with a distribution-matching objective that minimizes the discrepancy between $p_\pi(z,s)$ and $p_{\mathcal{M}}(z,s)$. This results in the following actor training loss:

$$\mathscr{L}_{\text{FB-CPR}}(\pi) = -\mathbb{E}_{z\sim\nu, s\sim\mathcal{D}_{\mathrm{online}}, a\sim\pi_z(\cdot|s)}\Big[F(s,a,z)^\top z\Big] + \alpha \mathrm{KL}\big(p_\pi, p_{\mathcal{M}}\big), \tag{7}$$

[3]In humanoid, we use motion capture datasets where trajectories may contain noise and artifacts and, in general, are not generated by "purposeful" or stationary policies.

where α is hyper-parameter that controls the strength of the regularization.

Distribution matching objective. We now explain how to turn Eq. 7 into a tractable RL procedure. The key idea is that we can interpret the KL-divergence as an expected return under the polices π_z where the reward is given by the log-ratio $p_{\mathcal{M}}(s,z)/p_\pi(s,z)$ of the two distributions,

$$\mathrm{KL}(p_\pi, p_{\mathcal{M}}) = \mathbb{E}_{\substack{z\sim\nu,\\ s\sim\rho^{\pi_z}}}\left[\log \frac{p_\pi(s,z)}{p_{\mathcal{M}}(s,z)}\right] = -\mathbb{E}_{z\sim\nu}\mathbb{E}\Big[\sum_{t=0}^{\infty}\gamma^t \log\frac{p_{\mathcal{M}}(s_{t+1},z)}{p_\pi(s_{t+1},z)}\Big| s_0\sim\mu,\pi_z\Big], \quad (8)$$

To estimate the reward term, we employ a variational representation of the Jensen-Shannon divergence. Specifically, we introduce a discriminator network $D : S \times Z \to [0,1]$ conditioned on the latent z and train it with a GAN-like objective (Goodfellow et al., 2014),

$$\mathscr{L}_{\text{discriminator}}(D) = -\mathbb{E}_{\tau\sim\mathcal{M},s\sim\rho^\tau}\left[\log(D(s,\mathrm{ER}_{\mathrm{FB}}(\tau)))\right] - \mathbb{E}_{z\sim\nu,s\sim\rho^{\pi_z}}\left[\log(1-D(s,z))\right]. \quad (9)$$

It is known that the optimal discriminator for the loss in Eq. 9 is $D^\star = \frac{p_{\mathcal{M}}}{p_\pi + p_{\mathcal{M}}}$ (e.g., Goodfellow et al., 2014; Nowozin et al., 2016), which allows us approximating the log-ratio reward function as $\log\frac{p_{\mathcal{M}}}{p_\pi} \approx \log\frac{D}{1-D}$. We can then fit a critic network Q to estimate the action-value of this approximate reward via off-policy TD learning,

$$\mathscr{L}_{\text{critic}}(Q) = \mathbb{E}_{\substack{(s,a,s')\sim\mathcal{D}_{\text{online}}\\ z\sim\nu,a'\sim\pi_z(\cdot|s')}}\left[\left(Q(s,a,z) - \log\frac{D(s',z)}{1-D(s',z)} - \gamma\overline{Q}(s',a',z)\right)^2\right]. \quad (10)$$

This leads us to the final actor loss for FB-CPR,

$$\mathscr{L}_{\text{FB-CPR}}(\pi) = -\mathbb{E}_{z\sim\nu,s\sim\mathcal{D}_{\text{online}},a\sim\pi_z(\cdot|s)}\left[F(s,a,z)^\top z + \alpha Q(s,a,z)\right]. \quad (11)$$

Latent space distribution. So far, we have not specified the distribution ν over the latent space Z. According to the FB optimality criteria (Touati & Ollivier, 2021), it is sufficient to choose a distribution that has support over the entire hypersphere. However, in practice, we can leverage ν to allocate more model capacity to meaningful latent tasks and to enhance the training signal provided by and to the discriminator, while ensuring generalization over a variety of tasks. In particular, we choose ν as a mixture of three components: **1)** $z = \mathrm{ER}_{\mathrm{FB}}(\tau)$ where $\tau \sim \mathcal{M}$, which encourages FB to accurately reproduce each trajectory in the unlabeled dataset, thus generating challenging samples for the discriminator and boosting its training signal; **2)** $z = B(s)$ where $s \in \mathcal{D}_{\text{online}}$, which focuses on goal-reaching tasks for states observed during the training process; and **3)** uniform over the hypersphere, which allocates capacity for broader tasks and covers the latent space exhaustively.

Online training and off-policy implementation. FB-CPR is pre-trained online, interleaving environment interactions with model updates. During interaction, we sample N policies with $z \sim \nu$ and rollout each for a fixed number steps. All the collected (unsupervised) transitions are added to a finite capacity replay buffer $\mathcal{D}_{\text{online}}$. We then use an off-policy procedure to update all components of FB-CPR: F and B using Eq. 5, the discriminator D using Eq. 9, the critic Q using Eq. 10, and the actor π using equation 11. The full pseudo-code of the algorithm is reported in App. B.

Discussion. While the distribution matching term in Eq. 8 is closely related to existing imitation learning schemes, it has crucial differences that makes it more suitable for our problem. Peng et al. (2022) and Vlastelica et al. (2024) focus on the state marginal version of p_π and $p_{\mathcal{M}}$, thus regularizing towards policies that globally cover the same states as the behaviors in $\mathcal{M}$. In general, this may lead to situations where no policy can accurately reproduce the trajectories in $\mathcal{M}$. Tessler et al. (2023) address this problem by employing a conditional objective similar to Eq. 8, where a trajectory encoder is learned end-to-end together with the policy space (π_z). In our case, distribution matching is used to regularize the FB unsupervised learning process and we directly use $\mathrm{ER}_{\mathrm{FB}}$ to embed trajectories into the latent policy space. Not only this simplifies the learning process by removing an ad-hoc trajectory encoding, but it also binds FB and policy training together, thus ensuring a more stable and consistent learning algorithm.

4 Experiments on Humanoid

We propose a novel suite of whole-body humanoid control tasks based on the SMPL humanoid (Loper et al., 2015), which is widely adopted in virtual character animation (e.g., Luo et al.,

2021; 2024a). The SMPL skeleton contains 24 rigid bodies, of which 23 are actuated. The body proportion can vary based on a body shape parameter, but in this work we use a neutral body shape. The state consists of proprioceptive observations containing body pose (70D), body rotation (144D), and linear and angular velocities (144D), resulting in a state space $S \subseteq \mathbb{R}^{358}$. All the components of the state are normalized w.r.t. the current facing direction and root position (e.g., Won et al., 2022; Luo et al., 2023). We use a proportional derivative (PD) controller and the action space $A \subseteq [-1, 1]^{69}$ thus specifies the "normalized" PD target. Unlike previous work, which considered an under-constrained skeleton and over-actuated controllers, we define joint ranges and torque limits to create "physically plausible" movements. The simulation is performed using MuJoCo (Todorov et al., 2012) at 450 Hz, while the control frequency is 30 Hz. More details in App. C.1.

Motion datasets. For the behavior dataset we use a subset of the popular AMASS motion-capture dataset (Mahmood et al., 2019), which contains a combination of short, task-specific motions (e.g., few seconds of running or walking), long mixed behaviors (e.g., more than 3 minutes of dancing or daily house activities) and almost static motions (e.g., greeting, throwing). Following previous approaches (e.g., Luo et al., 2021; 2023; 2024b), we removed motions involving interactions with objects (e.g., stepping on boxes). After a 10% train-test split, we obtained datasets consisting of 8902 motions for training $\mathcal{M}$ and 990 motions for testing $\mathcal{M}_{\text{TEST}}$, with a total duration of approximately 29 hours and 3 hours, respectively. Refer to Tab. 2 in App. C.2 for detailed description of the datasets. Motions are action-free and only contain body position and orientation data, but we use a finite difference method to add estimated velocities. Some motions may have a different frequency than what is used in our experiments, may not be continuous (e.g., joint flickering), or may contain artifacts (e.g., body penetration). This means that in some cases it may be impossible to reproduce them accurately in simulation, which makes the overall setting more challenging and realistic.

Downstream tasks and metrics. The evaluation suite consists of three categories (see App. C.3 for full specification of the tasks): **1)** *reward-based evaluation*: we designed 45 rewards with the objective of creating a variety of behaviors covering static/slow and dynamic/fast movements that requires the agent to control different body parts (arms, legs) and move at different heights (e.g., jump, crouching, sitting on the floor). For some reward functions good policies are similar to motions in the dataset (e.g., walk), whereas in some other cases they are very different (e.g., leg splits). For this category, we evaluate performance based on the average return over episodes of 300 steps. **2)** *goal-reaching evaluation*: we evaluate the ability of the model to reach a goal from an arbitrary initial condition. To this extent, we manually selected 50 "stable" poses (with joint velocities all equal to 0). For this category, we consider two metrics: *success rate*, where success is an indicator that the goal position has been attained at any point in time, and *proximity*, computed as the normalized distance to the goal position averaged in time. **3)** *tracking evaluation*: we evaluate the ability of the model to reproduce a target motion when starting from its initial pose.[4] A motion is successfully tracked if the agent remains within a given distance (in joint position and rotation) to the motion along the full length of the motion (Luo et al., 2021). We also use the earth mover's distance (Rubner et al., 2000, EMD), a less-restrictive metric that does not require the agent's trajectory to be perfectly time-aligned with the target motion.

Protocol and baselines. We compare our approach against a variety of baselines. We first define single-task baselines for each category. We use TD3 (Fujimoto et al., 2018) trained from scratch to learn a near-optimal policy for each reward-maximization and goal-reaching task. We also trained Goal-GAIL (Ding et al., 2019) and PHC (Luo et al., 2023) on each individual motion to have strong baselines for motion tracking. All the algorithms are trained online.[5] We then considered unsupervised RL algorithms that are in nature "multi-task". Goal-GAIL and Goal-TD3 are state-of-the-art goal-conditioned RL algorithms. PHC is a goal-conditioned algorithm specialized for motion tracking and CALM (Tessler et al., 2023) is an algorithm for behavior-conditioned imitation learning. All these baselines are trained online and leverage $\mathcal{M}$ in the process. ASE (Peng et al., 2022) is the closest BFM approach to ours as it allows for zero-shot learning and leverages motions for regularization. We train ASE online with $\mathcal{M}$ using an off-policy routine. We also tested planning-based approaches such as MPPI (Williams et al., 2017), DIFFUSER (Janner et al., 2022) and H-GAP (Jiang

[4]Unlike previous work (e.g., Pirotta et al., 2024) we do not consider imitation learning tasks due to the difficulty of obtaining human-like reward-driven policies to imitate.

[5]For reward and goal-based tasks, due to the high variance of TD3, we select the best performance across seeds. For single motion tracking, we run only one seed due to the high number of experiments. Hence we do not report any standard deviation in Tab. 1.

Algorithm	Reward (↑)	Goal		Tracking - EMD (↓)		Tracking - Success (↑)	
		Proximity (↑)	Success (↑)	Train	Test	Train	Test
TD3†	249.74	0.98	0.98				
GOAL-GAIL†				1.08	1.09	0.22	0.23
PHC†				1.14	1.14	0.94	0.94
ORACLE MPPI†	178.50	0.47	0.73				
GOAL-TD3		0.67 (0.34)	0.44 (0.47)	1.39 (0.08)	1.41 (0.09)	0.90 (0.01)	0.91 (0.01)
GOAL-GAIL		0.61 (0.35)	0.35 (0.44)	1.68 (0.02)	1.70 (0.02)	0.25 (0.01)	0.25 (0.02)
PHC		0.07 (0.11)	0.05 (0.11)	1.66 (0.06)	1.65 (0.07)	0.82 (0.01)	0.83 (0.02)
CALM		0.18 (0.27)	0.04 (0.17)	1.67 (0.02)	1.70 (0.03)	0.71 (0.02)	0.73 (0.02)
ASE	105.73 (3.82)	0.46 (0.37)	0.22 (0.37)	2.00 (0.02)	1.99 (0.02)	0.37 (0.02)	0.40 (0.03)
DIFFUSER	85.27 (0.99)	0.20 (0.03)	0.14 (0.01)				
FB-CPR	151.68 (7.53)	0.68 (0.35)	0.48 (0.46)	1.37 (0.00)	1.39 (0.01)	0.83 (0.01)	0.83 (0.01)
$\text{SCORE}_{\text{norm}}$	0.61	0.69	0.48	0.80	0.80	0.88	0.88

Table 1: Summary results comparing FB-CPR to different single-task baselines (i.e., retrained for each task) and "multi-task" unsupervised baselines across three different evaluation categories. We report mean and standard deviation across the 5 seeds. For FB-CPR we report the normalized performance against the best algorithm, i.e., $\text{SCORE}_{\text{norm}} = \mathbb{E}_{\text{task}}[\text{FB-CPR}(\text{task})/\text{BEST}(\text{task})]$. Note that the best algorithm may vary depending on the metric being evaluated (TD3 for reward and goal, Goal-GAIL for tracking EMD and PHC for tracking success). For each metric, we highlight the best "multi-task" baseline and the second best "multi-task" baseline. † are top-liner run on individual tasks, goals or motions (we use the best performance over seeds).

et al., 2024). All these methods are offline and require action-labeled datasets. For this purpose, we first create an action-labeled version of the AMASS dataset (by replaying policies from Goal-GAIL trained to track each individual motion) and then combined it with the replay buffer generated by FB-CPR to define a diverse dataset with good coverage properties that can be used for offline training (more details about this in App. C.1).

We use a comparable architecture and hyperparameter search for all models. Online algorithms are trained for 3M gradient steps corresponding to 30M interaction steps. Evaluation is done by averaging results over 100 episodes for reward and goal, and with a single episode for tracking, as the initial state is fixed. Due to the high computational cost, we were able to compute metrics over only 20 episodes for MPPI and DIFFUSER. We provide further implementation details in App. C.5.

4.1 MAIN RESULTS

Table 1 reports the aggregate performance of each algorithm for each evaluation category. Unfortunately, MPPI with a learned model and H-GAP performed poorly across all tasks and we do not report their performance in the table (see App. D.1). Instead, we report an *oracle* version of MPPI with direct sampling access to the dynamics as a planning-based top-line. Overall, FB-CPR achieves 73,4% of the performance of top-line algorithms on average across all categories. This results is remarkable since FB-CPR is not explicitly trained to solve any of the downstream tasks and it performs zero-shot inference without any additional learning or planning. Furthermore, FB-CPR is more than 1.4 times better than ASE in each task category and it performs on par or better than unsupervised RL algorithms specialized for specific categories. We now provide an in-depth analysis of each category, while a finer breakdown of the results is available in App. D.1.

Reward-maximization. In reward-based tasks FB-CPR achieves 61% of the performance of TD3, which is re-trained from scratch for each reward. Compared to unsupervised baselines, FB-CPR outperforms all the baselines that requires planning on a learned model. For example, FB-CPR achieves 177% of the performance of DIFFUSER that relies on a larger and more complex model to perform reward optimization. ORACLEMPPI performs better than FB-CPR, while still lagging behind model-free TD3. This improvement (+17.8% w.r.t. FB-CPR) comes at the cost of a significant increase in computational cost. ORACLEMPPI requires at least 30 minutes to complete a 300 step episode compared to the 12 seconds needed by FB-CPR to perform inference and execute the policy (about 7, 3 and 2 seconds for reward relabeling, inference, and policy rollout). DIFFUSER takes even more, about 5 hours for a single episode. While this comparison is subject to specific implementation details, it provides an interesting comparison between pre-training zero-shot policies and using test-time compute for planning. Finally, ASE, which has the same zero-shot properties as FB-CPR, only achieves 70% of its performance across all tasks.

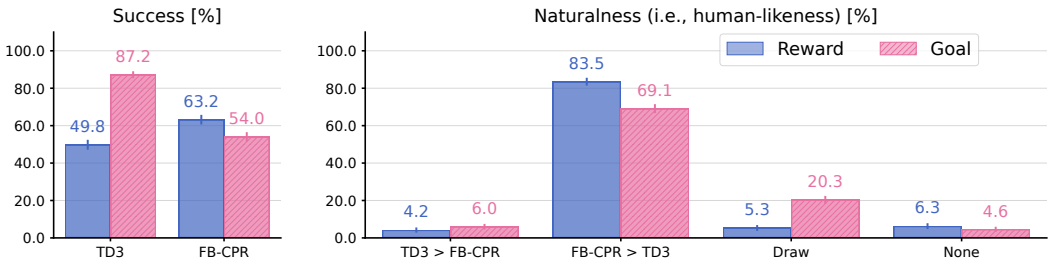

Figure 3: Human-evaluation. Left figure reports the percentage of times a behavior solved a reward-based (blue) or a goal-reaching (pink) task (tasks are independently evaluated). Right figure reports the score for human-likeness by direct comparison of the two algorithms.

Goal-reaching. Table 1 shows that FB-CPR performs similarly to specialized goal-based baselines (i.e., Goal-GAIL and Goal-TD3) and outperforms the zero-shot baseline (48% and 118% performance increase w.r.t. ASE on proximity and success). When compared with planning-based approaches, FB-CPR achieves a higher proximity but lower success rate. This means that FB-CPR is able to spend more time close to the goal, whereas ORACLEMPPI is able to reach the goal but not keeping a stable pose thereafter. We believe this is due to the fact that ORACLEMPPI aims to minimize only the distance w.r.t. position at planning without considering velocities.[6] Finally, similarly to the reward case, all other algorithms under-perform w.r.t. TD3 trained to reach each individual goal independently.[7] Since Goal-TD3 is trained using the same reward signal, the conjecture is that the unsupervised algorithm learns behaviors that are biased by the demonstrations. Indeed, by visually inspecting the motions, we noticed that TD3 tends to reach the goal in a faster way, while sacrificing the "quality" of the behaviors (further details below).

Tracking. We first notice that the same algorithm may have quite different success and EMD metrics. This is the case for Goal-GAIL, which achieves low EMD but quite poor success rate. This is due to the fact that Goal-GAIL is trained to reach the goal in a few steps, rather than in a single step. On the other hand, Goal-TD3 is trained to reach the goal in the shortest time possible and obtain good scores in both EMD and success metrics. We thus used two different algorithms trained on single motions for the top-line performance in EMD (Goal-GAIL) and success (PHC). The performance of FB-CPR is about 80% and 88% of the top-line scorer for EMD and success, and it achieves an overall 83% success rate on the test dataset. Similarly to previous categories, FB-CPR outperforms both zero-shot and planning-based baselines. Among "multi-task" baselines, only Goal-TD3 is able to do better than FB-CPR on average (about 9% improvement in success and a 1% drop in EMD). Interestingly, PHC achieves the same performance of FB-CPR despite being an algorithm designed specifically for tracking.[8] Due to the high computation cost, we were not able to test MPPI and DIFFUSER on tracking.

Qualitative Evaluation. While the quantitative evaluation shows that FB-CPR has a gap w.r.t. single-task toplines, it does not capture the *quality* of the learned behaviors. Similar to previous work (Hansen et al., 2024a), we conducted a *human evaluation study* in which 50 human evaluators were presented with pairs of clips corresponding to episodes of the same task generated with TD3 and FB-CPR. All videos used for this evaluation are available in the supplementary material. For reward-based tasks, they were asked to rate whether the model solves the task (as described in natural language) and which model is behaving more "naturally". For goal-reaching, they were asked to rate whether the goal (provided as image) was eventually achieved by the model and which model was behaving more "naturally" (see App. D.4 for more details). We evaluated all 45 rewards and 50 goals. In reward-based tasks, Fig. 3 shows that despite TD3 achieving higher reward, the two algorithms have very similar success rate, meaning that they both produce the intended behaviors (e.g., jumping, moving forward, rotating). Interestingly FB-CPR was considered more "human-

[6] We tried to train with a full distance (i.e., position and velocities) but we did not get any significant result.

[7] TD3 is trained using the full distance to the goal as reward function.

[8] Results in the literature (e.g. Luo et al., 2024b) reports near 100% success rate on AMASS. These results are not comparable since they use a much smaller test dataset (187 motions versus our 990 motions) and an over-actuated agent, which is able to move from any pose to any other pose within one or few steps.

Figure 4: **FB-CPR Ablations.** (TOP LEFT) Ablating the FB-CPR discriminator's policy conditioning. (TOP RIGHT) Ablating the contribution of $F(z)^\top z$ in the FB-CPR actor loss (Eq. 11). (BOTTOM LEFT) The effect of increasing model capacity along with the number of motions in the dataset $\mathcal{M}$. (BOTTOM RIGHT) Contrasting Advantage-Weighed FB (FB-AW) trained from a large diverse offline dataset versus FB-CPR trained fully online with policy regularization. All ablations are averaged over 5 seeds with ranges representing bootstrapped 95% confidence intervals.

like" in 83% of cases, while TD3 is more natural in only 4% of cases. This study highlights the well-known issue of reward functions that tend to "underspecify" the intended behavior, and how the motion-regularization used FB-CPR compensates for it by effectively capturing a human-like bias. In App. D.4.2, we provided further examples of this "human" bias both in under-specified and composed rewards (e.g., running with arms up). In goal-reaching tasks, the evaluation of success provided by human evaluators aligns with what our qualitative analysis reported (TD3 has an 11% drop while FB-CPR shows a 6% improvement). Also in this case, FB-CPR is considered more 'human-like' in 69% of cases despite TD3 having a higher success rate. Notably, in the remaining cases, the evaluators considered TD3 and FB-CPR to be equally good for 20% of the goals, while TD3 is better in only 6% of the goals.

4.2 ABLATIONS

Various design decisions have gone into FB-CPR that deserves further analysis. In the following, we seek to answer key questions surrounding the necessity of online interaction and how components of our algorithm affect different axes of performance. Additionally, Appendix D.2 provides further ablations on design decisions regarding the FB-CPR discriminator, sampling distribution ν, and other forms of policy regularization when provided action labels.

Is online policy regularization necessary given a large diverse dataset? Prior works on unsupervised RL have relied on large and diverse datasets that contain sufficient coverage of any downstream task. If such a dataset exists is there anything to be gained from the guided approach of online FB-CPR outlined herein? In order to test this hypothesis, we evaluate training offline FB with an advantage weighted actor update (Nair et al., 2020) (FB-AW) which compensates for overestimation when performing policy optimization with an offline dataset (Cetin et al., 2024). As no dataset with our criterion exists, we curate a dataset by collating all 30M transition from an online FB-CPR agent. The offline agent is trained for the same total number of gradients steps as the online agent and all hypereparameters shared between the two methods remain fixed. In the bottom right quadrant of Figure 4, we can see that FB-AW perform substantially worse than FB-CPR highlighting the difficulty of offline policy optimization and the efficacy of guiding online interactions through the conditional policy regularization of FB-CPR.

How important is maximizing the unsupervised RL term $F(z)^\top z$? The primary mechanism by which FB-CPR regularizes its policy is through the discriminator's critic (Eq. 10). This begs the question to what extent is maximizing the unsupervised value-function $F(s, a, z)^\top z$ contributes to the overall performance of FB-CPR. To answer this question, we train FB-CPR while omitting this unsupervised term when updating the actor. This has the effect of reducing FB-CPR to be more akin to CALM (Tessler et al., 2023), except that our motions are encoded with FB through ER_{FB}. These results are presented in top right quadrant of Figure 4 for both reward and tracking-based performance measures. We can see that including the unsupervised value-function from FB results in improved performance in both reward and tracking evaluation emphasizing that FB is providing much more than just a motion encoder through ER_{FB}.

How important is policy conditioning for the discriminator? FB-CPR relies on a latent-conditional discriminator to evaluate the distance between a specific motion and a policy selected through the trajectory embedding of ER_{FB}. We hypothesize that this policy-conditioned discriminator should provide a stronger signal to the agent and lead to better overall performance. We test this hypothesis by comparing FB-CPR with a discriminator that solely depends on state, thus converting the regularization term into a marginal state distribution matching. The top left quadrant of Figure 4 shows that the latent-conditioned discriminator outperforms the state-only configuration in tracking tasks while performing similarly in reward tasks. These findings demonstrate the importance of the ER_{FB} embedding in enabling FB-CPR to more accurately reproduce motions.

How does network capacity and expert dataset size impact FB-CPR performance? Many recent works in RL have shown vast performance improvements when scaling the capacity of neural networks (Schwarzer et al., 2023; Obando-Ceron et al., 2024; Nauman et al., 2024) along with dataset size (Brohan et al., 2023; Zitkovich et al., 2023) or task diversity (Kumar et al., 2023; Ali Taïga et al., 2023). Given these findings, we seek to understand the capabilities of FB-CPR when scaling both the network capacity and the number of expert demonstrations. To this end, we perform a grid sweep over three configurations of model sizes that alters the amount of compute by roughly $\{0.5\times, 1\times, 2\times\}$ of the base models; as well as datasets that are $\{6.25\%, 12.5\%, 25\%, 50\%, 100\%\}$ the size of our largest motion dataset via subsampling. For each of these combinations we report the tracking performance on all motions and present these results in the bottom left quadrant of Figure 4 with additional evaluation metrics in Appendix D.2. Consistent with prior results we can see that larger capacity models are better able to leverage larger motion datasets resulting in significantly improved performance for our $2\times$ larger model over the results of the $1\times$ model reported in Table 1.

5 Conclusions

We introduced FB-CPR, a novel algorithm combining the zero-shot properties of FB models with a regularization grounding online training and policy learning on a dataset of unlabeled behaviors. We demonstrated the effectiveness of FB-CPR by training the first BFM for zero-shot control of a complex humanoid agent with state-of-the-art performance across a variety of tasks.

Limitations. While FB-CPR effectively grounds unsupervised RL with behavior trajectories, a more formal and theoretical understanding of these components is still missing and alternative formulations may be possible. In practice, FB-CPR still fails at solving problems that are far from motion-capture datasets (e.g., tracking motions or solving reward-based tasks involving movements on the ground). Furthermore, despite producing more convincing human-like behaviors compared to pure reward-optimization algorithms and achieving good tracking performance, FB-CPR still produces imperfect and unnatural movements at times, in particular for behaviors involving falling or standing. We report videos of some of these failure modes in the supplementary material. The BFM trained with FB-CPR is still limited to proprioceptive observations and is unable to solve tasks that require navigating through the environment or interacting with objects. An interesting future direction is to integrate additional state variables (possibly including complex perception such as head-mounted cameras) to pre-train models that can solve more complex tasks. Arguably, in this case it may be hard to achieve satisfactory performance in zero-shot and some test-time planning capability or fast online adaptation may be needed. FB-CPR currently relies on motion capture datasets, which are usually expensive to obtain. In the future, it would be interesting to extend FB-CPR to directly leverage videos of different human activities to further refine and expand its capabilities. Finally, while language prompting could be added to the current by leveraging text-to-motion model and then set a motion tracking task, an interesting direction for future research is to align language and policies more directly.

REFERENCES

Adrien Ali Taïga, Rishabh Agarwal, Jesse Farebrother, Aaron Courville, and Marc G. Bellemare. Investigating multi-task pretraining and generalization in reinforcement learning. In *International Conference on Learning Representations (ICLR)*, 2023.

Marcin Andrychowicz, Filip Wolski, Alex Ray, Jonas Schneider, Rachel Fong, Peter Welinder, Bob McGrew, Josh Tobin, Pieter Abbeel, and Wojciech Zaremba. Hindsight experience replay. In *Neural Information Processing Systems (NeurIPS)*, 2017.

Rohan Anil, Sebastian Borgeaud, Yonghui Wu, Jean-Baptiste Alayrac, Jiahui Yu, Radu Soricut, Johan Schalkwyk, Andrew M. Dai, Anja Hauth, Katie Millican, David Silver, Slav Petrov, Melvin Johnson, Ioannis Antonoglou, Julian Schrittwieser, Amelia Glaese, Jilin Chen, Emily Pitler, Timothy P. Lillicrap, Angeliki Lazaridou, Orhan Firat, James Molloy, Michael Isard, Paul Ronald Barham, Tom Hennigan, Benjamin Lee, Fabio Viola, Malcolm Reynolds, Yuanzhong Xu, Ryan Doherty, Eli Collins, Clemens Meyer, Eliza Rutherford, Erica Moreira, Kareem Ayoub, Megha Goel, George Tucker, Enrique Piqueras, Maxim Krikun, Iain Barr, Nikolay Savinov, Ivo Danihelka, Becca Roelofs, Anaïs White, Anders Andreassen, Tamara von Glehn, Lakshman Yagati, Mehran Kazemi, Lucas Gonzalez, Misha Khalman, Jakub Sygnowski, and et al. Gemini: A family of highly capable multimodal models. *CoRR*, abs/2312.11805, 2023.

Bowen Baker, Ilge Akkaya, Peter Zhokhov, Joost Huizinga, Jie Tang, Adrien Ecoffet, Brandon Houghton, Raul Sampedro, and Jeff Clune. Video pretraining (VPT): learning to act by watching unlabeled online videos. In *Neural Information Processing Systems (NeurIPS)*, 2022.

Léonard Blier, Corentin Tallec, and Yann Ollivier. Learning successor states and goal-dependent values: A mathematical viewpoint. *CoRR*, abs/2101.07123, 2021.

David Brandfonbrener, Alberto Bietti, Jacob Buckman, Romain Laroche, and Joan Bruna. When does return-conditioned supervised learning work for offline reinforcement learning? In *Neural Information Processing Systems (NeurIPS)*, 2022.

David Brandfonbrener, Ofir Nachum, and Joan Bruna. Inverse dynamics pretraining learns good representations for multitask imitation. In *Neural Information Processing Systems (NeurIPS)*, 2023.

Anthony Brohan, Noah Brown, Justice Carbajal, Yevgen Chebotar, Joseph Dabis, Chelsea Finn, Keerthana Gopalakrishnan, Karol Hausman, Alexander Herzog, Jasmine Hsu, Julian Ibarz, Brian Ichter, Alex Irpan, Tomas Jackson, Sally Jesmonth, Nikhil J. Joshi, Ryan Julian, Dmitry Kalashnikov, Yuheng Kuang, Isabel Leal, Kuang-Huei Lee, Sergey Levine, Yao Lu, Utsav Malla, Deeksha Manjunath, Igor Mordatch, Ofir Nachum, Carolina Parada, Jodilyn Peralta, Emily Perez, Karl Pertsch, Jornell Quiambao, Kanishka Rao, Michael S. Ryoo, Grecia Salazar, Pannag R. Sanketi, Kevin Sayed, Jaspiar Singh, Sumedh Sontakke, Austin Stone, Clayton Tan, Huong T. Tran, Vincent Vanhoucke, Steve Vega, Quan Vuong, Fei Xia, Ted Xiao, Peng Xu, Sichun Xu, Tianhe Yu, and Brianna Zitkovich. RT-1: robotics transformer for real-world control at scale. In *Robotics: Science and Systems*, 2023.

Yuri Burda, Harrison Edwards, Amos Storkey, and Oleg Klimov. Exploration by random network distillation. In *International Conference on Learning Representations (ICLR)*, 2019.

Edoardo Cetin, Andrea Tirinzoni, Matteo Pirotta, Alessandro Lazaric, Yann Ollivier, and Ahmed Touati. Simple ingredients for offline reinforcement learning. In *International Conference on Machine Learning (ICML)*, 2024.

Lili Chen, Kevin Lu, Aravind Rajeswaran, Kimin Lee, Aditya Grover, Michael Laskin, Pieter Abbeel, Aravind Srinivas, and Igor Mordatch. Decision transformer: Reinforcement learning via sequence modeling. In *Neural Information Processing Systems (NeurIPS)*, 2021.

Xuxin Cheng, Yandong Ji, Junming Chen, Ruihan Yang, Ge Yang, and Xiaolong Wang. Expressive whole-body control for humanoid robots. *CoRR*, abs/2402.16796, 2024.

Zichen Jeff Cui, Yibin Wang, Nur Muhammad Mahi Shafiullah, and Lerrel Pinto. From play to policy: Conditional behavior generation from uncurated robot data. In *International Conference on Learning Representations (ICLR)*, 2023.

Peter Dayan. Improving generalization for temporal difference learning: The successor representation. *Neural Computation*, 5:613–624, 1993.

Yiming Ding, Carlos Florensa, Pieter Abbeel, and Mariano Phielipp. Goal-conditioned imitation learning. In *Neural Information Processing Systems (NeurIPS)*, 2019.

Zihan Ding, Amy Zhang, Yuandong Tian, and Qinqing Zheng. Diffusion world model. *CoRR*, abs/2402.03570, 2024.

Abhimanyu Dubey, Abhinav Jauhri, Abhinav Pandey, Abhishek Kadian, Ahmad Al-Dahle, Aiesha Letman, Akhil Mathur, Alan Schelten, Amy Yang, Angela Fan, Anirudh Goyal, Anthony Hartshorn, Aobo Yang, Archi Mitra, Archie Sravankumar, Artem Korenev, Arthur Hinsvark, Arun Rao, Aston Zhang, Aurélien Rodriguez, Austen Gregerson, Ava Spataru, Baptiste Rozière, Bethany Biron, Binh Tang, Bobbie Chern, Charlotte Caucheteux, Chaya Nayak, Chloe Bi, Chris Marra, Chris McConnell, Christian Keller, Christophe Touret, Chunyang Wu, Corinne Wong, Cristian Canton Ferrer, Cyrus Nikolaidis, Damien Allonsius, Daniel Song, Danielle Pintz, Danny Livshits, David Esiobu, Dhruv Choudhary, Dhruv Mahajan, Diego Garcia-Olano, Diego Perino, Dieuwke Hupkes, Egor Lakomkin, Ehab AlBadawy, Elina Lobanova, Emily Dinan, Eric Michael Smith, Filip Radenovic, Frank Zhang, Gabriel Synnaeve, Gabrielle Lee, Georgia Lewis Anderson, Graeme Nail, Grégoire Mialon, Guan Pang, Guillem Cucurell, Hailey Nguyen, Hannah Korevaar, Hu Xu, Hugo Touvron, Iliyan Zarov, Imanol Arrieta Ibarra, Isabel M. Kloumann, Ishan Misra, Ivan Evtimov, Jade Copet, Jaewon Lee, Jan Geffert, Jana Vranes, Jason Park, Jay Mahadeokar, Jeet Shah, Jelmer van der Linde, Jennifer Billock, Jenny Hong, Jenya Lee, Jeremy Fu, Jianfeng Chi, Jianyu Huang, Jiawen Liu, Jie Wang, Jiecao Yu, Joanna Bitton, Joe Spisak, Jongsoo Park, Joseph Rocca, Joshua Johnstun, Joshua Saxe, Junteng Jia, Kalyan Vasuden Alwala, Kartikeya Upasani, Kate Plawiak, Ke Li, Kenneth Heafield, Kevin Stone, and et al. The llama 3 herd of models. *CoRR*, abs/2407.21783, 2024.

Boston Dynamics. Atlas, 2024. URL www.bostondynamics.com/atlas.

Benjamin Eysenbach, Abhishek Gupta, Julian Ibarz, and Sergey Levine. Diversity is all you need: Learning skills without a reward function. In *International Conference on Learning Representations (ICLR)*, 2019.

Jesse Farebrother, Joshua Greaves, Rishabh Agarwal, Charline Le Lan, Ross Goroshin, Pablo Samuel Castro, and Marc G. Bellemare. Proto-value networks: Scaling representation learning with auxiliary tasks. In *International Conference on Learning Representations (ICLR)*, 2023.

Kevin Frans, Seohong Park, Pieter Abbeel, and Sergey Levine. Unsupervised zero-shot reinforcement learning via functional reward encodings. In *International Conference on Machine Learning (ICML)*, 2024.

Scott Fujimoto, Herke van Hoof, and David Meger. Addressing function approximation error in actor-critic methods. In *International Conference on Machine Learning (ICML)*, 2018.

Jonas Gehring, Gabriel Synnaeve, Andreas Krause, and Nicolas Usunier. Hierarchical skills for efficient exploration. In *Neural Information Processing Systems (NeurIPS)*, 2021.

Jonas Gehring, Deepak Gopinath, Jungdam Won, Andreas Krause, Gabriel Synnaeve, and Nicolas Usunier. Leveraging demonstrations with latent space priors. *Transactions on Machine Learning Research (TMLR)*, 2023.

Dibya Ghosh, Chethan Anand Bhateja, and Sergey Levine. Reinforcement learning from passive data via latent intentions. In *International Conference on Machine Learning (ICML)*, 2023.

Ian Goodfellow, Jean Pouget-Abadie, Mehdi Mirza, Bing Xu, David Warde-Farley, Sherjil Ozair, Aaron Courville, and Yoshua Bengio. Generative adversarial nets. In *Neural Information Processing Systems (NeurIPS)*, 2014.

Karol Gregor, Danilo Jimenez Rezende, and Daan Wierstra. Variational intrinsic control. *CoRR*, abs/1611.07507, 2016.

Ishaan Gulrajani, Faruk Ahmed, Martín Arjovsky, Vincent Dumoulin, and Aaron C. Courville. Improved training of wasserstein gans. In *Neural Information Processing Systems (NeurIPS)*, 2017.

Danijar Hafner, Jurgis Pasukonis, Jimmy Ba, and Timothy Lillicrap. Mastering diverse domains through world models. *CoRR*, abs/2301.04104, 2024.

Nicklas Hansen, Jyothir S V au2, Vlad Sobal, Yann LeCun, Xiaolong Wang, and Hao Su. Hierarchical world models as visual whole-body humanoid controllers. *CoRR*, abs/2405.18418, 2024a.

Nicklas Hansen, Hao Su, and Xiaolong Wang. TD-MPC2: scalable, robust world models for continuous control. In *International Conference on Learning Representations (ICLR)*, 2024b.

Haoran He, Chenjia Bai, Kang Xu, Zhuoran Yang, Weinan Zhang, Dong Wang, Bin Zhao, and Xuelong Li. Diffusion model is an effective planner and data synthesizer for multi-task reinforcement learning. In *Neural Information Processing Systems (NeurIPS)*, 2023.

Jonathan Ho and Stefano Ermon. Generative adversarial imitation learning. In *Neural Information Processing Systems (NeurIPS)*, pp. 4565–4573, 2016.

Taylor Howell, Nimrod Gileadi, Saran Tunyasuvunakool, Kevin Zakka, Tom Erez, and Yuval Tassa. Predictive sampling: Real-time behaviour synthesis with mujoco. *CoRR*, abs/2212.00541, 2022.

Tyler Ingebrand, Amy Zhang, and Ufuk Topcu. Zero-shot reinforcement learning via function encoders. In *International Conference on Machine Learning (ICML)*, 2024.

Michael Janner, Yilun Du, Joshua B. Tenenbaum, and Sergey Levine. Planning with diffusion for flexible behavior synthesis. In *International Conference on Machine Learning (ICML)*, 2022.

Scott Jeen, Tom Bewley, and Jonathan M. Cullen. Zero-shot reinforcement learning from low quality data. *CoRR*, abs/2309.15178, 2024.

Yunfan Jiang, Agrim Gupta, Zichen Zhang, Guanzhi Wang, Yongqiang Dou, Yanjun Chen, Li Fei-Fei, Anima Anandkumar, Yuke Zhu, and Linxi Fan. VIMA: Robot manipulation with multimodal prompts. In *International Conference on Machine Learning (ICML)*, 2023.

Zhengyao Jiang, Yingchen Xu, Nolan Wagener, Yicheng Luo, Michael Janner, Edward Grefenstette, Tim Rocktäschel, and Yuandong Tian. H-GAP: humanoid control with a generalist planner. In *International Conference on Learning Representations (ICLR)*, 2024.

Diederik P. Kingma and Jimmy Ba. Adam: A method for stochastic optimization. In *International Conference on Learning Representations (ICLR)*, 2015.

Martin Klissarov and Marlos C. Machado. Deep laplacian-based options for temporally-extended exploration. In *International Conference on Machine Learning (ICML)*, 2023.

Aviral Kumar, Rishabh Agarwal, Xinyang Geng, George Tucker, and Sergey Levine. Offline q-learning on diverse multi-task data both scales and generalizes. In *International Conference on Learning Representations (ICLR)*, 2023.

Ariel Kwiatkowski, Eduardo Alvarado, Vicky Kalogeiton, C. Karen Liu, Julien Pettré, Michiel van de Panne, and Marie-Paule Cani. A survey on reinforcement learning methods in character animation. *Computer Graphics Forum*, 41(2):613–639, 2022.

Michael Laskin, Denis Yarats, Hao Liu, Kimin Lee, Albert Zhan, Kevin Lu, Catherine Cang, Lerrel Pinto, and Pieter Abbeel. URLB: Unsupervised reinforcement learning benchmark. In *Neural Information Processing Systems (NeurIPS), Datasets and Benchmarks Track*, 2021.

Michael Laskin, Hao Liu, Xue Bin Peng, Denis Yarats, Aravind Rajeswaran, and Pieter Abbeel. CIC: contrastive intrinsic control for unsupervised skill discovery. *CoRR*, abs/2202.00161, 2022.

Fangchen Liu, Hao Liu, Aditya Grover, and Pieter Abbeel. Masked autoencoding for scalable and generalizable decision making. In *Neural Information Processing Systems (NeurIPS)*, 2022.

Hao Liu and Pieter Abbeel. Behavior from the void: unsupervised active pre-training. In *Proceedings of the 35th International Conference on Neural Information Processing Systems*, Red Hook, NY, USA, 2021. Curran Associates Inc. ISBN 9781713845393.

Matthew Loper, Naureen Mahmood, Javier Romero, Gerard Pons-Moll, and Michael J. Black. SMPL: a skinned multi-person linear model. *ACM Transactions on Graphics*, 34(6):248:1–248:16, 2015.

Zhengyi Luo. SMPLSim: Simulating smpl/smplx humanoids in mujoco and isaac gym. https://github.com/ZhengyiLuo/SMPLSim, 2023.

Zhengyi Luo, Ryo Hachiuma, Ye Yuan, and Kris Kitani. Dynamics-regulated kinematic policy for egocentric pose estimation. In *Neural Information Processing Systems (NeurIPS)*, 2021.

Zhengyi Luo, Jinkun Cao, Alexander Winkler, Kris Kitani, and Weipeng Xu. Perpetual humanoid control for real-time simulated avatars. In *International Conference on Computer Vision (ICCV)*, 2023.

Zhengyi Luo, Jinkun Cao, Rawal Khirodkar, Alexander Winkler, Kris Kitani, and Weipeng Xu. Real-time simulated avatar from head-mounted sensors. In *Conference on Computer Vision and Pattern Recognition (CVPR)*, 2024a.

Zhengyi Luo, Jinkun Cao, Josh Merel, Alexander Winkler, Jing Huang, Kris M. Kitani, and Weipeng Xu. Universal humanoid motion representations for physics-based control. In *International Conference on Learning Representations (ICLR)*, 2024b.

Zhengyi Luo, Jiashun Wang, Kangni Liu, Haotian Zhang, Chen Tessler, Jingbo Wang, Ye Yuan, Jinkun Cao, Zihui Lin, Fengyi Wang, Jessica Hodgins, and Kris Kitani. SMPLOlympics: Sports environments for physically simulated humanoids. *CoRR*, abs/2407.00187, 2024c.

Yecheng Jason Ma, Jason Yan, Dinesh Jayaraman, and Osbert Bastani. Offline goal-conditioned reinforcement learning via f-advantage regression. In *Neural Information Processing Systems (NeurIPS)*, 2022.

Yecheng Jason Ma, Shagun Sodhani, Dinesh Jayaraman, Osbert Bastani, Vikash Kumar, and Amy Zhang. VIP: Towards universal visual reward and representation via value-implicit pre-training. In *International Conference on Learning Representations (ICLR)*, 2023.

Marlos C. Machado, Marc G. Bellemare, and Michael Bowling. Count-based exploration with the successor representation. In *AAAI Conference on Artificial Intelligence*, 2020.

Naureen Mahmood, Nima Ghorbani, Nikolaus F. Troje, Gerard Pons-Moll, and Michael J. Black. AMASS: archive of motion capture as surface shapes. In *International Conference on Computer Vision (ICCV)*, 2019.

Viktor Makoviychuk, Lukasz Wawrzyniak, Yunrong Guo, Michelle Lu, Kier Storey, Miles Macklin, David Hoeller, Nikita Rudin, Arthur Allshire, Ankur Handa, and Gavriel State. Isaac gym: High performance GPU based physics simulation for robot learning. In *Neural Information Processing Systems (NeurIPS), Datasets and Benchmarks Track*, 2021.

Leland McInnes, John Healy, Nathaniel Saul, and Lukas Großberger. Umap: Uniform manifold approximation and projection. *Journal of Open Source Software*, 3(29):861, 2018.

Russell Mendonca, Oleh Rybkin, Kostas Daniilidis, Danijar Hafner, and Deepak Pathak. Discovering and achieving goals via world models. In *Neural Information Processing Systems (NeurIPS)*, 2021.

Josh Merel, Leonard Hasenclever, Alexandre Galashov, Arun Ahuja, Vu Pham, Greg Wayne, Yee Whye Teh, and Nicolas Heess. Neural probabilistic motor primitives for humanoid control. In *International Conference on Learning Representations (ICLR)*, 2019.

Lina Mezghani, Sainbayar Sukhbaatar, Piotr Bojanowski, Alessandro Lazaric, and Karteek Alahari. Learning goal-conditioned policies offline with self-supervised reward shaping. In *Conference on Robot Learning (CoRL)*, 2022.

Takeru Miyato, Toshiki Kataoka, Masanori Koyama, and Yuichi Yoshida. Spectral normalization for generative adversarial networks. In *International Conference on Learning Representations (ICLR)*, 2018.

Ashvin Nair, Abhishek Gupta, Murtaza Dalal, and Sergey Levine. AWAC: Accelerating online reinforcement learning with offline datasets. *CoRR*, abs/2006.09359, 2020.

Michal Nauman, Mateusz Ostaszewski, Krzysztof Jankowski, Piotr Milos, and Marek Cygan. Bigger, regularized, optimistic: scaling for compute and sample-efficient continuous control. In *Neural Information Processing Systems (NeurIPS)*, 2024.

Sebastian Nowozin, Botond Cseke, and Ryota Tomioka. f-gan: Training generative neural samplers using variational divergence minimization. In *Neural Information Processing Systems (NeurIPS)*, 2016.

Johan Samir Obando-Ceron, Ghada Sokar, Timon Willi, Clare Lyle, Jesse Farebrother, Jakob Nicolaus Foerster, Gintare Karolina Dziugaite, Doina Precup, and Pablo Samuel Castro. Mixtures of experts unlock parameter scaling for deep RL. In *International Conference on Machine Learning (ICML)*, 2024.

OpenAI, Josh Achiam, Steven Adler, Sandhini Agarwal, Lama Ahmad, Ilge Akkaya, Florencia Leoni Aleman, Diogo Almeida, Janko Altenschmidt, Sam Altman, Shyamal Anadkat, Red Avila, Igor Babuschkin, Suchir Balaji, Valerie Balcom, Paul Baltescu, Haiming Bao, Mohammad Bavarian, Jeff Belgum, Irwan Bello, Jake Berdine, Gabriel Bernadett-Shapiro, Christopher Berner, Lenny Bogdonoff, Oleg Boiko, Madelaine Boyd, Anna-Luisa Brakman, Greg Brockman, Tim Brooks, Miles Brundage, Kevin Button, Trevor Cai, Rosie Campbell, Andrew Cann, Brittany Carey, Chelsea Carlson, Rory Carmichael, Brooke Chan, Che Chang, Fotis Chantzis, Derek Chen, Sully Chen, Ruby Chen, Jason Chen, Mark Chen, Ben Chess, Chester Cho, Casey Chu, Hyung Won Chung, Dave Cummings, Jeremiah Currier, Yunxing Dai, Cory Decareaux, Thomas Degry, Noah Deutsch, Damien Deville, Arka Dhar, David Dohan, Steve Dowling, Sheila Dunning, Adrien Ecoffet, Atty Eleti, Tyna Eloundou, David Farhi, Liam Fedus, Niko Felix, Simón Posada Fishman, Juston Forte, Isabella Fulford, Leo Gao, Elie Georges, Christian Gibson, Vik Goel, Tarun Gogineni, Gabriel Goh, Rapha Gontijo-Lopes, Jonathan Gordon, Morgan Grafstein, Scott Gray, Ryan Greene, Joshua Gross, Shixiang Shane Gu, Yufei Guo, Chris Hallacy, Jesse Han, Jeff Harris, Yuchen He, Mike Heaton, Johannes Heidecke, Chris Hesse, Alan Hickey, Wade Hickey, Peter Hoeschele, Brandon Houghton, Kenny Hsu, Shengli Hu, Xin Hu, Joost Huizinga, Shantanu Jain, Shawn Jain, Joanne Jang, Angela Jiang, Roger Jiang, Haozhun Jin, Denny Jin, Shino Jomoto, Billie Jonn, Heewoo Jun, Tomer Kaftan, Łukasz Kaiser, Ali Kamali, Ingmar Kanitscheider, Nitish Shirish Keskar, Tabarak Khan, Logan Kilpatrick, Jong Wook Kim, Christina Kim, Yongjik Kim, Jan Hendrik Kirchner, Jamie Kiros, Matt Knight, Daniel Kokotajlo, Łukasz Kondraciuk, Andrew Kondrich, Aris Konstantinidis, Kyle Kosic, Gretchen Krueger, Vishal Kuo, Michael Lampe, Ikai Lan, Teddy Lee, Jan Leike, Jade Leung, Daniel Levy, Chak Ming Li, Rachel Lim, Molly Lin, Stephanie Lin, Mateusz Litwin, Theresa Lopez, Ryan Lowe, Patricia Lue, Anna Makanju, Kim Malfacini, Sam Manning, Todor Markov, Yaniv Markovski, Bianca Martin, Katie Mayer, Andrew Mayne, Bob McGrew, Scott Mayer McKinney, Christine McLeavey, Paul McMillan, Jake McNeil, David Medina, Aalok Mehta, Jacob Menick, Luke Metz, Andrey Mishchenko, Pamela Mishkin, Vinnie Monaco, Evan Morikawa, Daniel Mossing, Tong Mu, Mira Murati, Oleg Murk, David Mély, Ashvin Nair, Reiichiro Nakano, Rajeev Nayak, Arvind Neelakantan, Richard Ngo, Hyeonwoo Noh, Long Ouyang, Cullen O'Keefe, Jakub Pachocki, Alex Paino, Joe Palermo, Ashley Pantuliano, Giambattista Parascandolo, Joel Parish, Emy Parparita, Alex Passos, Mikhail Pavlov, Andrew Peng, Adam Perelman, Filipe de Avila Belbute Peres, Michael Petrov, Henrique Ponde de Oliveira Pinto, Michael, Pokorny, Michelle Pokrass, Vitchyr H. Pong, Tolly Powell, Alethea Power, Boris Power, Elizabeth Proehl, Raul Puri, Alec Radford, Jack Rae, Aditya Ramesh, Cameron Raymond, Francis Real, Kendra Rimbach, Carl Ross, Bob Rotsted, Henri Roussez, Nick Ryder, Mario Saltarelli, Ted Sanders, Shibani Santurkar, Girish Sastry, Heather Schmidt, David Schnurr, John Schulman, Daniel Selsam, Kyla Sheppard, Toki Sherbakov, Jessica Shieh, Sarah Shoker, Pranav Shyam, Szymon Sidor, Eric Sigler, Maddie Simens, Jordan Sitkin, Katarina Slama, Ian Sohl, Benjamin Sokolowsky, Yang Song, Natalie Staudacher, Felipe Petroski Such, Natalie Summers, Ilya Sutskever, Jie Tang,

Nikolas Tezak, Madeleine B. Thompson, Phil Tillet, Amin Tootoonchian, Elizabeth Tseng, Preston Tuggle, Nick Turley, Jerry Tworek, Juan Felipe Cerón Uribe, Andrea Vallone, Arun Vijayvergiya, Chelsea Voss, Carroll Wainwright, Justin Jay Wang, Alvin Wang, Ben Wang, Jonathan Ward, Jason Wei, CJ Weinmann, Akila Welihinda, Peter Welinder, Jiayi Weng, Lilian Weng, Matt Wiethoff, Dave Willner, Clemens Winter, Samuel Wolrich, Hannah Wong, Lauren Workman, Sherwin Wu, Jeff Wu, Michael Wu, Kai Xiao, Tao Xu, Sarah Yoo, Kevin Yu, Qiming Yuan, Wojciech Zaremba, Rowan Zellers, Chong Zhang, Marvin Zhang, Shengjia Zhao, Tianhao Zheng, Juntang Zhuang, William Zhuk, and Barret Zoph. GPT-4 technical report. *CoRR*, abs/2303.08774, 2024.

Seohong Park, Jongwook Choi, Jaekyeom Kim, Honglak Lee, and Gunhee Kim. Lipschitz-constrained unsupervised skill discovery. In *International Conference on Learning Representations*, 2022. URL https://openreview.net/forum?id=BGvt0ghNgA.

Seohong Park, Dibya Ghosh, Benjamin Eysenbach, and Sergey Levine. HIQL: offline goal-conditioned RL with latent states as actions. In *Neural Information Processing Systems (NeurIPS)*, 2023.

Seohong Park, Kevin Frans, Benjamin Eysenbach, and Sergey Levine. OGBench: Benchmarking offline goal-conditioned rl. *CoRR*, abs/2410.20092, 2024a.

Seohong Park, Tobias Kreiman, and Sergey Levine. Foundation policies with hilbert representations. In *International Conference on Machine Learning (ICML)*, 2024b.

Seohong Park, Oleh Rybkin, and Sergey Levine. METRA: scalable unsupervised RL with metric-aware abstraction. In *ICLR*. OpenReview.net, 2024c.

Deepak Pathak, Pulkit Agrawal, Alexei A. Efros, and Trevor Darrell. Curiosity-driven exploration by self-supervised prediction. In *International Conference on Machine Learning (ICML)*, 2017.

Tim Pearce, Tabish Rashid, Anssi Kanervisto, Dave Bignell, Mingfei Sun, Raluca Georgescu, Sergio Valcarcel Macua, Shan Zheng Tan, Ida Momennejad, Katja Hofmann, and Sam Devlin. Imitating human behaviour with diffusion models. In *International Conference on Learning Representations (ICLR)*, 2023.

Xue Bin Peng, Ze Ma, Pieter Abbeel, Sergey Levine, and Angjoo Kanazawa. AMP: adversarial motion priors for stylized physics-based character control. *ACM Transactions on Graphics*, 40 (4):144:1–144:20, 2021.

Xue Bin Peng, Yunrong Guo, Lina Halper, Sergey Levine, and Sanja Fidler. ASE: Large-scale reusable adversarial skill embeddings for physically simulated characters. *ACM Transactions On Graphics*, 41(4):1–17, 2022.

Matteo Pirotta, Andrea Tirinzoni, Ahmed Touati, Alessandro Lazaric, and Yann Ollivier. Fast imitation via behavior foundation models. In *International Conference on Learning Representations (ICLR)*, 2024.

Vitchyr Pong, Murtaza Dalal, Steven Lin, Ashvin Nair, Shikhar Bahl, and Sergey Levine. Skew-fit: State-covering self-supervised reinforcement learning. In *International Conference on Machine Learning (ICML)*, 2020.

Cheng Qian, Julen Urain, Kevin Zakka, and Jan Peters. Pianomime: Learning a generalist, dexterous piano player from internet demonstrations. *CoRR*, abs/2407.18178, 2024.

Sai Rajeswar, Pietro Mazzaglia, Tim Verbelen, Alexandre Piché, Bart Dhoedt, Aaron C. Courville, and Alexandre Lacoste. Mastering the unsupervised reinforcement learning benchmark from pixels. In *ICML*, volume 202 of *Proceedings of Machine Learning Research*, pp. 28598–28617. PMLR, 2023.

Daniele Reda, Jungdam Won, Yuting Ye, Michiel van de Panne, and Alexander Winkler. Physics-based motion retargeting from sparse inputs. *Proceedings of the ACM on Computer Graphics and Interactive Techniques*, 6(3), 2023.

Juntao Ren, Gokul Swamy, Steven Wu, Drew Bagnell, and Sanjiban Choudhury. Hybrid inverse reinforcement learning. In *International Conference on Machine Learning, (ICML)*, 2024.

Yossi Rubner, Carlo Tomasi, and Leonidas J. Guibas. The earth mover's distance as a metric for image retrieval. *International Journal of Computer Vision*, 40(2):99–121, 2000.

Jürgen Schmidhuber. Reinforcement learning upside down: Don't predict rewards - just map them to actions. *CoRR*, abs/1912.02875, 2019.

Max Schwarzer, Nitarshan Rajkumar, Michael Noukhovitch, Ankesh Anand, Laurent Charlin, R. Devon Hjelm, Philip Bachman, and Aaron C. Courville. Pretraining representations for data-efficient reinforcement learning. In *Neural Information Processing (NeurIPS)*, 2021.

Max Schwarzer, Johan Samir Obando-Ceron, Aaron C. Courville, Marc G. Bellemare, Rishabh Agarwal, and Pablo Samuel Castro. Bigger, better, faster: Human-level atari with human-level efficiency. In *International Conference on Machine Learning (ICML)*, 2023.

Mingyo Seo, Steve Han, Kyutae Sim, Seung Hyeon Bang, Carlos Gonzalez, Luis Sentis, and Yuke Zhu. Deep imitation learning for humanoid loco-manipulation through human teleoperation. *CoRR*, abs/2309.01952, 2023.

Carmelo Sferrazza, Dun-Ming Huang, Xingyu Lin, Youngwoon Lee, and Pieter Abbeel. Humanoidbench: Simulated humanoid benchmark for whole-body locomotion and manipulation. *CoRR*, abs/2403.10506, 2024.

Nur Muhammad Mahi Shafiullah, Zichen Jeff Cui, Ariuntuya Altanzaya, and Lerrel Pinto. Behavior transformers: Cloning k modes with one stone. In *Neural Information Processing Systems (NeurIPS)*, 2022.

Archit Sharma, Shixiang Gu, Sergey Levine, Vikash Kumar, and Karol Hausman. Dynamics-aware unsupervised discovery of skills. In *International Conference on Learning Representations (ICLR)*, 2020.

Harshit Sikchi, Wenxuan Zhou, and David Held. Learning off-policy with online planning. In *Conference on Robot Learning (CoRL)*, 2022.

Gokul Swamy, Sanjiban Choudhury, J. Andrew Bagnell, and Steven Wu. Of moments and matching: A game-theoretic framework for closing the imitation gap. In *International Conference on Machine Learning (ICML)*, 2021.

Gokul Swamy, Nived Rajaraman, Matthew Peng, Sanjiban Choudhury, J. Andrew Bagnell, Steven Wu, Jiantao Jiao, and Kannan Ramchandran. Minimax optimal online imitation learning via replay estimation. In *Neural Information Processing Systems (NeurIPS)*, 2022.

SIMA Team, Maria Abi Raad, Arun Ahuja, Catarina Barros, Frederic Besse, Andrew Bolt, Adrian Bolton, Bethanie Brownfield, Gavin Buttimore, Max Cant, Sarah Chakera, Stephanie C. Y. Chan, Jeff Clune, Adrian Collister, Vikki Copeman, Alex Cullum, Ishita Dasgupta, Dario de Cesare, Julia Di Trapani, Yani Donchev, Emma Dunleavy, Martin Engelcke, Ryan Faulkner, Frankie Garcia, Charles Gbadamosi, Zhitao Gong, Lucy Gonzales, Kshitij Gupta, Karol Gregor, Arne Olav Hallingstad, Tim Harley, Sam Haves, Felix Hill, Ed Hirst, Drew A. Hudson, Jony Hudson, Steph Hughes-Fitt, Danilo J. Rezende, Mimi Jasarevic, Laura Kampis, Rosemary Ke, Thomas Keck, Junkyung Kim, Oscar Knagg, Kavya Kopparapu, Andrew Lampinen, Shane Legg, Alexander Lerchner, Marjorie Limont, Yulan Liu, Maria Loks-Thompson, Joseph Marino, Kathryn Martin Cussons, Loic Matthey, Siobhan Mcloughlin, Piermaria Mendolicchio, Hamza Merzic, Anna Mitenkova, Alexandre Moufarek, Valeria Oliveira, Yanko Oliveira, Hannah Openshaw, Renke Pan, Aneesh Pappu, Alex Platonov, Ollie Purkiss, David Reichert, John Reid, Pierre Harvey Richemond, Tyson Roberts, Giles Ruscoe, Jaume Sanchez Elias, Tasha Sandars, Daniel P. Sawyer, Tim Scholtes, Guy Simmons, Daniel Slater, Hubert Soyer, Heiko Strathmann, Peter Stys, Allison C. Tam, Denis Teplyashin, Tayfun Terzi, Davide Vercelli, Bojan Vujatovic, Marcus Wainwright, Jane X. Wang, Zhengdong Wang, Daan Wierstra, Duncan Williams, Nathaniel Wong, Sarah York, and Nick Young. Scaling instructable agents across many simulated worlds. *CoRR*, abs/2404.10179, 2024.

Chen Tessler, Yoni Kasten, Yunrong Guo, Shie Mannor, Gal Chechik, and Xue Bin Peng. Calm: Conditional adversarial latent models for directable virtual characters. In *ACM SIGGRAPH*, 2023.

Emanuel Todorov, Tom Erez, and Yuval Tassa. Mujoco: A physics engine for model-based control. In *International Conference on Intelligent Robots and Systems*, 2012.

Ahmed Touati and Yann Ollivier. Learning one representation to optimize all rewards. In *Neural Information Processing Systems (NeurIPS)*, 2021.

Ahmed Touati, Jérémy Rapin, and Yann Ollivier. Does zero-shot reinforcement learning exist? In *International Conference on Learning Representations (ICLR)*, 2023.

Saran Tunyasuvunakool, Alistair Muldal, Yotam Doron, Siqi Liu, Steven Bohez, Josh Merel, Tom Erez, Timothy Lillicrap, Nicolas Heess, and Yuval Tassa. dm_control: Software and tasks for continuous control. *Software Impacts*, 6:100022, 2020. ISSN 2665-9638.

UniTree. H1, 2024. URL www.unitree.com/h1.

Marin Vlastelica, Jin Cheng, Georg Martius, and Pavel Kolev. Offline diversity maximization under imitation constraints. In *Reinforcement Learning Conference (RLC)*, 2024.

Nolan Wagener, Andrey Kolobov, Felipe Vieira Frujeri, Ricky Loynd, Ching-An Cheng, and Matthew J. Hausknecht. Mocapact: A multi-task dataset for simulated humanoid control. In *Neural Information Processing Systems (NeurIPS)*, 2022.

Guanzhi Wang, Yuqi Xie, Yunfan Jiang, Ajay Mandlekar, Chaowei Xiao, Yuke Zhu, Linxi Fan, and Anima Anandkumar. Voyager: An open-ended embodied agent with large language models. *Transactions on Machine Learning Research (TMLR)*, 2024.

Yinhuai Wang, Jing Lin, Ailing Zeng, Zhengyi Luo, Jian Zhang, and Lei Zhang. Physhoi: Physics-based imitation of dynamic human-object interaction. *CoRR*, abs/2312.04393, 2023.

David Warde-Farley, Tom Van de Wiele, Tejas D. Kulkarni, Catalin Ionescu, Steven Hansen, and Volodymyr Mnih. Unsupervised control through non-parametric discriminative rewards. In *International Conference on Learning Representations (ICLR)*, 2019.

Grady Williams, Andrew Aldrich, and Evangelos A. Theodorou. Model predictive path integral control: From theory to parallel computation. *Journal of Guidance, Control, and Dynamics*, 40 (2):344–357, 2017. doi: 10.2514/1.G001921.

Jungdam Won, Deepak Gopinath, and Jessica K. Hodgins. Physics-based character controllers using conditional vaes. *ACM Transactions on Graphics*, 41(4):96:1–96:12, 2022.

Philipp Wu, Arjun Majumdar, Kevin Stone, Yixin Lin, Igor Mordatch, Pieter Abbeel, and Aravind Rajeswaran. Masked trajectory models for prediction, representation, and control. In *International Conference on Machine Learning (ICML)*, 2023.

Denis Yarats, Rob Fergus, Alessandro Lazaric, and Lerrel Pinto. Reinforcement learning with prototypical representations. In *International Conference on Machine Learning (ICML)*, 2021.

Wenhao Yu, Nimrod Gileadi, Chuyuan Fu, Sean Kirmani, Kuang-Huei Lee, Montserrat Gonzalez Arenas, Hao-Tien Lewis Chiang, Tom Erez, Leonard Hasenclever, Jan Humplik, Brian Ichter, Ted Xiao, Peng Xu, Andy Zeng, Tingnan Zhang, Nicolas Heess, Dorsa Sadigh, Jie Tan, Yuval Tassa, and Fei Xia. Language to rewards for robotic skill synthesis. In *Conference on Robot Learning (CoRL)*, 2023.

Chuning Zhu, Xinqi Wang, Tyler Han, Simon S. Du, and Abhishek Gupta. Transferable reinforcement learning via generalized occupancy models. In *Neural Information Processing Systems (NeurIPS)*, 2024.

Brianna Zitkovich, Tianhe Yu, Sichun Xu, Peng Xu, Ted Xiao, Fei Xia, Jialin Wu, Paul Wohlhart, Stefan Welker, Ayzaan Wahid, Quan Vuong, Vincent Vanhoucke, Huong Tran, Radu Soricut, Anikait Singh, Jaspiar Singh, Pierre Sermanet, Pannag R. Sanketi, Grecia Salazar, Michael S. Ryoo, Krista Reymann, Kanishka Rao, Karl Pertsch, Igor Mordatch, Henryk Michalewski, Yao Lu, Sergey Levine, Lisa Lee, Tsang-Wei Edward Lee, Isabel Leal, Yuheng Kuang, Dmitry Kalashnikov, Ryan Julian, Nikhil J. Joshi, Alex Irpan, Brian Ichter, Jasmine Hsu, Alexander Herzog, Karol Hausman, Keerthana Gopalakrishnan, Chuyuan Fu, Pete Florence, Chelsea Finn, Kumar Avinava Dubey, Danny Driess, Tianli Ding, Krzysztof Marcin Choromanski, Xi Chen, Yevgen Chebotar, Justice Carbajal, Noah Brown, Anthony Brohan, Montserrat Gonzalez Arenas, and Kehang Han. RT-2: Vision-language-action models transfer web knowledge to robotic control. In *Conference on Robot Learning (CoRL)*, 2023.

Appendices

Appendix A Related Work **20**

Appendix B Algorithmic details **22**

Appendix C Experimental Details for the Humanoid Environment **22**

C.1 The SMPL MuJoCo Model 22

C.2 Data 22

C.3 Tasks and Metrics 22

C.4 Training Protocols 26

C.5 Algorithms Implementation and Parameters 27

Appendix D Additional Experimental Results **35**

D.1 Detailed Results 35

D.2 Ablations 39

D.3 Diversity, Dataset Coverage and Transitions 42

D.4 Qualitative Evaluation 44

Appendix E Ablations on Bipedal Walker **50**

Appendix F Ablations on AntMaze **51**

Appendix G Understanding the Behavioral Latent Space **51**

G.1 Dimensionality Reduction of the Behavioral Latent Space 52

G.2 Behavior Interpolation 53

Appendix H Comparison to Unsupervised Skill Discovery Methods **54**

A Related Work

RL for Humanoid Control. Controlling a humanoid agent is considered a major objective for both in robotic (UniTree, 2024; Dynamics, 2024) and simulated (Peng et al., 2021; Won et al., 2022; Luo et al., 2024a) domains and it has emerged as a major challenge for reinforcement learning due to its high dimensionality and intrinsic instability. In robotics, a predominant approach is to perform direct behavior cloning of task-specific demonstrations (e.g., Seo et al., 2023) or combing imitation and reinforcement learning (RL) to regularize task-driven policies by using human-like priors (e.g., Cheng et al., 2024). In virtual domains, RL is often used for physics-based character animation by leveraging motion-capture datasets to perform motion tracking (Luo et al., 2023; Merel et al., 2019; Wagener et al., 2022; Reda et al., 2023) or to learn policies solving specific tasks, such as locomotion or manipulation (Luo et al., 2024c; Wang et al., 2023; Hansen et al., 2024a). Despite its popularity across different research communities, no well-established platform, data, or benchmark for multi-task whole-body humanoid control is available. Standard simulation platforms such as `dm_control` (Tunyasuvunakool et al., 2020) or IsaacGym (Makoviychuk et al., 2021) employ different humanoid skeletons and propose only a handful of reward-based tasks. Luo et al.

(2024c) and Sferrazza et al. (2024) recently introduced a broader suite of humanoid tasks, but they all require task-specific observations to include object interaction and world navigation. Regarding datasets, MoCapAct Wagener et al. (2022) relies on CMU motion capture data mapped onto a CMU humanoid skeleton, Peng et al. (2022) uses a well curated animation dataset related to a few specific movements mapped onto the IsaacGym humanoid, and Luo et al. (2023) use the AMASS dataset mapped to an SMPL skeleton.

Unsupervised RL. Pre-trained unsupervised representations from interaction data (Yarats et al., 2021; Schwarzer et al., 2021; Farebrother et al., 2023) or passive data (Baker et al., 2022; Ma et al., 2023; Brandfonbrener et al., 2023; Ghosh et al., 2023), such as unlabeled videos, significantly reduce the sample complexity and improve performance in solving downstream tasks such as goal-based, reward-based, or imitation learning by providing effective state embeddings that simplify observations (e.g., image-based RL) and capture the dynamical features of the dynamics. Another option is to pre-train a set of policies through skill diversity metrics (e.g. Gregor et al., 2016; Eysenbach et al., 2019; Sharma et al., 2020; Laskin et al., 2022; Klissarov & Machado, 2023; Park et al., 2024c) or exploration-driven metrics (e.g. Pathak et al., 2017; Machado et al., 2020; Mendonca et al., 2021; Rajeswar et al., 2023) that can serve as behavior priors. While both pre-trained representations and policies can greatly reduce sample complexity and improve performance, a full RL model still needs to be trained from scratch to solve any downstream task.

Zero-shot RL. Goal-conditioned methods (Andrychowicz et al., 2017; Pong et al., 2020; Warde-Farley et al., 2019; Mezghani et al., 2022; Ma et al., 2022; Park et al., 2023) train goal-conditioned policies to reach any goal state from any other state. While they are the most classical form of zero-shot RL, they are limited to learn goal-reaching behaviors. Successor features based methods are the most related to our approach. They achieve zero-shot capabilities by modeling a discounted sum of state features learned via low-rank decomposition (Touati & Ollivier, 2021; Touati et al., 2023; Pirotta et al., 2024; Jeen et al., 2024) or Hilbert representation (Park et al., 2024b). One of the key advantages of these methods is their low inference complexity, as they can infer a near-optimal policy for a given task through a simple regression problem. Generalized occupancy models (Zhu et al., 2024) learn a distribution of successor features but requires planning for solving novel downstream tasks. Building general world models is another popular technique (Yu et al., 2023; Ding et al., 2024; Jiang et al., 2024) for zero-shot RL when combined with search/planning algorithms (e.g. Williams et al., 2017; Howell et al., 2022). While this category hold the promise of being zero-shot, several successful world-modeling algorithms uses a task-aware training to obtain the best downstream task performance (Hansen et al., 2024b;a; Hafner et al., 2024; Sikchi et al., 2022). Finally, recent works (Frans et al., 2024; Ingebrand et al., 2024) have achieved zero-shot capabilities by learning an encoding of reward function at pre-train time by generating random unsupervised rewards.

Integrating demonstrations. Our method is related to the vast literature of learning from demonstrations. Transformer-based approaches have became a popular solution for integrating expert demonstrations in the learning process. The simplest solution is to pre-train a model through conditioned or masked behavioral cloning (Cui et al., 2023; Shafiullah et al., 2022; Schmidhuber, 2019; Chen et al., 2021; Liu et al., 2022; Wu et al., 2023; Jiang et al., 2023). If provided with sufficiently curated expert datasets at pre-training, these models can be prompted with different information (e.g., state, reward, etc) to solve various downstream tasks. While these models are used in a purely generative way, H-GAP (Jiang et al., 2024) combines them with model predictive control to optimize policies that solve downstream tasks. Similar works leverage diffusion models as an alternative to transformer architectures for conditioned trajectory generation (e.g., Pearce et al., 2023; He et al., 2023) or to solve downstream tasks via planning (Janner et al., 2022). Another popular approach is to rely on discriminator-based techniques to integrate demonstrations into an RL model either for imitation (e.g., Ho & Ermon, 2016; Ding et al., 2019; Tessler et al., 2023), reward-driven (hierarchical) tasks (Peng et al., 2021; Gehring et al., 2021; 2023; Vlastelica et al., 2024) or zero-shot (Peng et al., 2022)[9]. When the demonstrations are of "good" quality, the demonstrated behaviors can be distilled into the learned policies by constructing a one-step tracking problem (e.g., Luo et al., 2023; 2024b; Qian et al., 2024). These skills can be then used as behavior priors to train task-oriented controllers using hierarchical RL. Finally, recent papers leverage internet-scale data to learn general controllers for video games or robotic control. These methods leverage curated data with action

[9]While the original ASE algorithm is designed to create behavior priors that are then used in a hierarchical RL routine, we show in our experiments that it is possible to leverage the learned discriminator to solve downstream tasks in a zero-shot manner.

labeling (Wang et al., 2024; Team et al., 2024; Zitkovich et al., 2023) or the existence of high-level API for low-level control (Zitkovich et al., 2023).

B ALGORITHMIC DETAILS

In Alg. 1 we provide a detailed pseudo-code of FB-CPR including how all losses are computed. Following Touati et al. (2023), we add two regularization losses to improve FB training: an orthonormality loss pushing the covariance $\Sigma_B = \mathbb{E}[B(s)B(s)^\top]$ of B towards the identity, and a temporal difference loss pushing $F(s, a, z)^\top z$ toward the action-value function of the corresponding reward $B(s)^\top \Sigma_B^{-1} z$. The former is helpful to make sure that B is well-conditioned and does not collapse, while the latter makes F spend more capacity on the directions in z space that matter for policy optimization.

C EXPERIMENTAL DETAILS FOR THE HUMANOID ENVIRONMENT

C.1 THE SMPL MUJOCO MODEL

Our implementation of the humanoid agent is build on the MuJoCo model for SMPL humanoid by Luo (2023). Previous work in this domain considers unconstrained joint and over-actuated controllers with the objective of perfectly matching any behavior in motion datasets and then use the learned policies as frozen behavioral priors to perform hierarchical RL (e.g., Luo et al., 2024b). Unfortunately, this approach strongly relies on motion tracking as the only modality to extract behaviors and it often leads to simulation instabilities during training. Instead, we refined the agent specification and designed more natural joint ranges and PD controllers by building on the `dm_control` (Tunyasuvunakool et al., 2020) CMU humanoid definition and successive iterations based on qualitative evaluation. While this does not prevent the agent to express non-natural behaviors (see e.g., policies optimized purely by reward maximization), it does provide more stability and defines a more reasonable control space. We will release the full agent specification and environment code at a later time for full reproducibility.

C.2 DATA

The AMASS dataset (Mahmood et al., 2019) unifies 15 different motion capture datasets into a single SMPL-based dataset (Loper et al., 2015). For our purposes, we only consider the kinematic aspects of the dataset and ignore the full meshed body reconstruction. In order to enable the comparison to algorithms that require action-labeled demonstration datasets, we follow a similar procedure to (Wagener et al., 2022) and train a single instance of Goal-GAIL to accurately match each motion in the dataset and then roll out the learned policies to generate a dataset of trajectories with actions. The resulting dataset, named AMASS-Act, contains as many motions as the original AMASS dataset.

As mentioned in the main paper, we select only a subset of the AMASS (AMASS-Act) dataset. Following previous approaches (e.g., Luo et al., 2021; 2023; 2024b), we removed motions involving interactions with objects (e.g., stepping on boxes). We also sub-sampled the BMLhandball dataset to just 50 motions since it contains many redundant behaviors. Finally, we removed two dataset `SSM_synced` and `TCD`. We report several statistics about the datasets in Tab. 2.

C.3 TASKS AND METRICS

In this section we provide a complete description of the tasks and metrics.

C.3.1 REWARD-BASED EVALUATION

Similarly to (Tunyasuvunakool et al., 2020), rewards are defined as a function of next state and optionally action and are normalized, i.e., the reward range is $[0, 1]$. Here we provide a high level description of the 8 categories of rewards, we refer the reader to the code (that we aim to release after the submission) for details.

Algorithm 1 FB-CPR

Inputs: unlabeled dataset $\mathcal{M}$, Polyak coefficient ζ, number of parallel networks m, randomly initialized networks $\{F_{\theta_k}\}_{k\in[m]}$, B_ω, π_ϕ, $\{Q_{\eta_k}\}_{k\in[m]}$, D_ψ, learning rate ξ, batch size n, B regularization coefficient λ, Fz-regularization coefficient β, actor regularization coefficient α, number of rollouts per update N_{rollouts}, rollout length T_{rollout}, z sampling distribution $\nu = (\nu_{\text{online}}, \nu_{\text{unlabeled}})$, sequence length T_{seq}, z relabeling probability p_{relabel}

Initialize empty train buffer: $\mathcal{D}_{\text{online}} \leftarrow \emptyset$
for $t = 1, \dots$ **do**
  /* Rollout
  for $i = 1, \dots, N_{\text{rollouts}}$ **do**
    Sample $z = \begin{cases} B(s) & \text{where } s \sim \mathcal{D}_{\text{online}}, & \text{with prob } \nu_{\text{online}} \\ \frac{1}{T_{\text{seq}}} \sum_{t=1}^{T_{\text{seq}}} B(s_t) & \text{where } \{s_1, \dots, s_{T_{\text{seq}}}\} \sim \mathcal{M}, & \text{with prob } \tau_{\text{unlabeled}} \\ \sim \mathcal{N}(0, I_d) & & \text{with prob } 1 - \tau_{\text{online}} - \tau_{\text{unlabeled}} \end{cases}$
    $z \leftarrow \sqrt{d} \frac{z}{\|z\|_2}$
    Rollout $\pi_\phi(\cdot, z)$ for T_{rollout} steps, and store data into $\mathcal{D}_{\text{train}}$
  end for
  /* Sampling
  Sample a mini-batch of n transitions $\{(s_i, a_i, s'_i, z_i)\}_{i=1}^n$ from $\mathcal{D}_{\text{online}}$
  Sample a mini-batch of $\frac{n}{T_{\text{seq}}}$ sequences $\{(s_{j,1}, s_{j,2} \dots, s_{j,T_{\text{seq}}})\}_{j=1}^{\frac{n}{T_{\text{seq}}}}$ from $\mathcal{M}$
  /* Encode Expert sequences
  $z_j \leftarrow \frac{1}{T_{\text{seq}}} \sum_{t=1}^{T_{\text{seq}}} B(s_{j,t})$; $z_j \leftarrow \sqrt{d} \frac{z_j}{\|z_j\|_2}$
  /* Compute discriminator loss
  $\mathscr{L}_{\text{discriminator}}(\psi) = -\frac{1}{n} \sum_{j=1}^{\frac{n}{T_{\text{seq}}}} \sum_{t=1}^{T_{\text{seq}}} \log D_\psi(s_{j,t}, z_j) - \frac{1}{n} \sum_{i=1}^n \log(1 - D_\psi(s_i, z_i))$
  /* Sampling and Relabeling latent variables z
  Set $\forall i \in [i], z_i = \begin{cases} z_i & \text{(no relabel)} & \text{with prob } 1 - p_{\text{relabel}} \\ B(s_k) & \text{where } k \sim \mathcal{U}([n]), & \text{with prob } p_{\text{relabel}} * \tau_{\text{online}} \\ \frac{1}{T_{\text{seq}}} \sum_{t=1}^{T_{\text{seq}}} B(s_{j,t}) & \text{where } j \sim \mathcal{U}([\frac{n}{T_{\text{seq}}}]), & \text{with prob } p_{\text{relabel}} * \tau_{\text{unlabeled}} \\ \sim \mathcal{N}(0, I_d) & & \text{with prob } p_{\text{relabel}} * (1 - \tau_{\text{online}} - \tau_{\text{unlabeled}}) \end{cases}$
  /* Compute FB loss
  Sample $a'_i \sim \pi_\phi(s'_i, z_i)$ for all $i \in [n]$
  $\mathscr{L}_{\text{FB}}(\theta_k, \omega) = \frac{1}{2n(n-1)} \sum_{i \neq j} \left(F_{\theta_k}(s_i, a_i, z_i)^\top B_\omega(s'_j) - \gamma \frac{1}{m} \sum_{l \in [m]} \overline{F_{\theta_l}}(s'_i, a'_i, z_i)^\top \overline{B_\omega}(s'_j) \right)^2$
  $\quad - \frac{1}{n} \sum_i F_{\theta_k}(s_i, a_i, z_i)^\top B_\omega(s'_i) \forall k \in [m]$
  /* Compute orthonormality regularization loss
  $\mathscr{L}_{\text{ortho}}(\omega) = \frac{1}{2n(n-1)} \sum_{i \neq j} (B_\omega(s'_i)^\top B_\omega(s'_j))^2 - \frac{1}{n} \sum_i B_\omega(s'_i)^\top B_\omega(s'_i)$
  /* Compute Fz-regularization loss
  $\mathscr{L}_{\text{Fz}}(\theta_k) = \frac{1}{n} \sum_{i \in [n]} \left(F_{\theta_k}(s_i, a_i, z_i)^\top z_i - \overline{B_\omega(s'_i)^\top \Sigma_B^{-1} z_i} - \gamma \min_{l \in [m]} \overline{F_{\theta_l}}(s'_i, a'_i, z_i)^\top z_i \right)^2, \forall k$
  /* Compute critic loss
  Compute discriminator reward: $r_i \leftarrow \log(D_\psi(s_i, z_i)) - \log(1 - D_\psi(s_i, z_i)), \quad \forall i \in [n]$
  $\mathscr{L}_{\text{critic}}(\eta_k) = \frac{1}{n} \sum_{i \in [n]} \left(Q_{\eta_k}(s_i, a_i, z_i) - r_i - \gamma \min_{l \in [m]} \overline{Q_{\eta_l}}(s'_i, a'_i, z_i) \right)^2, \quad \forall k \in [m]$
  /* Compute actor loss
  Sample $a_i^\phi \sim \pi_\phi(s_i, z_i)$ for all $i \in [n]$
  Let $\overline{F} \leftarrow \text{stopgrad} \left(\frac{1}{n} \sum_{i=1}^n | \min_{l \in [m]} F_{\theta_l}(s_i, a_i^\phi, z_i)^T z_i | \right)$
  $\mathscr{L}_{\text{actor}}(\phi) = -\frac{1}{n} \sum_{i=1}^n \left(\min_{l \in [m]} F_{\theta_l}(s_i, a_i^\phi, z_i)^T z_i + \alpha \overline{F} \min_{l \in [m]} J_{\theta_l}(s_i, a_i^\phi, z_i) \right)$
  /* Update all networks
  $\psi \leftarrow \psi - \xi \nabla_\psi \mathscr{L}_{\text{discriminator}}(\psi)$
  $\theta_k \leftarrow \theta_k - \xi \nabla_{\theta_k} (\mathscr{L}_{\text{FB}}(\theta_k, \omega) + \beta \mathscr{L}_{\text{Fz}}(\theta_k))$ for all $k \in [m]$
  $\omega \leftarrow \omega - \xi \nabla_\omega (\sum_{l \in [m]} \mathscr{L}_{\text{FB}}(\theta_l, \omega) + \lambda \cdot \mathscr{L}_{\text{ortho}}(\omega))$
  $\eta_k \leftarrow \eta_k - \xi \nabla_{\eta_k} \mathscr{L}_{\text{critic}}(\eta_k) \forall k \in [m]$
  $\phi \leftarrow \phi - \xi \nabla_\phi \mathscr{L}_{\text{actor}}(\phi)$
end for

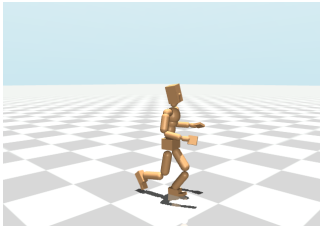

Locomotion. This category includes all the reward functions that require the agent to move at a certain speed, in a certain direction and at a certain height. The speed is the xy-linear velocity of the center of mass of the kinematic subtree rooted at the chest. We require the velocity to lie in a small band around the target velocity. The direction defined as angular displacement w.r.t. the robot facing direction, that is computed w.r.t. the x chest body. We defined high and low tasks. In high locomotion tasks, we constrain the head z-coordinate to be above a threshold, while in low tasks the agent is encouraged to keep the pelvis z-coordinate inside a predefined range

Dataset	Train dataset $\mathcal{M}$				Test dataset $\mathcal{M}_{\text{test}}$			
	Motion count	Average length	Total Steps	Total Time (s)	Motion count	Average length	Total Steps	Total Time (s)
ACCAD	223	189.00	42146	1404.87	25	174.48	4362	145.40
BMLhandball	45	291.18	13103	436.77	5	292.40	1462	48.73
BMLmovi	1456	167.36	243683	8122.77	162	165.98	26888	896.27
BioMotionLab	1445	348.88	504134	16804.47	161	266.89	42969	1432.30
CMU	1638	445.85	730307	24343.57	182	485.52	88364	2945.47
DFaust	80	179.39	14351	478.37	9	134.67	1212	40.40
DanceDB	23	1768.91	40685	1356.17	2	855.00	1710	57.00
EKUT	124	157.49	19529	650.97	14	153.00	2142	71.40
Eyes	562	862.41	484677	16155.90	62	872.95	54123	1804.10
HumanEva	25	540.68	13517	450.57	3	582.33	1747	58.23
KIT	2858	235.56	673239	22441.30	318	232.09	73806	2460.20
MPI	264	974.24	257199	8573.30	29	908.59	26349	878.30
SFU	30	569.37	17081	569.37	3	849.67	2549	84.97
TotalCapture	33	2034.06	67124	2237.47	4	1715.50	6862	228.73
Transitions	96	247.86	23795	793.17	11	228.82	2517	83.90
Total	8,902		3,144,570	29h6m59s	990		337,062	3h7m15s

Table 2: AMASS statistics split into $\mathcal{M}$ (train) and $\mathcal{M}_{\text{test}}$ (test) datasets.

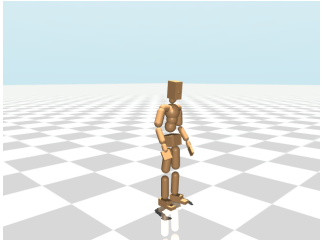

Standing. This category includes tasks that require a vertical stable position. Similarly to locomotion we defined standing "high" and "low". These two tasks are obtained from locomotion tasks by setting the speed to 0 (i.e., `smpl_move-ego-[low-]-0-0`).

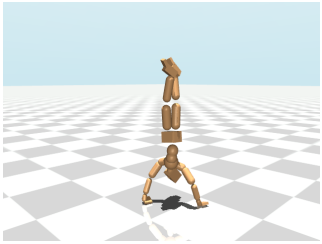

Handstand. This is a reverse standing position on the hands (i.e., `smpl_handstand`). To achieve this, the robot must place its feet and head above specific thresholds, with the feet being the highest point and the head being the lowest. Additionally, the robot's velocities and rotations should be zero, and control inputs should be minimal.

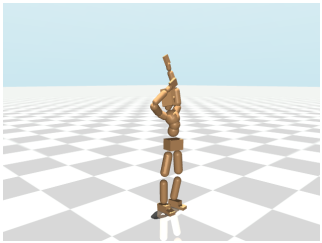

Arm raising. Similar to the previous category, this task requires the robot to maintain a standing position while reaching specific vertical positions with its hands, measured at the wrist joints. We define three hand positions: Low (z-range: 0-0.8), Medium (z-range: 1.4-1.6), and High (z-range: 1.8 and above). The left and right hands are controlled independently, resulting in nine distinct tasks. Additionally, we incorporate a penalty component for unnecessary movements and high actions. These tasks are denoted as `smpl_raisearms-{left_pos}-{right_pos}`.

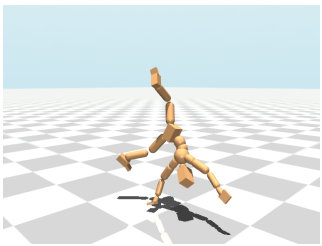

Rotation. The tasks in this category require the robot to achieve a specific angular velocity around one of the cardinal axes (x, y, or z) while maintaining proper body alignment. This alignment component is crucial to prevent unwanted movement in other directions. Similar to locomotion tasks, the robot must keep its angular velocity within a narrow range of the target velocity, use minimal control inputs, and maintain a minimum height above the ground, as measured by the pelvis z-coordinate. The tasks in this category are denoted as `smpl_rotate-{axis}-{speed}-{height}`.

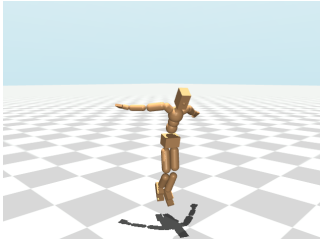

Jump. The jump task is defined as reaching a target height with the head while maintaining a sufficiently high vertical velocity. These tasks are named `smpl_jump-{height}`.

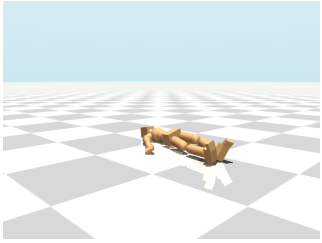

Ground poses. This category includes tasks that require the robot to achieve a stable position on the ground, such as sitting, crouching, lying down, and splitting. The sitting task (`smpl_sitonground`) requires the robot's knees to touch the ground, whereas crouching does not have this constraint. The lie-down task has two variants: facing upward (`smpl_lieonground-up`) and facing downward (`smpl_lieonground-down`). Additionally, we define the split task, which is similar to sitting on the ground but requires the robot to spread its feet apart by a certain distance (`smpl_split-{distance}`).

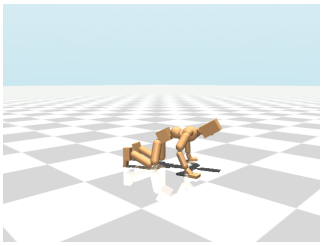

Crawl. The crawl task requires the agent to move across the floor in a crawling position, maintaining a specific target height at the spine link. Similar to locomotion tasks, the agent must move in its facing direction at a desired speed. The crawl tasks are denoted as `smpl_crawl-{height}-{speed}-{facing}`. We provide two options for the agent's orientation: crawling while facing downwards (towards the floor) or upwards (towards the sky), with the latter being significantly more challenging.

While our suite allows to generate virtually infinite tasks, we extracted 55 representative tasks for evaluation. See Tab. 18 and Tab. 19 for the complete list. We evaluate the performance of a policy in solving the task via the cumulative return over episodes of $H = 300$ steps: $\mathbb{E}_{s_0 \sim \mu_{\text{test}}, \pi}\left[\sum_{t=1}^{H} r(a_t, s_{t+1})\right]$. The initial distribution used in test is a mixture between a random falling position and a subset of the whole AMASS dataset, this is different from the distribution used in training (see App. C.4).

C.3.2 Motion Tracking Evaluation

This evaluation aims to assess the ability of the model to accurately replicate a motion, ideally by exactly matching the sequence of motion states. At the beginning of each episode, we initialize the agent in the first state of the motion and simulate as many steps as the motion length. Similarly to (Luo et al., 2021; 2023), we use success to evaluate the ability of the agent to replicate a set of motions. Let $\mathcal{M} = \{\tau_i\}_{i=1}^{M}$ the set of motions to track and denote by $\tau_i^{\mathfrak{A}}$ the trajectory generated by agent $\mathfrak{A}$ when asked to track τ_i. Then, given a threshold $\xi = 0.5$, we define

$$\text{success}(\mathcal{M}) = \frac{1}{M} \sum_{i=1}^{M} \mathbb{I}\Big\{\forall t \leq \text{len}(\tau_i) : d_{\text{smpl}}\big(s_t^{\tau_i}, s_t^{\tau_i^{\mathfrak{A}}}\big) \leq \xi\Big\}$$

where s_t^{τ} is the state of trajectory τ at step t, $d_{\text{smpl}}(s, s') = \|[X, \theta] - [X', \theta']\|_2$ and $[X, \theta]$ is the subset of the state containing joint positions and rotations. This metric is very restrictive since it requires accurate alignment at each step. Unfortunately, exactly matching the motion at each time step may not be possible due discontinuities (the motion may flicker, i.e., joint position changes abruptly in a way that is not physical), physical constraints (the motion is not physically realizable by our robot), object interaction[11], etc. We thus consider the Earth Mover's Distance (Rubner et al., 2000, EMD) with d_{smpl} as an additional metric. EMD measures the cost of transforming one distribution into another. In our case, two trajectories that are slightly misaligned in time may still be similar in

[11] We curated our datasets but we cannot exclude we missed some non-realizable motion given that this process was hand made.

EMD because the alignment cost is small, while the success metric may still be zero. While these metrics capture different dimensions, if motions are accurately tracked on average, we expect low EMD and high success rate.

C.3.3 GOAL-BASED EVALUATION

The main challenge in defining goal-based problems for humanoid is to generate target poses that are attainable and (mostly) stable. For this reason, we have manually extracted 50 poses from the motion dataset, 38 from motions in the training dataset and 12 from motions in the test dataset, trying to cover poses involving different heights and different positions for the body parts. In Fig. 5 we report a sample of 10 poses.

In order to assess how close the agent is to the target pose, we use $d_{\text{smpl}}(s, s')$ as in tracking, where the distance is only measured between position and rotation variables, while velocity variables are ignored. Let g be the goal state obtained by setting positions and rotations to the desired pose and velocities to 0, $\beta = 2$ be a threshold parameter, and $\sigma = 2$ be a margin parameter, we then define two evaluation metrics

$$\text{success} = \mathbb{E}_{s_0 \sim \mu_{\text{test}}} \Big[\mathbb{I}\Big\{ \exists t \leq 300 : d_{\text{smpl}}(s_t, g) \leq \beta \Big\} \Big];$$

$$\text{proximity} = \mathbb{E}_{s_0 \sim \mu_{\text{test}}} \Bigg[\frac{1}{300} \sum_{t=1}^{300} \Bigg(\mathbb{I}\Big\{ d_{\text{smpl}}(s_t, g) \leq \beta \Big\} + \mathbb{I}\Big\{ d_{\text{smpl}}(s_t, g) > \beta \wedge d_{\text{smpl}}(s_t, g) \leq \beta + \sigma \Big\} \Big(\frac{\beta + \sigma - d_{\text{smpl}}(s_t, g)}{\sigma} \Big) \Big\} \Bigg) \Bigg].$$

The *success* metric matches the standard shortest-path metric, where the problem is solved as soon as the agent reaches a state that is close enough to the goal. The *proximity* metric is computing a "soft" average distance across the full episode of 300 steps. The "score" for each step is 1 if the distance is within the threshold β, while it decreases linearly down to 0 when the current state is further than $\beta + \sigma$ from the goal. Finally, the metrics are averaged over multiple episodes when starting from initial states randomly sampled from μ_{test}.

When evaluating FB-CPR, CALM, ASE, and GOAL-GAIL, we need to pass a full goal state g, which includes the zero-velocity variables. On the other hand, PHC and GOAL-TD3 are directly trained to match only the position and rotation part of the goal state. Finally, for both MPPI and TD3 directly optimizing for the distance to the pose (i.e., no velocity) led to the better results.

C.4 TRAINING PROTOCOLS

In this section we provide a description of the training protocol, you can refer to the next section for algorithm dependent details. We have two train protocols depending on whether the algorithm is trained online or offline.

Online training. The agent interacts with the environment via episodes of fix length $H = 300$ steps. We simulate 50 parallel (and independent) environments at each step. The algorithm has also

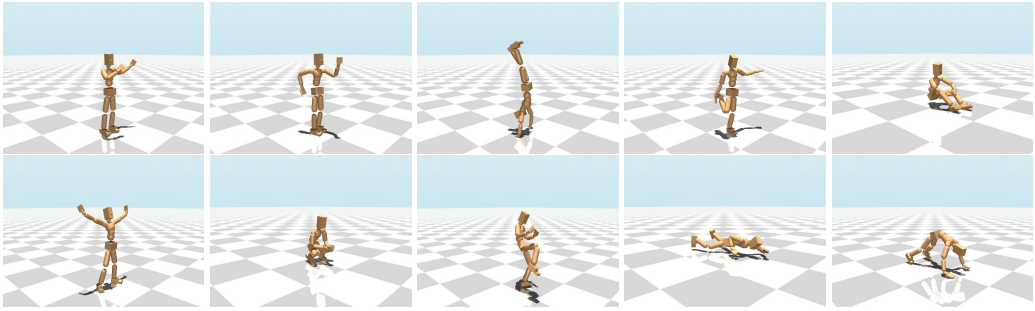

Figure 5: Examples of the poses used for goal-based evaluation.

access to the dataset $\mathcal{M}$ containing observation-only motions. The initial state distribution of an episode is a mixture between randomly generated falling positions (named "Fall" initialization) and states in $\mathcal{M}$ (named "MoCap" initialization[12]). We select the "Fall" modality with probability 0.2. For "MoCap", we use prioritization to sample motions from $\mathcal{M}$ and, inside a motion, the state is uniformly sampled. We change the prioritization during training based on the ability of the agent to track motions. Every 1M interaction steps, we evaluate the tracking performance of the agent on all the motions in $\mathcal{M}$ and update the priorities based on the following scheme. We clip the EMD in $[0.5, 5]$ and construct bins of length 0.5. This leads to 10 bins. Let $b(m)$ the bin to which motion m is mapped to and $|b(m)|$ the cardinality of the bin. Then,

$$\forall m \in \mathcal{D}_{\text{train}}, \quad \text{priority}(m) = \frac{1}{|b(m)|}.$$

We train all the agents for 3M gradient steps corresponding to 30M environment steps. The only exception is PHC where we had to change the update/step ratio and run 300M steps to achieve 3M gradient steps (we also updated the priorities every 10M steps instead of 1M).

Offline training. Offline algorithms (i.e., Diffuser and H-GAP) require a dataset label with actions and sufficiently diverse. We thus decided to use a combination of the in-house generated AMASS-Act and the replay buffer of a trained FB-CPR agent. We selected the same motions in $\mathcal{M}$ from the AMASS-Act dataset. The FB-CPR replay buffer corresponds to the buffer of the agent after being trained for 30M environment steps. The resulting dataset contains about 8.1M transitions.

C.5 Algorithms Implementation and Parameters

In this section, we describe how each considered algorithm was implemented and the hyperparameters used to obtain the results of Tab. 1.

C.5.1 Shared configurations

We first report some configurations shared across multiple algorithms, unless otherwise stated in each section below.

General training parameters. We use a replay buffer of capacity 5M transitions and update agents by sampling mini-batches of 1024 transitions. Algorithms that need trajectories from the unlabeled dataset sample segments of these of length 8 steps. During online training, we interleave a rollout phase, where we collect 500 transitions across 50 parallel environments, with a model update phase, where we update each network 50 times. During rollouts of latent- or goal-conditioned agents, we store into the online buffer transitions (s, a, s', z), where z is the latent parameter of the policy that generated the corresponding trajectory. To make off-policy training of all networks (except for discriminators) more efficient, we sample mini-batches containing (s, a, s', z) from the online buffer but relabel each z with a randomly-generated one from the corresponding distribution ν with some "relabeling probability" (reported in the tables below).

All algorithms keep the running mean and standard deviation of states in batches sampled from the online buffer and the unlabeled dataset at each update. These are used to normalize states before feeding them into each network. Unless otherwise stated we use the Adam optimizer (Kingma & Ba, 2015) with $(\beta_1, \beta_2) = (0.9, 0.999)$ and $\epsilon = 10^{-8}$.

Table 3: Summary of general traning parameters.

Hyperparameter	Value
Number of environment steps	30M
Number of parallel environments	50
Number of rollout steps between each agent update	500
Number of gradient steps per agent update	50
Number of initial steps with random actions	50000
Replay buffer size	5M
Batch size	1024
Discount factor	0.98

[12]We use both velocity and position information for the initialization.

We report also the parameters used for motion prioritization.

Table 4: Summary of prioritization parameters.

Hyperparameter	Value
Update priorities every N environment steps	1M
EMD clip	[0.5, 5]
Bin width	0.5

Network architectures. All networks are MLPs with ReLU activations, except for the first hidden layer which uses a layernorm followed by tanh. Each z-conditioned network has two initial "embedding layers", one processing (s, z), and the other processing s alone (or s and a). The second embedding layer has half the hidden units of the first layer, and their outputs are concatenated and fed into the main MLP. On the other hand, networks that do not depend on z directly concatenate all inputs and feed them into a simple MLP. The shared parameters used for these two architectures are reported in the table below. Each actor network outputs the mean of a Gaussian distribution with fixed standard deviation of 0.2.

Table 5: Hyperparameters used for the "simple MLP" architectures.

Hyperparameter	critics	actors	state embeddings
Input variables	(s, a)	s	s
Hidden layers	4	4	1
Hidden units	1024	1024	256
Activations	ReLU	ReLU	ReLU
First-layer activation	layernorm + tanh	layernorm + tanh	layernorm + tanh
Output activation	linear	tanh	l2-normalization
Number of parallel networks	2	1	1

Table 6: Hyperparameters used for the architectures with embedding layers.

Hyperparameter	critics (e.g., F, Q)	actors
Input variables	(s, a, z)	(s, z)
Embeddings	one over (s, a) and one over (s, z)	one over (s) and one over (s, z)
Embedding hidden layers	2	2
Embedding hidden units	1024	1024
Embedding output dim	512	512
Hidden layers	2	2
Hidden units	1024	1024
Activations	ReLU	ReLU
First-layer activation	layernorm + tanh	layernorm + tanh
Output activation	linear	tanh
Number of parallel networks	2	1

Discriminator. The discriminator is an MLP with 3 hidden layers of 1024 hidden units, each with ReLU activations except for the first hidden layer which uses a layernorm followed by tanh. It takes as input a state observation s and a latent variable z, and has a sigmoidal unit at the output. It is trained by minimizing the standard cross-entropy loss with a learning rate of 10^{-5} regularized by the gradient penalty used in Wasserstein GANs (Gulrajani et al., 2017) with coefficient 10. Note that this is a different gradient penalty than the one used by Peng et al. (2022); Tessler et al. (2023). We provide an in depth ablation into the choice of gradient penalty in App. D.2.

Table 7: Hyperparameters used for the discriminator.

Hyperparameter	FB-CPR	CALM	ASE	Goal-GAIL
Input variables	(s, z)	(s, z)	s	(s, g)
Hidden layers	3	3	3	3
Hidden units	1024	1024	1024	1024
Activations	ReLU	ReLU	ReLU	ReLU
Output activation	sigmoid	sigmoid	sigmoid	sigmoid
WGAN gradient penalty coefficient	10	10	10	10
Learning rate	10^{-5}	10^{-5}	10^{-5}	10^{-5}

C.5.2 TD3

We follow the original implementation of algorithm by Fujimoto et al. (2018), except that we replace the minimum operator over target networks to compute the TD targets and the actor loss by a penalization wrt the absolute difference between the Q functions in the ensemble, as proposed by Cetin et al. (2024). This penalty is used in the actor and the critic of all TD3-based algorithms, with the coefficients reported in the tables below. Note that we will report only the values 0, for which the target is the average of the Q networks in the ensemble, and 0.5, for which the target is the minimum of these networks.

Table 8: Hyperparameters used for TD3 training.

Hyperparameter	Value
General training parameters	See Tab. 3
General prioritization parameters	See Tab. 4
actor network	third column of Tab. 5, output dim = action dim
critic network	second column of Tab. 5, output dim 1
Learning rate for actor	10^{-4}
Learning rate for critic	10^{-4}
Polyak coefficient for target network update	0.005
Actor penalty coefficient	0
Critic penalty coefficient	0

C.5.3 FB-CPR

The algorithm is implemented following the pseudocode App. B. The values of its hyperparameters are reported in the table below.

Inference methods. For reward-based inference, we use a weighted regression method $z_r \propto \mathbb{E}_{s' \sim \mathcal{D}_{\text{online}}}[\exp(10r(s'))B(s')r(s')]$, where we estimate the expectation with 100k samples from the online buffer. We found this to work better than standard regression, likely due to the high diversity of behaviors present in the data. For goal-based inference, we use the original method $z_g = B(g)$, while for motion tracking of a motion τ we infer one z for each time step t in the motion as $z_t \propto \sum_{j=t+1}^{t+L+1} B(s_j)$, where s_j is the j-th state in the motion and L is the same encoding sequence length used during pre-training.

Table 9: Hyperparameters used for FB-CPR pretraining.

Hyperparameter	Value
General training parameters	See Tab. 3
General prioritization parameters	See Tab. 4
Sequence length for trajectory sampling from $\mathcal{D}$	8
z update frequency during rollouts	once every 150 steps
z dimension d	256
Regularization coefficient α	0.01
F network	second column of Tab. 6, output dim 256
actor network	third column of Tab. 6, output dim = action dim
critic network	second column of Tab. 6, output dim 1
B network	fourth column of Tab. 5, output dim 256
Discriminator	Tab. 7
Learning rate for F	10^{-4}
Learning rate for actor	10^{-4}
Learning rate for critic	10^{-4}
Learning rate for B	10^{-5}
Coefficient for orthonormality loss	100
z distribution ν	
-encoding of unlabeled trajectories	60%
-goals from the online buffer	20%
-uniform on unit sphere	20%
Probability of relabeling zs	0.8
Polyak coefficient for target network update	0.005
FB penalty coefficient	0
Actor penalty coefficient	0.5
Critic penalty coefficient	0.5
Coefficient for Fz-regularization loss	0.1

C.5.4 ASE

We implemented an off-policy version of ASE to be consistent with the training protocol of FB-CPR. In particular, we use a TD3-based scheme to optimize all networks instead of PPO as in the original implementation of Peng et al. (2022). As for FB-CPR, we fit a critic to predict the expected discounted sum of rewards from the discriminator by temporal difference (see Eq. 10), and another critic to predict $\mathbb{E}[\sum_{t=0}^{\infty} \gamma^t \phi(s_{t+1})^\top z | s, a, \pi_z]$, where ϕ is the representation learned by the DIAYN-based (Eysenbach et al., 2019) skill discovery part of the algorithm. We train such representation by an off-policy version of Eq. 13 in (Peng et al., 2022), where we sample couples (s', z) from the online buffer and maximize $\mathbb{E}_{(s',z)\sim\mathcal{D}_{\text{online}}}[\phi(s')^T z]$. Note that this is consistent with the original off-policy implementation of DIAYN (Eysenbach et al., 2019). The output of ϕ is normalized on the hypersphere of radius $\sqrt{d}$. We also add an othornormality loss (same as the one used by FB) as we found this to be essential for preventing collapse of the encoder.

Inference methods. For reward-based and goal-based inference we use the same methods as FB-CPR, with B replaced with ϕ. For tracking we use $z_t \propto B(s_{t+1})$ for each timestep t in the target motion.

Table 10: Hyperparameters used for ASE pretraining.

Hyperparameter	Value
General training parameters	See Tab. 3
General prioritization parameters	See Tab. 4
z update frequency during rollouts	once every 150 steps
z dimension d	64
Regularization coefficient α	0.01
actor network	third column of Tab. 6, output dim = action dim
critic networks	second column of Tab. 6, output dim 1
ϕ encoder network	fourth column of Tab. 5, output dim 64
Discriminator	Tab. 7
Learning rate for actor	10^{-4}
Learning rate for critic	10^{-4}
Learning rate for ϕ	10^{-8}
Coefficient for orthonormality loss	100
z distribution ν	
-goals from unlabeled dataset	60%
-goals from the online buffer	20%
-uniform on unit sphere	20%
Probability of relabeling zs	0.8
Polyak coefficient for target network update	0.005
Coefficient for diversity loss (Eq. 15 in (Peng et al., 2022))	0
Actor penalty coefficient	0.5
Critic penalty coefficient	0.5

C.5.5 CALM

As for ASE, we implemented an off-policy TD3-based version of CALM to be consistent with the training protocol of FB-CPR. We fit a critic $Q(s, a, z)$ to predict the expected discounted sum of rewards from the discriminator by temporal difference (see Eq. 10). We also train a sequence encoder $\phi(\tau)$ which embeds a sub-trajectory τ from the unlabeled dataset into z space through a transformer. The encoder and the actor are trained end-to-end by maximizing $Q(s, \pi(s, z = \phi(\tau)), z = \phi(\tau)$, plus the constrastive regularization loss designed to prevent the encoder from collapsing (Eq. 5,6 in (Tessler et al., 2023)). The transformer interleaves attention and feed-forward blocks. The former uses a layernorm followed by multi-head self-attention plus a residual connection, while the latter uses a layernorm followed by two linear layers interleaved by a GELU activation. Its output is normalized on the hypersphere of radius $\sqrt{d}$.

Inference methods. We use the same methods as FB-CPR for goal-based and tracking inference.

Table 11: Hyperparameters used for CALM pretraining.

Hyperparameter	Value
General training parameters	See Tab. 3
General prioritization parameters	See Tab. 4
Sequence length for trajectory sampling from $\mathcal{D}$	8
z update frequency during rollouts	once every 150 steps
z dimension d	256
actor network	third column of Tab. 6, output dim = action dim
critic network	second column of Tab. 6, output dim 1
ϕ encoder network	transformer (see text above)
-attention blocks	2
-embedding dim	256
-MLP first linear layer	256x1024
-MLP second linear layer	1024x256
Discriminator	Tab. 7
Learning rate for actor	10^{-4}
Learning rate for critic	10^{-4}
Learning rate for ϕ	10^{-7}
Coefficient for constrastive loss	0.1
z distribution ν	
-encoding of unlabeled trajectories	100%
-goals from the online buffer	0%
-uniform on unit sphere	0%
Probability of relabeling zs	1
Polyak coefficient for target network update	0.005
Actor penalty coefficient	0.5
Critic penalty coefficient	0.5

C.5.6 PHC

PHC is similar to a goal-conditioned algorithm except that the goal is "forced" to be the next state in the motion. This makes PHC an algorithm specifically designed for one-step tracking. We use a TD3-based variant of the original implementation (Luo et al., 2023). Concretely the implementation is exactly the same of TD3 but we changed the underlying environment. In this tracking environment the state is defined as the concatenation of the current state s and the state g to track. The resulting state space is $\mathbb{R}^{716}$. At the beginning of an episode, we sample a motion m from the motion set (either $\mathcal{M}$ or $\mathcal{D}_{\text{test}}$) and we initialize the agent to a randomly selected state of the motion. Let $\bar{t}$ being the randomly selected initial step of the motion, then at any episode step $t \in [1, \text{len}(m) - \bar{t} - 1]$ the target state g_t correspond to the motion state $m_{\bar{t}+t+1}$. We use the negative distance in position/orientation as reward function, i.e., $r((s, g), a, (s', g')) = -d_{\text{smpl}}(g, s')$.

Inference methods. By being a goal-conditioned algorithm we just need to pass the desired goal as target reference and can be evaluated for goal and tracking tasks.

Table 12: Hyperparameters used for PHC pretraining.

Hyperparameter	Value
General training parameters	See Tab. 3
General prioritization parameters	See Tab. 4
Update priorities every N environment steps	10M
Number of environment steps	$300M$
Number of gradient steps per agent update	5
TD3 configuration	See Tab. 8

C.5.7 GOAL-GAIL

We use a TD3-based variant of the original implementation (Ding et al., 2019). Concretely, the implementation is very similar to the one of CALM, except that there is no trajectory encoder and the discriminator directly receives couples (s, g), where g is a goal state sampled from the online buffer or the unlabeled dataset. In particular, the negative pairs (s, g) for updating the discriminator are sampled uniformly from the online buffer (where g is the goal that was targeted when rolling out the policy that generated s), while the positive pairs are obtained by sampling a sub-trajectory τ of length 8 from the unlabeled dataset and taking g as the last state and s as another random state. Similarly to CALM, we train a goal-conditioned critic $Q(s, a, g)$ to predict the expected discounted sum of discriminator rewards, and an goal-conditioned actor $\pi(s, g)$ to maximize the predictions of such a critic.

Inference methods. We use the same methods as ASE for goal-based and tracking inference.

Table 13: Hyperparameters used for GOAL-GAIL pretraining.

Hyperparameter	Value
General training parameters	See Tab. 3
General prioritization parameters	See Tab. 4
Sequence length for trajectory sampling from $\mathcal{D}$	8
goal update frequency during rollouts	once every 150 steps
actor network	third column of Tab. 6, output dim = action dim
critic network	second column of Tab. 6, output dim 1
Discriminator	Tab. 7
Learning rate for actor	10^{-4}
Learning rate for critic	10^{-4}
goal sampling distribution	
-goals from the unlabeled dataset	50%
-goals from the online buffer	50%
Probability of relabeling zs	0.8
Polyak coefficient for target network update	0.005
Actor penalty coefficient	0.5
Critic penalty coefficient	0.5

C.5.8 GOAL-TD3

We closely follow the implementation of Pirotta et al. (2024). For reaching each goal g, we use the reward function $r(s', g) = -\|\text{pos}(s') - \text{pos}(g)\|_2$, where $\text{pos}(\cdot)$ extracts only the position of each joint, ignoring their velocities. We then train a goal-conditioned TD3 agent to optimize such a reward for all g. We sample a percentage of training goals from the unlabeled dataset, and a percentage using hindsight experience replay (HER, Andrychowicz et al., 2017) on trajectories from the online buffer.

Inference methods. We use the same methods as ASE for goal-based and tracking inference.

Table 14: Hyperparameters used for GOAL-TD3 pretraining.

Hyperparameter	Value
General training parameters	See Tab. 3
General prioritization parameters	See Tab. 4
Sequence length for HER sampling	8
goal update frequency during rollouts	once every 150 steps
actor network	third column of Tab. 6, output dim = action dim
critic network	second column of Tab. 6, output dim 1
Learning rate for actor	10^{-4}
Learning rate for critic	10^{-4}
goal sampling distribution	
-goals from the unlabeled dataset	100%
-goals from the online buffer (HER)	0%
Probability of relabeling zs	0.5
Polyak coefficient for target network update	0.005
Actor penalty coefficient	0.5
Critic penalty coefficient	0.5

C.5.9 MPPI

We use MPPI with the real dynamic and real reward function for each task. For each evaluation state, action plans are sampled according to a factorized Gaussian distribution. Initially, mean and standard variation of the Gaussian are set with 0 and 1, respectively. actions plans are evaluated by deploying them in the real dynamics and computed the cumulative return over some planning horizon. Subsequently, the Gaussian parameters are updated using the top-k most rewarding plans. For goal-reaching tasks, we use the reward $r(s', g) = -\|\text{pos}(s') - \text{pos}(g)\|_2$

Table 15: Hyperparameters used for MPPI planning.

Hyperparameter	Value
Number of plans	256
Planning horizon	32 for reward-based tasks, 8 for goals
k for the top-k	64
Maximum of standard deviation	2
Minimum of standard deviation	0.2
Temperature	1
Number of optimization steps	10

C.5.10 DIFFUSER

We train Diffuser offline on FB-CPR replay buffer and AMASS-Act dataset as described in C.4. We follow the original implementation in Janner et al. (2022). We use diffusion probabilistic model to learn a generative model over sequence of state-action pairs. Diffusion employs a forward diffusion process $q(\tau^i|\tau^{i-1})$ (typically pre-specified) to slowly corrupt the data by adding noise and learn a parametric reverse denoising process $p_\theta(\tau^{i-1}|\tau^i), \forall i \in [0, n]$ which induces the following data distribution:

$$p_\theta(\tau^0) = \int p(\tau^n) \prod_{i=1}^{n} p_\theta(\tau^{i-1} \mid \tau^i) \mathrm{d}\tau^1 \dots \mathrm{d}\tau^n \tag{12}$$

where τ^0 denotes the real data and τ^n is sampled from a standard Gaussian prior. The parametric models is trained using a variationnal bound on the log-likelihood objective $\mathbb{E}_{\tau^0 \sim \mathcal{D}}[\log p_\theta(\tau^0)]$. We use Temporal U-net architecture as in Janner et al. (2022) for p_θ.

At test time, we learn a value function to predict the cumulative sum of reward given a sequence τ: $R_\psi(\tau) \approx \sum_{t=1}^{l(\tau)} \gamma^{t-1} r(s_t)$. To do that, we relabel the offline dataset according to the task's reward and we train R_ψ by regression on the same noise distribution used in the diffusion training:

$$\mathbb{E}_{\tau^0 \sim \mathcal{D}} \mathbb{E}_{i \in \mathcal{U}[n]} \mathbb{E}_{\tau^i \sim q(\tau^i|\tau^0)} \left[\left(R_\psi(\tau^i) - \sum_{t=1}^{l(\tau^0)} \gamma^{t-1} r(s_t) \right)^2 \right] \tag{13}$$

We use then guiding sampling to solve the task by following the gradient of the value function $\nabla_{\tau^i} R_\psi(\tau^i)$ at each denoising step. For goal-reaching tasks, we condition the diffuser sampling by replacing the last state of the sampled sequence τ^i by the goal state after each diffusion steps. We sample several sequences and we select the one that maximizes the cumulative sum of the reward $r(s', g) = -\|\mathrm{pos}(s') - \mathrm{pos}(g)\|_2$.

Table 16: Hyperparameters used for Diffuser pretraining and planning.

Hyperparameter	Value
Learning rate	4×10^{-5}
Number of gradient steps	3×10^6
Sequence length	32
U-Net hidden dimension	1024
Number of diffusion steps	50
Weight of the action loss	10
Planning horizon	32
Gradient scale	0.1
Number of plans	128
Number of guided steps	2
Number of guided-free denoising steps	4

C.5.11 H-GAP

We train the H-GAP model on the FB-CPR replay buffer and the AMASS-Act dataset as outlined in C.4. Following the methodology described in Jiang et al. (2024), we first train a VQ-VAE on the dataset to discretize the state-action trajectories. Subsequently, we train a decoder-only Prior Transformer to model the latent codes autoregressively. In line with the procedures detailed in Jiang et al. (2024), we integrate H-GAP within a Model Predictive Control (MPC) framework. This integration involves employing top-p sampling to generate a set of probable latent trajectories, which

were then decoded back into the original state-action space. At test time, we selected the most optimal trajectory based on the task-specific reward functions, assuming access to these functions.

Table 17: Hyperparameters used for H-GAP.

Hyperparameter	Value
batch size	128
training steps	10^8
Modeling horizon	32
VQ-VAE chunk size	4
VQ-VAE code per chunk	32
VQ-VAE number of code	512
VQ-VAE learning rate	3×10^{-4}
VQ-VAE number of heads	4
VQ-VAE number of layers	4
Prior Transformer number of heads	10
Prior Transformer number of layers	10
Prior Transformer learning rate	3×10^{-4}

Task	TD3	MPPI	Norm.	Diffuser	Normalized	ASE	Normalized	FB-CPR	Normalized
move-ego-0-0	275.08	203.33	0.74	227.27 (3.09)	0.83 (0.01)	266.03 (1.41)	0.97 (0.01)	274.68 (1.48)	1.00 (0.01)
move-ego-low-0-0	273.67	249.12	0.91	118.50 (15.56)	0.43 (0.06)	222.14 (19.48)	0.81 (0.07)	215.61 (27.63)	0.79 (0.10)
handstand	251.30	3.58	0.01	5.21 (3.76)	0.02 (0.01)	0.04 (0.08)	0.00 (0.00)	41.27 (10.20)	0.16 (0.04)
move-ego-0-2	255.57	263.67	1.03	238.99 (5.79)	0.94 (0.02)	224.29 (50.58)	0.88 (0.20)	260.93 (5.21)	1.02 (0.02)
move-ego-0-4	242.66	251.13	1.03	179.82 (19.33)	0.74 (0.08)	211.65 (32.39)	0.87 (0.13)	235.44 (29.42)	0.97 (0.12)
move-ego--90-2	255.45	260.71	1.02	206.48 (7.00)	0.81 (0.03)	230.46 (9.72)	0.90 (0.04)	210.99 (6.55)	0.83 (0.03)
move-ego--90-4	245.76	250.29	1.02	137.80 (9.33)	0.56 (0.04)	143.12 (26.14)	0.58 (0.11)	202.99 (9.33)	0.83 (0.04)
move-ego-90-2	253.77	262.62	1.03	207.27 (4.74)	0.82 (0.02)	194.18 (64.48)	0.77 (0.25)	224.68 (9.15)	0.89 (0.04)
move-ego-90-4	247.49	251.61	1.02	132.93 (10.93)	0.54 (0.04)	134.14 (12.22)	0.54 (0.05)	185.60 (14.42)	0.75 (0.06)
move-ego-180-2	258.28	251.46	0.97	195.45 (7.26)	0.76 (0.03)	237.73 (21.51)	0.92 (0.08)	227.34 (27.01)	0.88 (0.10)
move-ego-180-4	249.81	252.28	1.01	132.89 (9.70)	0.53 (0.04)	134.54 (13.34)	0.54 (0.05)	205.54 (14.40)	0.82 (0.06)
move-ego-low-0-2	274.71	273.65	1.00	100.64 (8.61)	0.37 (0.03)	56.46 (10.91)	0.21 (0.04)	207.27 (58.01)	0.75 (0.21)
move-ego-low--90-2	270.69	266.74	0.99	80.33 (4.51)	0.30 (0.02)	65.01 (44.17)	0.24 (0.16)	221.37 (35.35)	0.82 (0.13)
move-ego-low-90-2	259.97	267.52	1.03	96.12 (6.79)	0.37 (0.03)	58.71 (47.10)	0.23 (0.18)	222.81 (21.94)	0.86 (0.08)
move-ego-low-180-2	280.15	273.37	0.98	65.61 (7.73)	0.23 (0.03)	13.77 (16.25)	0.05 (0.06)	65.20 (32.64)	0.23 (0.12)
jump-2	90.66	67.45	0.74	15.85 (0.64)	0.17 (0.01)	8.73 (6.86)	0.10 (0.08)	34.88 (3.52)	0.38 (0.04)
rotate-x--5-0.8	222.60	163.35	0.73	8.31 (1.82)	0.04 (0.01)	0.04 (0.05)	0.00 (0.00)	7.42 (5.69)	0.03 (0.03)
rotate-x-5-0.8	219.28	176.23	0.80	13.04 (3.12)	0.06 (0.01)	0.04 (0.01)	0.00 (0.00)	2.29 (1.78)	0.01 (0.01)
rotate-y--5-0.8	272.15	270.84	1.00	107.14 (14.51)	0.39 (0.05)	124.52 (32.52)	0.46 (0.12)	217.70 (43.67)	0.80 (0.16)
rotate-y-5-0.8	273.74	272.66	1.00	97.70 (10.05)	0.36 (0.04)	149.48 (36.92)	0.55 (0.13)	199.08 (51.78)	0.73 (0.19)
rotate-z--5-0.8	257.30	208.39	0.81	6.67 (1.50)	0.03 (0.01)	0.39 (0.77)	0.00 (0.00)	95.23 (15.75)	0.37 (0.06)
rotate-z-5-0.8	266.16	206.59	0.78	5.83 (2.46)	0.02 (0.01)	0.01 (0.00)	0.00 (0.00)	124.95 (17.61)	0.47 (0.07)
raisearms-l-l	264.61	194.60	0.74	221.11 (5.14)	0.84 (0.02)	265.15 (1.35)	1.00 (0.01)	270.43 (0.37)	1.02 (0.00)
raisearms-l-m	266.03	187.43	0.70	133.55 (8.85)	0.50 (0.03)	63.67 (18.97)	0.24 (0.07)	97.66 (81.17)	0.37 (0.31)
raisearms-l-h	268.30	41.05	0.15	87.44 (13.21)	0.33 (0.05)	258.00 (1.36)	0.96 (0.01)	243.16 (19.18)	0.91 (0.07)
raisearms-m-l	269.36	178.85	0.66	116.25 (13.75)	0.43 (0.05)	70.66 (36.32)	0.26 (0.13)	134.83 (70.28)	0.50 (0.26)
raisearms-m-m	267.55	137.62	0.51	139.84 (12.04)	0.52 (0.04)	11.52 (0.14)	0.04 (0.00)	87.25 (98.42)	0.33 (0.37)
raisearms-m-h	264.12	34.64	0.13	91.54 (8.02)	0.35 (0.03)	52.79 (1.61)	0.20 (0.01)	75.05 (69.32)	0.28 (0.26)
raisearms-h-l	273.91	40.19	0.15	62.35 (9.37)	0.23 (0.03)	240.23 (22.36)	0.88 (0.08)	167.98 (82.03)	0.61 (0.30)
raisearms-h-m	264.67	36.41	0.14	78.29 (16.38)	0.30 (0.06)	54.58 (3.27)	0.21 (0.01)	104.26 (81.69)	0.39 (0.31)
raisearms-h-h	265.17	8.23	0.03	69.31 (19.10)	0.26 (0.07)	255.83 (0.69)	0.96 (0.00)	199.88 (42.03)	0.75 (0.16)
crouch-0	268.83	222.66	0.83	82.36 (12.78)	0.31 (0.05)	181.96 (58.21)	0.68 (0.22)	226.28 (28.17)	0.84 (0.10)
sitonground	271.76	243.64	0.90	61.18 (9.02)	0.23 (0.03)	114.03 (57.40)	0.42 (0.21)	199.44 (22.15)	0.73 (0.08)
lieonground-up	278.66	249.31	0.89	29.05 (7.71)	0.10 (0.03)	204.26 (18.93)	0.73 (0.07)	193.66 (33.18)	0.69 (0.12)
lieonground-down	277.51	242.08	0.87	73.70 (10.52)	0.27 (0.04)	158.10 (68.06)	0.57 (0.25)	193.50 (18.89)	0.70 (0.07)
split-0.5	276.13	250.66	0.91	104.29 (12.85)	0.38 (0.05)	112.46 (71.92)	0.41 (0.26)	232.18 (20.26)	0.84 (0.07)
split-1	279.25	253.28	0.91	27.28 (5.74)	0.10 (0.02)	13.92 (20.72)	0.05 (0.07)	117.67 (61.27)	0.42 (0.22)
crawl-0.4-0-u	145.11	124.76	0.86	10.47 (6.81)	0.07 (0.05)	77.46 (36.91)	0.53 (0.25)	101.76 (15.97)	0.70 (0.11)
crawl-0.4-2-u	287.01	60.50	0.21	1.81 (1.25)	0.01 (0.00)	4.03 (4.03)	0.01 (0.01)	15.02 (6.03)	0.05 (0.02)
crawl-0.5-0-u	146.02	124.75	0.85	4.84 (3.67)	0.03 (0.03)	77.72 (37.07)	0.53 (0.25)	101.92 (16.39)	0.70 (0.11)
crawl-0.5-2-u	234.51	60.16	0.26	1.77 (1.27)	0.01 (0.01)	3.97 (4.04)	0.02 (0.02)	15.81 (6.10)	0.07 (0.03)
crawl-0.4-0-d	145.79	112.27	0.77	27.44 (9.15)	0.19 (0.06)	20.32 (14.02)	0.14 (0.10)	191.75 (43.60)	1.32 (0.30)
crawl-0.4-2-d	289.55	105.70	0.37	4.00 (0.78)	0.01 (0.00)	15.50 (3.19)	0.05 (0.01)	19.00 (4.07)	0.07 (0.01)
crawl-0.5-0-d	146.46	112.00	0.76	24.68 (3.74)	0.17 (0.03)	7.03 (2.07)	0.05 (0.01)	131.13 (64.97)	0.90 (0.44)
crawl-0.5-2-d	291.74	64.94	0.22	4.64 (2.01)	0.02 (0.01)	19.41 (9.51)	0.07 (0.03)	22.93 (5.31)	0.08 (0.02)
Average	249.74	178.50	0.72	85.27	0.33	105.73	0.41	151.68	0.61
Median	265.17	206.59	0.83	80.33	0.30	77.46	0.41	191.75	0.73

Table 18: Humanoid Environment. Average return per task for reward-optimization evaluation.

Group	Num. Tasks	TD3	MPPI	Normalized	Diffuser	Normalized	ASE	Normalized	FB-CPR	Normalized
Stand	2	274.38 (0.71)	226.22 (22.89)	0.82 (0.09)	172.89 (54.38)	0.63 (0.20)	244.09 (21.94)	0.89 (0.08)	245.14 (29.53)	0.89 (0.11)
Handstand	1	251.30 (0.00)	3.58 (0.00)	0.01 (0.00)	5.21 (0.00)	0.02 (0.00)	0.04 (0.00)	0.00 (0.00)	41.27 (0.00)	0.16 (0.00)
Locomotion	8	251.10 (5.15)	255.47 (5.39)	1.02 (0.02)	178.95 (37.70)	0.71 (0.14)	188.76 (41.77)	0.75 (0.16)	219.19 (21.64)	0.87 (0.08)
Locom.-Low	4	271.38 (7.39)	270.32 (3.20)	1.00 (0.02)	85.67 (13.83)	0.32 (0.06)	48.49 (20.28)	0.18 (0.08)	179.16 (66.08)	0.67 (0.25)
Jump	1	90.66 (0.00)	67.45 (0.00)	0.74 (0.00)	15.85 (0.00)	0.17 (0.00)	8.73 (0.00)	0.10 (0.00)	34.88 (0.00)	0.38 (0.00)
Rotation	6	251.87 (22.52)	216.34 (42.26)	0.85 (0.10)	39.78 (44.43)	0.15 (0.16)	45.75 (64.93)	0.17 (0.24)	107.78 (83.74)	0.40 (0.31)
RaiseArms	9	267.08 (2.96)	95.45 (72.90)	0.36 (0.27)	111.08 (46.67)	0.42 (0.18)	141.38 (102.78)	0.53 (0.38)	153.39 (67.09)	0.57 (0.25)
On-Ground	6	275.36 (3.80)	243.61 (10.14)	0.88 (0.03)	62.98 (27.77)	0.23 (0.10)	130.79 (61.96)	0.48 (0.23)	193.79 (37.32)	0.71 (0.14)
Crawl	8	210.77 (67.08)	95.63 (26.87)	0.54 (0.28)	9.96 (9.66)	0.06 (0.07)	28.18 (29.15)	0.18 (0.21)	74.91 (62.42)	0.48 (0.45)

Table 19: Humanoid Environment. Average return per category for reward-optimization evaluation.

D Additional Experimental Results

In this section we report a more detailed analysis of the experiments.

D.1 Detailed Results

In this section we report detailed results split across tasks.

- Table 18 shows the average return for each reward-based task and Table 19 groups the results per task category.
- Table 20 shows the proximity metric for each goal pose, while Table 21 shows the success rate.
- Table 22 shows the train and test tracking performance for both EMD and success rate grouped over the AMASS datasets.

Goal	TD3	MPPI	Diffuser	Goal-GAIL	Goal-TD3	PHC	CALM	ASE	FB-CPR
Proximity									
t_pose	0.99	0.21	0.60 (0.07)	0.98 (0.00)	0.99 (0.00)	0.24 (0.03)	0.53 (0.34)	0.98 (0.01)	0.99 (0.00)
t_pose_lower_arms	0.99	0.28	0.52 (0.04)	0.96 (0.05)	0.99 (0.00)	0.44 (0.04)	0.81 (0.17)	0.95 (0.06)	0.99 (0.00)
t_pose_bow_head	0.99	0.23	0.60 (0.13)	0.98 (0.00)	0.99 (0.00)	0.21 (0.06)	0.63 (0.27)	0.82 (0.12)	0.99 (0.00)
u_stretch_y_right	0.99	0.19	0.12 (0.12)	0.79 (0.17)	0.87 (0.07)	0.02 (0.01)	0.16 (0.14)	0.55 (0.20)	0.70 (0.21)
u_stretch_y_left	0.98	0.20	0.01 (0.01)	0.55 (0.11)	0.77 (0.06)	0.02 (0.01)	0.10 (0.20)	0.37 (0.23)	0.73 (0.18)
u_stretch_z_right	0.99	0.28	0.02 (0.01)	0.66 (0.28)	0.81 (0.14)	0.04 (0.00)	0.09 (0.14)	0.31 (0.23)	0.83 (0.10)
u_stretch_z_left	0.99	0.16	0.25 (0.09)	0.95 (0.04)	0.95 (0.07)	0.06 (0.01)	0.09 (0.15)	0.45 (0.25)	0.97 (0.03)
u_stretch_x_back	0.98	0.07	0.10 (0.11)	0.81 (0.14)	0.72 (0.17)	0.02 (0.01)	0.01 (0.01)	0.76 (0.22)	0.93 (0.04)
u_stretch_x_front_part	0.99	0.63	0.55 (0.13)	0.94 (0.07)	0.99 (0.00)	0.14 (0.02)	0.34 (0.20)	0.74 (0.16)	0.99 (0.00)
u_stretch_x_front_full	0.98	0.98	0.06 (0.03)	0.84 (0.09)	0.90 (0.07)	0.01 (0.00)	0.34 (0.29)	0.60 (0.22)	0.95 (0.02)
crossed_arms	0.98	0.20	0.26 (0.10)	0.80 (0.06)	0.86 (0.08)	0.02 (0.01)	0.14 (0.17)	0.56 (0.07)	0.89 (0.05)
scratching_head	0.99	0.24	0.29 (0.14)	0.98 (0.00)	0.99 (0.01)	0.06 (0.02)	0.15 (0.25)	0.97 (0.01)	0.99 (0.00)
right_hand_wave	0.99	0.23	0.42 (0.17)	0.92 (0.01)	0.98 (0.00)	0.12 (0.01)	0.32 (0.20)	0.94 (0.02)	0.95 (0.00)
x_strech	0.98	0.11	0.42 (0.13)	0.90 (0.08)	0.93 (0.05)	0.06 (0.02)	0.12 (0.14)	0.82 (0.13)	0.94 (0.05)
i_strecth	0.86	0.07	0.20 (0.15)	0.71 (0.07)	0.74 (0.09)	0.01 (0.00)	0.02 (0.03)	0.69 (0.08)	0.88 (0.08)
arms_stretch	0.98	0.08	0.22 (0.13)	0.58 (0.08)	0.72 (0.14)	0.07 (0.01)	0.05 (0.10)	0.39 (0.13)	0.68 (0.06)
drinking_from_bottle	0.98	0.23	0.17 (0.07)	0.69 (0.09)	0.88 (0.08)	0.04 (0.02)	0.07 (0.10)	0.80 (0.08)	0.97 (0.04)
arm_on_chest	0.98	0.15	0.17 (0.07)	0.92 (0.05)	0.99 (0.00)	0.04 (0.01)	0.16 (0.17)	0.95 (0.02)	0.98 (0.00)
pre_throw	0.56	0.03	0.00 (0.00)	0.08 (0.07)	0.23 (0.13)	0.04 (0.01)	0.00 (0.00)	0.02 (0.03)	0.08 (0.10)
egyptian	0.99	0.18	0.18 (0.08)	0.80 (0.10)	0.94 (0.06)	0.12 (0.03)	0.28 (0.28)	0.60 (0.27)	0.98 (0.00)
zombie	0.98	0.14	0.47 (0.09)	0.96 (0.03)	0.99 (0.00)	0.15 (0.04)	0.33 (0.30)	0.92 (0.05)	0.98 (0.00)
stand_martial_arts	0.99	0.41	0.41 (0.17)	0.94 (0.05)	0.99 (0.01)	0.05 (0.03)	0.34 (0.23)	0.94 (0.02)	0.98 (0.00)
peekaboo	0.90	0.25	0.27 (0.12)	0.91 (0.10)	0.75 (0.20)	0.06 (0.03)	0.18 (0.23)	0.87 (0.15)	0.95 (0.04)
dance	0.98	0.17	0.31 (0.06)	0.97 (0.02)	0.99 (0.00)	0.07 (0.04)	0.34 (0.24)	0.86 (0.16)	0.99 (0.00)
kneel_left	0.99	0.97	0.10 (0.07)	0.79 (0.12)	0.94 (0.05)	0.04 (0.00)	0.23 (0.30)	0.34 (0.19)	0.95 (0.02)
crouch_high	0.99	0.89	0.39 (0.05)	0.98 (0.00)	0.99 (0.00)	0.46 (0.08)	0.76 (0.18)	0.85 (0.12)	0.99 (0.00)
crouch_medium	0.99	0.95	0.47 (0.06)	0.99 (0.00)	1.00 (0.00)	0.38 (0.07)	0.81 (0.12)	0.86 (0.12)	0.99 (0.00)
crouch_low	0.99	0.63	0.08 (0.03)	0.73 (0.20)	0.85 (0.09)	0.07 (0.03)	0.16 (0.15)	0.47 (0.11)	0.85 (0.06)
squat_pre_jump	0.98	0.97	0.03 (0.01)	0.17 (0.13)	0.22 (0.20)	0.02 (0.01)	0.03 (0.05)	0.31 (0.20)	0.56 (0.04)
squat_hands_on_ground	0.98	0.77	0.21 (0.07)	0.72 (0.08)	0.93 (0.04)	0.02 (0.01)	0.21 (0.25)	0.30 (0.19)	0.74 (0.10)
side_high_kick	0.98	0.38	0.00 (0.00)	0.02 (0.02)	0.02 (0.01)	0.01 (0.01)	0.00 (0.00)	0.01 (0.01)	0.03 (0.03)
pre_front_kick	0.99	0.33	0.01 (0.00)	0.54 (0.22)	0.75 (0.09)	0.06 (0.03)	0.08 (0.06)	0.20 (0.16)	0.69 (0.21)
arabesque_hold_foot	0.85	0.17	0.03 (0.03)	0.11 (0.06)	0.30 (0.13)	0.01 (0.00)	0.02 (0.04)	0.02 (0.02)	0.11 (0.05)
hold_right_foot	0.99	0.17	0.04 (0.03)	0.28 (0.11)	0.56 (0.20)	0.03 (0.01)	0.01 (0.03)	0.10 (0.07)	0.64 (0.12)
hold_left_foot	0.99	0.44	0.04 (0.01)	0.51 (0.09)	0.76 (0.08)	0.20 (0.02)	0.29 (0.10)	0.17 (0.17)	0.72 (0.07)
bend_on_left_leg	0.98	0.69	0.01 (0.00)	0.09 (0.10)	0.40 (0.08)	0.02 (0.01)	0.04 (0.08)	0.09 (0.08)	0.57 (0.12)
lie_front	0.97	0.87	0.16 (0.16)	0.67 (0.11)	0.52 (0.08)	0.01 (0.00)	0.05 (0.04)	0.46 (0.14)	0.61 (0.10)
crawl_backward	0.98	0.92	0.13 (0.13)	0.36 (0.19)	0.37 (0.15)	0.00 (0.00)	0.01 (0.02)	0.03 (0.04)	0.13 (0.13)
lie_back_knee_bent	0.97	0.79	0.07 (0.07)	0.15 (0.13)	0.03 (0.03)	0.02 (0.01)	0.00 (0.00)	0.09 (0.14)	0.04 (0.08)
lie_side	0.97	0.89	0.20 (0.08)	0.36 (0.18)	0.19 (0.11)	0.02 (0.01)	0.00 (0.00)	0.08 (0.08)	0.36 (0.04)
crunch	0.98	0.44	0.00 (0.00)	0.00 (0.00)	0.04 (0.07)	0.01 (0.00)	0.00 (0.00)	0.00 (0.00)	0.00 (0.00)
lie_back	0.97	0.86	0.24 (0.14)	0.59 (0.28)	0.28 (0.18)	0.05 (0.01)	0.19 (0.19)	0.54 (0.23)	0.43 (0.22)
sit_side	0.98	0.93	0.03 (0.01)	0.18 (0.10)	0.35 (0.17)	0.00 (0.00)	0.01 (0.03)	0.05 (0.10)	0.28 (0.17)
sit_hand_on_legs	0.98	0.97	0.29 (0.14)	0.42 (0.10)	0.53 (0.06)	0.00 (0.00)	0.04 (0.08)	0.04 (0.03)	0.59 (0.13)
sit_hand_behind	0.99	0.93	0.23 (0.16)	0.66 (0.08)	0.60 (0.11)	0.02 (0.02)	0.03 (0.06)	0.15 (0.16)	0.60 (0.11)
knees_and_hands	0.98	0.92	0.38 (0.15)	0.71 (0.08)	0.83 (0.06)	0.03 (0.01)	0.18 (0.15)	0.46 (0.13)	0.73 (0.11)
bridge_front	0.98	0.82	0.12 (0.10)	0.50 (0.41)	0.74 (0.07)	0.05 (0.02)	0.23 (0.11)	0.44 (0.02)	0.67 (0.19)
push_up	0.97	0.89	0.04 (0.05)	0.35 (0.24)	0.46 (0.11)	0.01 (0.01)	0.01 (0.01)	0.02 (0.02)	0.11 (0.05)
handstand	0.84	0.00	0.00 (0.00)	0.01 (0.01)	0.00 (0.00)	0.02 (0.01)	0.00 (0.00)	0.00 (0.00)	0.05 (0.04)
handstand_right_leg_bent	0.96	0.05	0.00 (0.00)	0.00 (0.00)	0.00 (0.00)	0.01 (0.01)	0.00 (0.00)	0.00 (0.00)	0.02 (0.02)
Average	0.96	0.47	0.20	0.61	0.67	0.07	0.18	0.46	0.68
Median	0.98	0.31	0.17	0.70	0.77	0.04	0.11	0.46	0.74

Table 20: Humanoid Environment. Proximity over goal poses for goal-reaching evaluation.

We further mention results for two baselines that performed poorly in our tests. First, similarly to DIFFUSER, we tested H-GAP (Jiang et al., 2024) trained on the union of the AMASS-ACT dataset and FB-CPR replay buffer. Despite conducting extensive hyper-parameter search based on the default settings reported in Jiang et al. (2024) and scaling the model size, we encountered challenges in training an accurate Prior Transformer and we were unable to achieve satisfactory performance on the downstream tasks. We obtained an average normalized performance of 0.05 in reward optimization on a subset of stand and locomotion tasks. We did not test the other modalities. Second, we also tested planning with a learned model. Specifically, we trained an MLP network on the same offline dataset to predict the next state given a state-action pair. We then used this learned model in MPPI and evaluated its performance on the same subset of tasks as H-GAP. The results showed that MPPI with the learned model achieved a low normalized return of 0.03. We believe that this is due to MPPI's action sampling leading to out-of-distribution action plans, which can cause the model to struggle with distribution shift and compounding errors when chaining predictions. Some form of pessimistic planning is necessary when using a learned model to avoid deviating too much from the observed samples. Unlike MPPI, Diffuser achieves this by sampling action plans that are likely under the offline data distribution. For more details on the results of H-GAP and MPPI with the learned model, see Table 23.

Goal	TD3	MPPI	Diffuser	Goal-GAIL	Goal-TD3	PHC	CALM	ASE	FB-CPR
Success									
t_pose	1.00	0.75	0.80 (0.07)	1.00 (0.00)	1.00 (0.00)	0.09 (0.04)	0.21 (0.40)	0.98 (0.04)	1.00 (0.00)
t_pose_lower_arms	1.00	0.75	0.78 (0.13)	1.00 (0.00)	1.00 (0.00)	0.35 (0.13)	0.49 (0.43)	0.90 (0.19)	1.00 (0.00)
t_pose_bow_head	1.00	0.90	0.77 (0.15)	1.00 (0.00)	1.00 (0.00)	0.06 (0.06)	0.29 (0.39)	0.37 (0.32)	1.00 (0.00)
u_stretch_y_right	1.00	0.65	0.01 (0.02)	0.36 (0.28)	0.80 (0.27)	0.01 (0.02)	0.00 (0.00)	0.04 (0.05)	0.53 (0.32)
u_stretch_y_left	1.00	0.65	0.00 (0.00)	0.10 (0.17)	0.16 (0.31)	0.00 (0.00)	0.00 (0.00)	0.00 (0.00)	0.30 (0.20)
u_stretch_z_right	1.00	0.80	0.00 (0.00)	0.23 (0.30)	0.38 (0.44)	0.04 (0.01)	0.00 (0.00)	0.01 (0.02)	0.55 (0.24)
u_stretch_z_left	1.00	0.70	0.02 (0.02)	0.82 (0.36)	0.99 (0.01)	0.02 (0.02)	0.00 (0.00)	0.06 (0.09)	0.96 (0.07)
u_stretch_x_back	1.00	0.25	0.00 (0.00)	0.26 (0.36)	0.40 (0.42)	0.04 (0.03)	0.00 (0.00)	0.39 (0.45)	0.87 (0.08)
u_stretch_x_front_part	1.00	1.00	0.59 (0.18)	0.93 (0.11)	1.00 (0.00)	0.05 (0.03)	0.05 (0.09)	0.36 (0.24)	1.00 (0.00)
u_stretch_x_front_full	1.00	1.00	0.02 (0.02)	0.34 (0.32)	0.64 (0.36)	0.00 (0.00)	0.00 (0.00)	0.21 (0.18)	0.82 (0.30)
crossed_arms	1.00	0.60	0.04 (0.05)	0.40 (0.29)	0.56 (0.32)	0.01 (0.02)	0.01 (0.02)	0.06 (0.07)	0.63 (0.22)
scratching_head	1.00	0.80	0.30 (0.25)	1.00 (0.00)	0.99 (0.02)	0.04 (0.02)	0.01 (0.02)	0.96 (0.04)	1.00 (0.00)
right_hand_wave	1.00	0.70	0.37 (0.16)	0.99 (0.02)	1.00 (0.00)	0.02 (0.02)	0.06 (0.12)	0.99 (0.02)	1.00 (0.00)
x_strech	1.00	0.60	0.12 (0.09)	0.54 (0.40)	0.87 (0.15)	0.03 (0.03)	0.00 (0.00)	0.45 (0.37)	0.80 (0.23)
i_strecth	0.67	0.00	0.00 (0.00)	0.00 (0.00)	0.30 (0.40)	0.00 (0.00)	0.00 (0.00)	0.00 (0.00)	0.25 (0.38)
arms_stretch	1.00	0.60	0.04 (0.05)	0.00 (0.00)	0.21 (0.25)	0.04 (0.03)	0.00 (0.00)	0.00 (0.00)	0.00 (0.00)
drinking_from_bottle	1.00	0.70	0.01 (0.02)	0.00 (0.00)	0.40 (0.49)	0.02 (0.02)	0.00 (0.00)	0.00 (0.00)	0.86 (0.28)
arm_on_chest	1.00	0.80	0.02 (0.04)	0.88 (0.16)	1.00 (0.00)	0.00 (0.00)	0.01 (0.01)	0.81 (0.21)	0.99 (0.02)
pre_throw	0.00	0.00	0.00 (0.00)	0.00 (0.00)	0.00 (0.00)	0.06 (0.04)	0.00 (0.00)	0.00 (0.00)	0.00 (0.00)
egyptian	1.00	0.65	0.03 (0.02)	0.43 (0.36)	0.80 (0.30)	0.02 (0.02)	0.00 (0.00)	0.30 (0.35)	1.00 (0.00)
zombie	1.00	0.75	0.35 (0.16)	0.97 (0.06)	1.00 (0.00)	0.04 (0.03)	0.00 (0.00)	0.74 (0.26)	1.00 (0.00)
stand_martial_arts	1.00	0.90	0.41 (0.18)	1.00 (0.00)	1.00 (0.00)	0.04 (0.04)	0.00 (0.00)	0.82 (0.17)	1.00 (0.00)
peekaboo	0.66	0.60	0.00 (0.00)	0.76 (0.35)	0.51 (0.39)	0.04 (0.05)	0.00 (0.00)	0.58 (0.35)	0.89 (0.22)
dance	1.00	0.70	0.16 (0.08)	0.94 (0.12)	1.00 (0.00)	0.00 (0.00)	0.02 (0.03)	0.67 (0.39)	1.00 (0.00)
kneel_left	1.00	1.00	0.10 (0.12)	0.31 (0.30)	1.00 (0.00)	0.00 (0.00)	0.00 (0.00)	0.00 (0.00)	0.90 (0.10)
crouch_high	1.00	1.00	0.75 (0.10)	1.00 (0.00)	1.00 (0.00)	0.55 (0.11)	0.37 (0.41)	0.67 (0.28)	1.00 (0.00)
crouch_medium	1.00	1.00	0.97 (0.04)	1.00 (0.00)	1.00 (0.00)	0.42 (0.14)	0.44 (0.38)	0.53 (0.33)	1.00 (0.00)
crouch_low	1.00	0.95	0.00 (0.00)	0.57 (0.38)	0.45 (0.45)	0.02 (0.01)	0.00 (0.00)	0.01 (0.03)	0.72 (0.27)
squat_pre_jump	1.00	1.00	0.02 (0.02)	0.01 (0.02)	0.02 (0.03)	0.01 (0.02)	0.00 (0.00)	0.09 (0.16)	0.25 (0.25)
squat_hands_on_ground	1.00	0.40	0.00 (0.00)	0.00 (0.00)	0.64 (0.45)	0.00 (0.00)	0.00 (0.00)	0.00 (0.00)	0.10 (0.20)
side_high_kick	1.00	0.65	0.00 (0.00)	0.00 (0.00)	0.00 (0.00)	0.00 (0.00)	0.00 (0.00)	0.00 (0.00)	0.00 (0.00)
pre_front_kick	1.00	0.70	0.01 (0.02)	0.23 (0.39)	0.40 (0.49)	0.04 (0.03)	0.00 (0.00)	0.02 (0.03)	0.57 (0.36)
arabesque_hold_foot	0.66	0.60	0.01 (0.02)	0.00 (0.00)	0.00 (0.00)	0.01 (0.01)	0.00 (0.00)	0.00 (0.00)	0.00 (0.00)
hold_right_foot	1.00	0.70	0.00 (0.00)	0.00 (0.00)	0.01 (0.01)	0.01 (0.01)	0.00 (0.00)	0.11 (0.21)	0.44 (0.42)
hold_left_foot	1.00	0.70	0.00 (0.00)	0.20 (0.26)	0.25 (0.36)	0.00 (0.00)	0.00 (0.00)	0.00 (0.00)	0.25 (0.38)
bend_on_left_leg	1.00	1.00	0.00 (0.00)	0.00 (0.00)	0.00 (0.00)	0.05 (0.04)	0.00 (0.00)	0.00 (0.00)	0.00 (0.00)
lie_front	1.00	0.90	0.10 (0.20)	0.01 (0.02)	0.00 (0.00)	0.00 (0.00)	0.00 (0.00)	0.01 (0.02)	0.00 (0.00)
crawl_backward	1.00	0.95	0.00 (0.00)	0.00 (0.00)	0.00 (0.00)	0.00 (0.00)	0.00 (0.00)	0.00 (0.00)	0.00 (0.00)
lie_back_knee_bent	1.00	0.85	0.00 (0.00)	0.00 (0.00)	0.00 (0.00)	0.02 (0.03)	0.00 (0.00)	0.00 (0.00)	0.00 (0.00)
lie_side	1.00	0.90	0.00 (0.00)	0.00 (0.00)	0.00 (0.00)	0.02 (0.02)	0.00 (0.00)	0.00 (0.00)	0.00 (0.00)
crunch	1.00	0.55	0.00 (0.00)	0.00 (0.00)	0.00 (0.00)	0.00 (0.00)	0.00 (0.00)	0.00 (0.00)	0.00 (0.00)
lie_back	1.00	0.90	0.02 (0.04)	0.31 (0.39)	0.00 (0.00)	0.08 (0.03)	0.00 (0.00)	0.13 (0.27)	0.00 (0.00)
sit_side	1.00	0.95	0.00 (0.00)	0.00 (0.00)	0.00 (0.00)	0.00 (0.00)	0.00 (0.00)	0.00 (0.00)	0.00 (0.00)
sit_hand_on_legs	1.00	1.00	0.00 (0.00)	0.00 (0.00)	0.00 (0.00)	0.00 (0.00)	0.00 (0.00)	0.00 (0.00)	0.00 (0.00)
sit_hand_behind	1.00	0.95	0.01 (0.02)	0.00 (0.00)	0.00 (0.00)	0.02 (0.05)	0.00 (0.00)	0.00 (0.00)	0.00 (0.00)
knees_and_hands	1.00	0.95	0.06 (0.07)	0.00 (0.00)	0.18 (0.27)	0.04 (0.02)	0.00 (0.00)	0.00 (0.00)	0.01 (0.02)
bridge_front	1.00	0.85	0.00 (0.00)	0.06 (0.08)	0.00 (0.00)	0.08 (0.04)	0.00 (0.00)	0.00 (0.00)	0.17 (0.31)
push_up	1.00	0.95	0.00 (0.00)	0.00 (0.00)	0.00 (0.00)	0.00 (0.00)	0.00 (0.00)	0.00 (0.00)	0.00 (0.00)
handstand	0.67	0.00	0.00 (0.00)	0.00 (0.00)	0.00 (0.00)	0.01 (0.02)	0.00 (0.00)	0.00 (0.00)	0.00 (0.00)
handstand_right_leg_bent	1.00	0.10	0.00 (0.00)	0.00 (0.00)	0.00 (0.00)	0.01 (0.02)	0.00 (0.00)	0.00 (0.00)	0.00 (0.00)
Average	0.95	0.73	0.14	0.35	0.44	0.05	0.04	0.22	0.48
Median	1.00	0.75	0.01	0.22	0.39	0.02	0.00	0.01	0.48

Table 21: Humanoid Environment. Success rate over different goal poses in the goal-reaching evaluation.

Task	H-GAP		MPPI with learned world model	
	Normalized		Normalized	
move-ego-0-0	0.123	33.78	0.069	19.05
move-ego-0-2	0.036	9.16	0.040	10.24
move-ego-0-4	0.028	6.82	0.038	9.21
move-ego--90-2	0.041	10.56	0.032	8.26
move-ego--90-4	0.032	7.97	0.026	6.41
move-ego-90-2	0.049	12.46	0.036	9.19
move-ego-90-4	0.039	9.54	0.024	6.00
move-ego-180-2	0.053	13.68	0.024	6.26
move-ego-180-4	0.042	10.41	0.019	4.76
Average	0.05	12.71	0.03	8.82
Median	0.04	10.41	0.03	8.26

Table 23: Humanoid Environment. Average Return of H-GAP and MPPI with learned world model on a subset of stand and locomotion tasks.

Dataset	Goal-GAIL (1motion)		PHC (1motion)		ASE		CALM		Goal-GAIL		Goal-TD3		PHC		FB-CPR	
	train	test	train	test	train	test	train	test	train	test	train	test	train	test	train	test
								EMD								
ACCAD	1.18 (0.37)	1.22 (0.35)	1.13 (1.44)	0.87 (0.27)	2.34 (0.03)	2.53 (0.03)	2.05 (0.07)	2.25 (0.04)	2.02 (0.04)	2.22 (0.03)	1.65 (0.09)	1.77 (0.09)	1.95 (0.06)	2.08 (0.04)	1.67 (0.01)	1.84 (0.03)
BMLhandball	1.55 (0.14)	1.55 (0.18)	1.44 (1.83)	0.96 (0.14)	2.63 (0.08)	2.66 (0.07)	2.16 (0.05)	2.24 (0.06)	2.14 (0.03)	2.19 (0.06)	1.73 (0.08)	1.77 (0.13)	2.06 (0.09)	2.07 (0.11)	1.75 (0.03)	1.76 (0.05)
BMLmovi	1.06 (0.26)	1.08 (0.29)	1.13 (1.54)	1.15 (1.47)	2.00 (0.05)	1.96 (0.02)	1.71 (0.04)	1.74 (0.04)	1.67 (0.01)	1.69 (0.02)	1.42 (0.08)	1.44 (0.10)	1.76 (0.07)	1.74 (0.09)	1.37 (0.01)	1.38 (0.02)
BioMotionLab	1.24 (0.25)	1.25 (0.36)	1.23 (1.56)	1.26 (1.63)	2.10 (0.02)	2.06 (0.02)	1.78 (0.02)	1.76 (0.02)	1.86 (0.02)	1.86 (0.04)	1.48 (0.07)	1.47 (0.08)	1.70 (0.06)	1.67 (0.06)	1.48 (0.01)	1.47 (0.01)
CMU	1.17 (0.35)	1.18 (0.38)	1.15 (1.64)	1.06 (1.27)	2.23 (0.02)	2.23 (0.02)	1.86 (0.04)	1.90 (0.03)	1.87 (0.02)	1.92 (0.02)	1.51 (0.08)	1.54 (0.09)	1.78 (0.07)	1.79 (0.06)	1.52 (0.01)	1.54 (0.01)
DFaust	0.96 (0.26)	1.15 (0.33)	1.71 (2.87)	0.83 (0.26)	2.05 (0.06)	2.28 (0.14)	1.74 (0.05)	1.86 (0.06)	1.72 (0.03)	1.96 (0.03)	1.41 (0.07)	1.51 (0.08)	1.71 (0.06)	1.74 (0.07)	1.43 (0.01)	1.57 (0.02)
DanceDB	1.48 (0.22)	1.63 (0.07)	2.11 (2.35)	1.54 (0.04)	2.70 (0.04)	3.05 (0.06)	2.39 (0.02)	2.76 (0.09)	2.38 (0.03)	2.78 (0.06)	1.96 (0.11)	2.16 (0.11)	2.19 (0.06)	2.42 (0.08)	1.94 (0.02)	2.08 (0.03)
EKUT	0.79 (0.17)	0.89 (0.22)	0.95 (1.63)	1.49 (2.42)	1.70 (0.03)	1.79 (0.03)	1.33 (0.03)	1.44 (0.02)	1.35 (0.02)	1.45 (0.03)	1.17 (0.07)	1.21 (0.06)	1.38 (0.07)	1.45 (0.05)	1.10 (0.00)	1.23 (0.04)
Eyes	1.32 (0.22)	1.32 (0.23)	1.35 (1.12)	1.44 (1.60)	2.14 (0.03)	2.15 (0.04)	1.90 (0.03)	1.92 (0.01)	1.83 (0.03)	1.85 (0.04)	1.62 (0.10)	1.63 (0.11)	1.85 (0.07)	1.81 (0.07)	1.57 (0.01)	1.55 (0.01)
HumanEva	1.02 (0.23)	1.11 (0.21)	0.88 (0.37)	1.06 (0.14)	2.05 (0.04)	2.16 (0.12)	1.74 (0.08)	1.87 (0.09)	1.82 (0.02)	1.86 (0.06)	1.42 (0.08)	1.52 (0.13)	1.64 (0.08)	1.74 (0.11)	1.41 (0.03)	1.59 (0.05)
KIT	0.89 (0.25)	0.89 (0.23)	1.00 (1.24)	0.98 (1.07)	1.71 (0.03)	1.68 (0.03)	1.35 (0.01)	1.37 (0.05)	1.36 (0.03)	1.36 (0.02)	1.17 (0.08)	1.17 (0.08)	1.42 (0.07)	1.40 (0.07)	1.12 (0.01)	1.13 (0.01)
MPI	1.28 (0.28)	1.26 (0.27)	1.23 (1.19)	1.57 (1.90)	2.42 (0.02)	2.42 (0.05)	2.08 (0.02)	2.14 (0.06)	2.04 (0.03)	2.10 (0.04)	1.68 (0.08)	1.72 (0.08)	1.96 (0.06)	2.00 (0.07)	1.68 (0.01)	1.76 (0.01)
SFU	1.20 (0.37)	1.43 (0.14)	0.95 (0.39)	1.29 (0.42)	2.63 (0.01)	3.24 (0.08)	2.25 (0.06)	2.68 (0.08)	2.26 (0.06)	2.69 (0.04)	1.77 (0.08)	2.11 (0.08)	2.04 (0.08)	2.41 (0.11)	1.88 (0.01)	2.27 (0.04)
TotalCapture	1.15 (0.14)	1.17 (0.16)	1.23 (1.21)	1.10 (0.28)	2.06 (0.06)	2.16 (0.05)	1.74 (0.02)	1.85 (0.02)	1.76 (0.03)	1.86 (0.03)	1.45 (0.09)	1.51 (0.12)	1.73 (0.11)	1.71 (0.10)	1.44 (0.03)	1.50 (0.02)
Transitions	1.15 (0.08)	1.17 (0.07)	2.12 (2.90)	2.65 (3.37)	2.31 (0.05)	2.40 (0.04)	1.99 (0.04)	2.04 (0.06)	2.01 (0.05)	2.05 (0.02)	1.53 (0.08)	1.59 (0.09)	1.77 (0.05)	1.83 (0.05)	1.54 (0.01)	1.59 (0.02)
								SUCCESS								
ACCAD	0.20 (0.40)	0.24 (0.43)	0.94 (0.23)	1.00 (0.00)	0.31 (0.02)	0.25 (0.02)	0.58 (0.05)	0.46 (0.05)	0.24 (0.01)	0.22 (0.04)	0.80 (0.02)	0.66 (0.04)	0.68 (0.03)	0.56 (0.08)	0.67 (0.03)	0.49 (0.03)
BMLhandball	0.00 (0.00)	0.00 (0.00)	0.91 (0.28)	1.00 (0.00)	0.02 (0.03)	0.00 (0.00)	0.10 (0.07)	0.04 (0.08)	0.00 (0.00)	0.00 (0.00)	0.80 (0.12)	0.88 (0.16)	0.50 (0.04)	0.40 (0.18)	0.30 (0.13)	0.24 (0.15)
BMLmovi	0.22 (0.41)	0.19 (0.39)	0.96 (0.20)	0.96 (0.20)	0.51 (0.01)	0.57 (0.02)	0.78 (0.02)	0.82 (0.03)	0.28 (0.02)	0.25 (0.02)	0.97 (0.00)	0.96 (0.01)	0.87 (0.01)	0.87 (0.03)	0.88 (0.02)	0.89 (0.02)
BioMotionLab	0.04 (0.18)	0.06 (0.23)	0.91 (0.28)	0.92 (0.27)	0.12 (0.02)	0.14 (0.03)	0.53 (0.06)	0.60 (0.04)	0.04 (0.00)	0.06 (0.01)	0.80 (0.03)	0.83 (0.02)	0.72 (0.02)	0.76 (0.01)	0.75 (0.02)	0.79 (0.02)
CMU	0.16 (0.37)	0.18 (0.39)	0.93 (0.26)	0.95 (0.23)	0.27 (0.02)	0.31 (0.02)	0.60 (0.02)	0.63 (0.04)	0.21 (0.01)	0.22 (0.02)	0.86 (0.01)	0.86 (0.01)	0.77 (0.01)	0.78 (0.03)	0.75 (0.01)	0.74 (0.02)
DFaust	0.47 (0.50)	0.33 (0.47)	0.89 (0.32)	1.00 (0.00)	0.48 (0.03)	0.47 (0.19)	0.74 (0.02)	0.71 (0.05)	0.48 (0.03)	0.53 (0.04)	0.95 (0.01)	1.00 (0.00)	0.86 (0.03)	0.96 (0.05)	0.86 (0.01)	0.84 (0.05)
DanceDB	0.04 (0.20)	0.00 (0.00)	0.61 (0.49)	1.00 (0.00)	0.04 (0.00)	0.00 (0.00)	0.10 (0.02)	0.00 (0.00)	0.05 (0.02)	0.00 (0.00)	0.62 (0.08)	0.70 (0.24)	0.30 (0.08)	0.40 (0.20)	0.27 (0.06)	0.50 (0.00)
EKUT	0.30 (0.46)	0.36 (0.48)	0.96 (0.20)	0.86 (0.35)	0.49 (0.05)	0.51 (0.11)	0.90 (0.02)	0.84 (0.03)	0.32 (0.02)	0.34 (0.08)	0.99 (0.01)	1.00 (0.00)	0.94 (0.02)	0.84 (0.05)	0.94 (0.04)	0.81 (0.07)
Eyes	0.00 (0.04)	0.00 (0.00)	0.91 (0.29)	0.85 (0.35)	0.24 (0.05)	0.29 (0.10)	0.65 (0.02)	0.66 (0.02)	0.11 (0.02)	0.18 (0.08)	0.92 (0.01)	0.91 (0.02)	0.76 (0.01)	0.83 (0.03)	0.79 (0.02)	0.79 (0.03)
HumanEva	0.20 (0.40)	0.00 (0.00)	0.96 (0.20)	1.00 (0.00)	0.43 (0.08)	0.27 (0.39)	0.83 (0.08)	0.87 (0.16)	0.17 (0.02)	0.00 (0.00)	0.99 (0.02)	1.00 (0.00)	0.94 (0.03)	0.93 (0.13)	0.92 (0.04)	0.93 (0.13)
KIT	0.41 (0.49)	0.44 (0.50)	0.97 (0.17)	0.97 (0.18)	0.56 (0.04)	0.59 (0.05)	0.91 (0.01)	0.92 (0.01)	0.40 (0.02)	0.40 (0.04)	0.98 (0.00)	0.98 (0.00)	0.95 (0.00)	0.94 (0.01)	0.95 (0.01)	0.96 (0.01)
MPI	0.07 (0.25)	0.07 (0.25)	0.86 (0.35)	0.83 (0.38)	0.12 (0.01)	0.14 (0.04)	0.35 (0.02)	0.39 (0.04)	0.09 (0.01)	0.13 (0.03)	0.71 (0.02)	0.74 (0.03)	0.53 (0.02)	0.50 (0.08)	0.51 (0.02)	0.56 (0.05)
SFU	0.00 (0.00)	0.00 (0.00)	0.97 (0.18)	0.67 (0.47)	0.05 (0.03)	0.00 (0.00)	0.38 (0.05)	0.07 (0.13)	0.00 (0.00)	0.00 (0.00)	0.73 (0.03)	0.60 (0.13)	0.55 (0.03)	0.47 (0.27)	0.50 (0.06)	0.13 (0.16)
TotalCapture	0.00 (0.00)	0.00 (0.00)	0.73 (0.45)	0.75 (0.43)	0.00 (0.00)	0.00 (0.00)	0.16 (0.04)	0.20 (0.19)	0.00 (0.00)	0.00 (0.00)	0.79 (0.03)	0.70 (0.10)	0.46 (0.04)	0.40 (0.12)	0.55 (0.07)	0.35 (0.12)
Transitions	0.00 (0.00)	0.00 (0.00)	0.84 (0.36)	0.82 (0.39)	0.04 (0.02)	0.04 (0.04)	0.33 (0.03)	0.36 (0.16)	0.00 (0.00)	0.00 (0.00)	0.81 (0.03)	0.78 (0.09)	0.58 (0.04)	0.40 (0.04)	0.62 (0.04)	0.65 (0.11)

Table 22: Humanoid Environment. Average performance over each sub-set of the AMASS dataset used in the tracking evaluation.

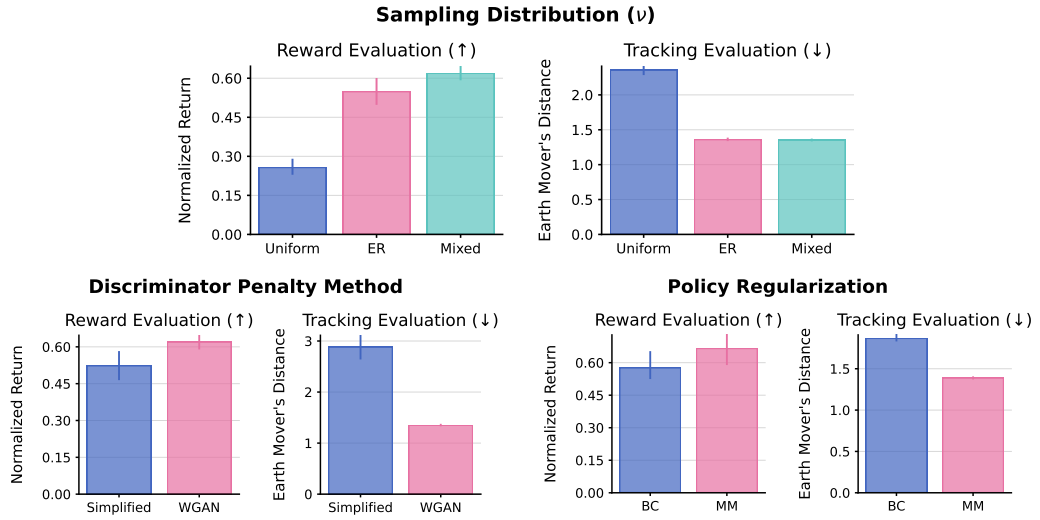

Figure 6: **Additional FB-CPR Ablations**. (TOP) Ablating the sampling distribution ν. (BOTTOM LEFT) Ablating the discriminator gradient penalty method. (BOTTOM RIGHT) Ablating the policy regularization method between behavior cloning and moment matching when given action labels. All ablations are averaged over 5 seeds with ranges denoting bootstrapped 95% confidence intervals.

D.2 ABLATIONS

In this section we detail additional ablations into the components of FB-CPR.

Which gradient penalty better stabilizes the discriminator in FB-CPR? Algorithms requiring bi-level optimization through a min-max game are known to be unstable and typically require strong forms of regularization (e.g., Gulrajani et al., 2017; Miyato et al., 2018). Prior works like CALM (Tessler et al., 2023), ASE (Peng et al., 2022), and AMP (Peng et al., 2021) employ what we will refer to as the simplified gradient penalty on the discriminator to stabilize training:

$$\lambda_{\text{GP}} \, \mathbb{E}_{\tau \sim \mathcal{M}, s \sim \tau} \left[\left\| \nabla_{x,z} D(x,z) \big|_{(x,z)=(s,\text{ER}_{\text{FB}}(\tau))} \right\|_2^2 \right] .$$

Alternatively, other works in Inverse Reinforcement Learning (e.g., Swamy et al., 2021; 2022; Ren et al., 2024) have had success employing the Wasserstein gradient penalty of Gulrajani et al. (2017):

$$\lambda_{\text{GP}} \, \mathbb{E}_{\substack{z \sim \nu, s \sim \rho^{\pi_z}, \tau \sim \mathcal{M}, s' \sim \tau \\ t \sim \text{Unif}(0,1)}} \left[\left(\left\| \nabla_{x,z'} D(x,z') \big|_{x=ts+(1-t)s', z'=tz+(1-t)\text{ER}_{\text{FB}}(\tau)} \right\|_2^2 - 1 \right)^2 \right] .$$

We want to verify which of these two methods better stabilizes training of the discriminator in FB-CPR. To this end, we perform a sweep over $\lambda_{\text{GP}} \in \{0, 1, 5, 10, 15\}$ for both the aforementioned gradient penalties and further averaged over 5 independent seeds. We found that without a gradient penalty, i.e., $\lambda_{\text{GP}} = 0$ training was unstable and lead to subpar performance. For both gradient penalty methods we found that $\lambda_{\text{GP}} = 10$ performed best and as seen in Figure 6 (Left) the Wasserstein gradient penalty ultimately performed best.

What is gained or lost when ablating the mixture components of ν? By modelling ν as a mixture distribution we hypothesize that a tradeoff is introduced depending on the proportion of each component. One of the most natural questions to ask is whether there is anything to be gained by only sampling $\tau \sim \mathcal{M}$ and encoding with $z = \text{ER}_{\text{FB}}(\tau)$. If indeed this component is enabling FB-CPR to accurately reproduce trajectories in $\mathcal{M}$ we may see an improvement in tracking performance perhaps at the cost of diversity impacting reward-optimization performance. On the other hand, increased diversity by only sampling uniformly from the hypersphere may improve reward evaluation performance for reward functions that are not well aligned with any motion in $\mathcal{M}$. We test these hypotheses by training FB-CPR on 1) only ER_{FB} encoded subtrajectories from $\mathcal{M}$, 2) only uniformly sampled embeddings from the hypersphere, and 3) the default mixture weights reported in Table 9.

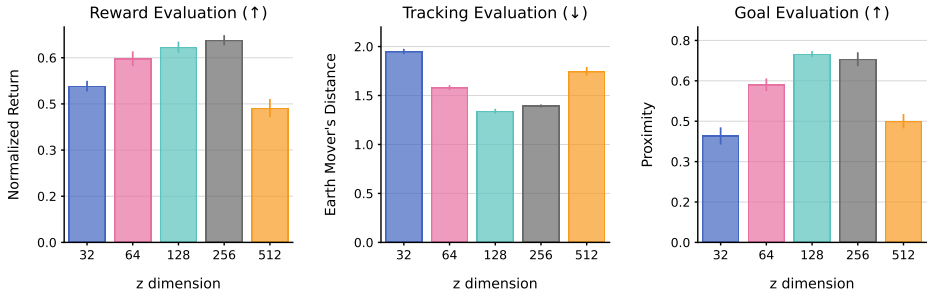

Figure 7: Performance of FB-CPR in the same setting as Table 1 but with different dimensions of the latent space. Results are averaged over 5 seeds with ranges denoting bootstrapped 95% confidence intervals.

Figure 6 confirms that mixed sampling strikes a nice balance between these trade-offs. Indeed, only using ER_{FB} encoded subtrajectories from $\mathcal{M}$ harms reward evaluation performance but surprisingly does not improve on tracking performance. Perhaps unsurprisingly sampling only uniformly from the hypersphere is a weak prior and does not fully leverage the motion dataset resulting in substantially degraded performance across the board.

Is CPR regularization better than BC if given action labels? In our work we adopt the moment matching framework to perform policy regularization (Swamy et al., 2021). This framework can be naturally extended to the action-free setting whereas most imitation learning methods require action labels. If we are provided a dataset with action-labels should we continue to adopt the moment matching framework with the conditional discriminator presented herein? To answer this question we curate our own action labelled dataset by relabelling the AMASS dataset with a pre-trained FB-CPR policy. Given this dataset we directly compare the conditional discriminator (Eq. 11) with a modified form of the FB-CPR actor loss that instead performs regularization via behavior cloning,

$$\mathscr{L}_{\text{FB-CPR-BC}}(\pi) = -\mathbb{E}_{z\sim\nu, s\sim\mathcal{D}_{\text{online}}, a\sim\pi_z(\cdot|s)}\left[F(s,a,z)^\top z\right] - \alpha_{\text{BC}}\,\mathbb{E}_{z\sim\nu,(s,a)\sim\mathcal{M}}\left[\log \pi_z(a\,|\,s)\right]. \tag{14}$$

We perform a sweep over the strength of the behavior cloning regularization term $\alpha_{\text{BC}} \in \{0.1, 0.2, 0.4, 0.5\}$ and further average these results over 5 seeds. Furthermore, we re-train FB-CPR on the relabelled dataset and also perform a sweep over the CPR regularization coefficient $\alpha_{\text{CPR}} \in \{0.01, 0.03, 0.05\}$. Ultimately, $\alpha_{\text{BC}} = 0.2$ and $\alpha_{\text{CPR}} = 0.01$ performed best with results on reward and tracking evaluation presented in the bottom right panel of Figure 6. We can see that even when given action-labels our action-free discriminator outperforms the BC regularization in both reward and tracking evaluation. This highlights the positive interaction of the conditional discriminator with FB to provide a robust method capable of leveraging action-free demonstrations and notably outperforming a strong action-dependent baseline.

How does the latent space dimension affect the performance of FB-CPR? Choosing the dimension d of the latent space built by FB-CPR involves an important trade-off: on the one hand, we would like d to be large so as to have an accurate estimation of the successor measure of the learned policies, which in turns would yield accurate evaluation of the Q function for many rewards and accurate trajectory encoding through ER_{FB} (cf. Section 2). Moreover, as we recall that task inference involves mapping functions of the state space to latent vectors (e.g., by $z = \mathbb{E}_\rho[B(s)R(s)]$ for a reward function R and $z = B(g)$ for a goal g), a large dimension d is desirable to make sure as many tasks/behaviors as possible are learned reliably. On the other hand, it is desirable to use a small d to learn a set of behaviors which is as succinct as possible, which would be more efficient to train and to query at inference time, as argued in several works on unsupervised skill discovery (e.g., Eysenbach et al., 2019; Peng et al., 2022; Tessler et al., 2023; Park et al., 2024c).

We demonstrate this trade-off empirically in Figure 7, where we repeat the same experiment as in Table 1 for different values of d. We observe a nearly monotonic performance improvement up to dimensions 128 and 256, were performance saturate (with the latter being slightly better on reward tasks and the former being slightly better on tracking and goal reaching). As expected, we qualitatively observe that $d = 32$ and $d = 64$ limit too much the capacity of the latent space, as

Algorithm	Reward (↑)	Goal		Tracking - EMD (↓)		Tracking - Success (↑)	
		Proximity (↑)	Success (↑)	Train	Test	Train	Test
FB	24.47 (1.88)	0 (0)	0 (0)	8.09 (0.21)	8.19 (0.14)	0 (0)	0 (0)
$\text{SCORE}_{\text{norm}}$	0.10	0	0	0.13	0.13	0	0

Table 24: Performance of the FB algorithm (Touati & Ollivier, 2021) in the same setting as Table 1, where $\text{SCORE}_{\text{norm}}$ are normalized w.r.t. the performance of the best baseline in such table.

several of the hardest tasks (e.g., cartwheels or backflips) or the hardest goals (e.g., yoga poses) are not learned at all. On the other hand, we observe a collapse in the learned representation B when moving to very large d, which results in the performance drop at $d = 512$. This is mostly due to the fact that several parameters used for the "default" configuration reported in Table 1, and kept constant for all runs in this ablation, are not suitable for training with such large d. For instance, the network architecture of F is too small to predict successor features over 512 dimensions, and should be scaled proportionally to d. Similarly, a batch size of 1024 is likely not sufficient to accurately estimate the covariance matrix of B, which is required by the orthonormality and temporal difference losses (cf. Appendix B). Overall we found $d = 256$ to be a good trade-off between capacity, succinctness, and training stability, as FB+CPR with such dimension does not suffer the collapsing issue of $d = 512$ and learns more difficult behaviors than $d = 128$.

What is the importance of regularizing with unlabeled data? One may wonder whether regularizing the learned policies towards behaviors in the unlabeled dataset is really needed, or whether the plain FB algorithm of Touati & Ollivier (2021) (i.e., without the CPR part) trained online can already learn useful behaviors and solve many tasks. We report the results of such algorithm, trained with the same parameters used for FB-CPR, in Table 24. The algorithm achieves near-zero performance in all tasks, with only a small improvement over a randomly-initialized untrained policy in reward-based problems and tracking. Such small improvements is due to the fact that the algorithm learned how to roughly stand up, although without being able to maintain a standing position. The main reason behind this failure is that the FB algorithm has no explicit component to encourage discovery of diverse behaviors, except for the purely myopic exploration of TD3 (i.e., perturbing each action component with random noise) which obviously would fail in problems with large state and action spaces. On the other hand, the regularization in FB-CPR overcomes this problem by directing the agent towards learning behaviors in the unlabeled dataset.

D.3 Diversity, Dataset Coverage and Transitions

In this section we intend to further investigate the behaviors learned by FB-CPR beyond its performance in solving downstream tasks.

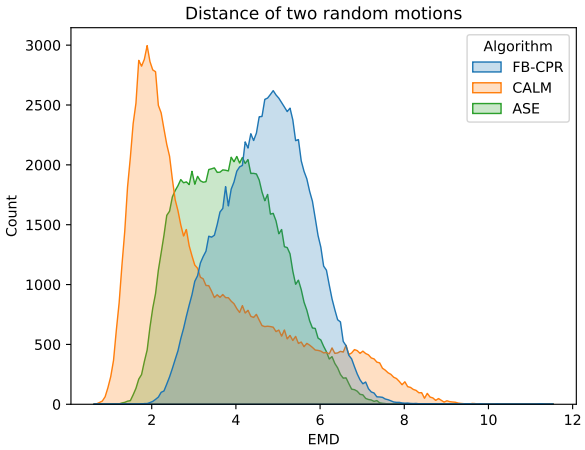

Figure 8: Distribution of EMD distance between trajectories generated by two randomly sampled policies π_z and $\pi_{z'}$.

Algorithm	Diversity
FB-CPR	4.70 (0.66)
CALM	3.36 (1.15)
ASE	3.91 (0.73)

Figure 9: Average diversity.

How diverse are the behaviors learned by FB-CPR? We want to evaluate the diversity of behaviors encoded in (π_z). Given two randomly drawn z and z', we run the two associated policies from the same initial state and we compute the EMD distance between the two resulting trajectories. We repeat this procedure for $n = 100,000$ times and compute

$$\text{Diversity} = \frac{1}{n} \sum_{i=1}^{n} \text{EMD}(\tau_i, \tau_i'). \tag{15}$$

The values of diversity are presented in Table 9. FB-CPR has the highest diversity. This result is confirmed by looking at the distribution of EMD values between τ_i and τ_i' in Fig. 8. FB-CPR has consistently the most diverse results. ASE distribution is shifted toward lower EMD values, which means that its behaviors are less diverse. CALM has mode around 2, which means that its representation has clusters of similar motions, but it is also the algorithm with the wider distribution with EMD distance above 7.0.

Are FB-CPR behaviors grounded in the behavior dataset $\mathcal{M}$? While this question is partially answered in the tracking evaluation, we would like to evaluate how much of the motion dataset is actually covered. In fact, a common failure mode of imitation regularization algorithms is the collapse of the learned policies towards accurately matching only a small portion of the demonstrated behaviors. In order to evaluate the level of coverage of the training motion dataset[13], we use a similar metric to the one proposed in (Peng et al., 2022), while accounting for the differences in the dataset: we have a much larger (8902 vs 187 motions) and less curated dataset, where the length of the motions has much larger variance.

We first sample a random z and generate a trajectory τ_z by executing the corresponding policy π_z for 200 steps starting from a T-pose configuration. Then, we calculate the EMD between τ_z and each motion in $\mathcal{M}$ and we select the motion m_z^* with the lowest EMD as the one best matching τ:

$$m_z^\star = \arg\min_{m^i \in \mathcal{M}} \text{EMD}(\tau_z, m^i). \tag{16}$$

We use EMD instead of time-aligned distance metrics to account for the fact that τ_z is executed from an initial state that could be fairly far from a motion in $\mathcal{M}$. We repeat this procedure 10,000

[13]Notice that here we are not trying to evaluate the generalization capabilities of the model, which is the focus of Sect. 4.

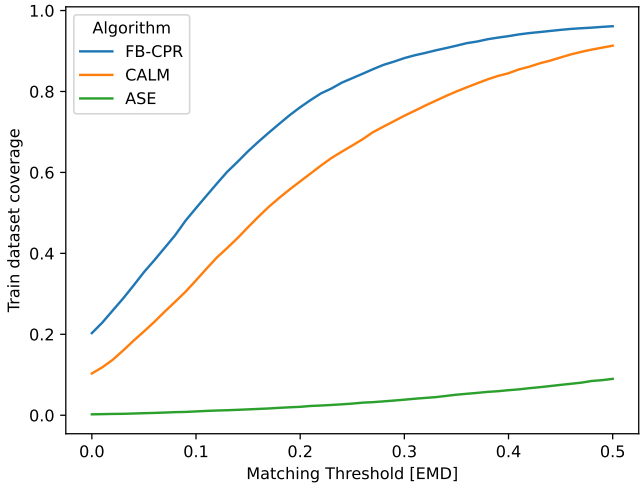

Figure 10: Relation between the threshold used to determine motion matching and the coverage of the train dataset by the randomly sampled policies.

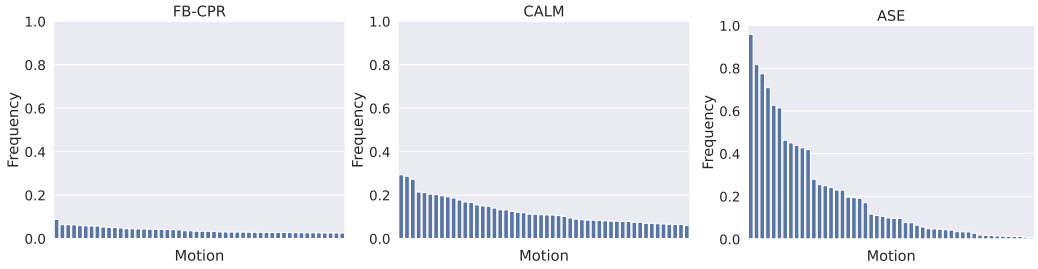

Figure 11: The frequency of the 50 most matched motions with multi-matching and $\text{MATCH}_{\text{THRESHOLD}} = 0.1$. Note that each algorithm matches to a different set of most frequent motions.

times and calculate the frequency of selecting each motion from the dataset. The dataset coverage is defined as the ratio of the number of the motions selected at least once to the number of motions in the training dataset.

As the train motion dataset is two orders of magnitude larger than the one used in (Peng et al., 2022), it is naturally harder to cover $\mathcal{M}$. To mitigate this issue, we propose a multiple-matching approach: a motion m is considered as matching, if its EMD to the closest motion from $\mathcal{M}$ is no larger than

$$\text{EMD}(\tau_z, m_z^\star) + \text{MATCH}_{\text{THRESHOLD}}. \tag{17}$$

By definition, greater values of the $\text{MATCH}_{\text{THRESHOLD}}$ results in greater coverage, as further motions are matched. Additionally, we observed by qualitative assessment, that when EMD is larger than 4.5, then the two trajectories are distinct enough to be considered as different behaviors. We therefore discard a matching if the EMD distance of m^* is above 4.5. The relation between $\text{MATCH}_{\text{THRESHOLD}}$ and the coverage is presented on Fig. 10. It can be observed that FB-CPR has consistently the highest coverage and it smoothly increases with the EMD threshold. CALM has lower coverage, but presents similar coverage pattern. In comparison, the coverage of ASE remains consistently low.

In order to calculate the matching of the top 50 most matched motions used in the further comparison, we used this multi-matching variant with $\text{MATCH}_{\text{THRESHOLD}} = 0.1$. In Fig. 11 we report the frequency of the top 50 most matched motions through this procedure for FB-CPR, CALM, and ASE. ASE has a very skewed distribution, meaning that many policies π_z tend to produce trajecto-

ries similar to a very small subset of motions, which suggests some form of coverage collapse. On the other extreme, FB-CPR has a very flat distribution, suggesting that it has a more even coverage of the motions dataset.

Is FB-CPR capable of motion stitching? Another possible failure mode is to learn policies that are accurately tracking individual motions but are unable to *stitch* together different motions, i.e., to smoothly transition from one behavior to another. In this case, we sample two embeddings z_S and z_D (respectively source and destination) and we use them to generate a trajectory τ which is composed of two disjoint sub-trajectories: the first 200 steps are generated with π_{z_S} and form sub-trajectory τ_S; after that, the second sub-trajectory τ_D is generated as the continuation of τ_S, while running policy π_{z_D}. After their generation, τ_S and τ_D are separately matched to the motions using Eq. 16, and a pair of source and destination motion is recorded. To make the process computationally feasible, we restrict our attention to the 50 most frequently matched motions selected in the previous evaluation with Eq. 16, and presented in Fig. 11. The procedure of generating transitioning trajectory is repeated 10,000 times. The *pairwise transition probability* is defined as the probability of matching a destination motion, conditioned on the source motion.

We also define pairwise transition coverage on a dataset as the ratio of the number of pairwise transitions with frequency larger than 0, to the number of all possible pairwise transitions. The pairwise transition probability and respective coverage is reported in Fig. 12. All algorithms have similar overall coverage.

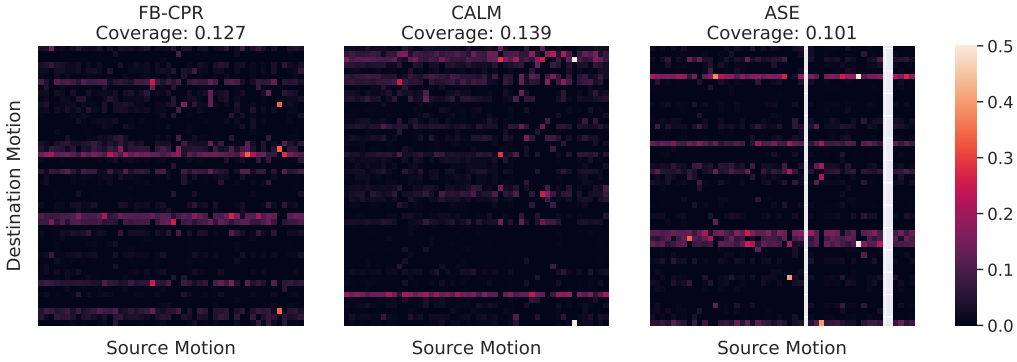

Figure 12: The probability of transitioning to destination motion conditioned on the source motion. For ASE, there was no random trajectory matched to source motion in three cases, and the corresponding columns of the heatmap are left empty.

Is FB-CPR learning more than imitating the motions in $\mathcal{M}$? While the good coverage highlighted above and the good tracking performance shown in Sect. 4 illustrate that FB-CPR successfully ground its behaviors on the training motions, a remaining question is whether it has learned *more* than what is strictly in $\mathcal{M}$. In order to investigate this aspect we analyze the distribution of the closest EMD distance $EMD(\tau_z, m_z^\star)$ w.r.t. random policies π_z. Fig. 13 highlights the most of the behaviors in (π_z) do not necessarily have a very tight connection with motions in the dataset. This is contrast with CALM and ASE, which have much smaller EMD distances, thus showing that they tend to use a larger part of the policy capacity to accurately reproduce motions rather than learning other behaviors.

D.4 Qualitative Evaluation

D.4.1 Human Evaluation

In most of reward-based tasks, the reward function is under-specified and different policies may achieve good performance while having different levels of *human-likeness*. In the worst case, the agent can learn to *hack* the reward function and maximize performance while performing very unnatural behaviors. On the other hand, in some cases, more human-like policies may not be "optimal". Similarly, in goal-based tasks, different policies may achieve similar success rate and proximity, while expressing very different behaviors.

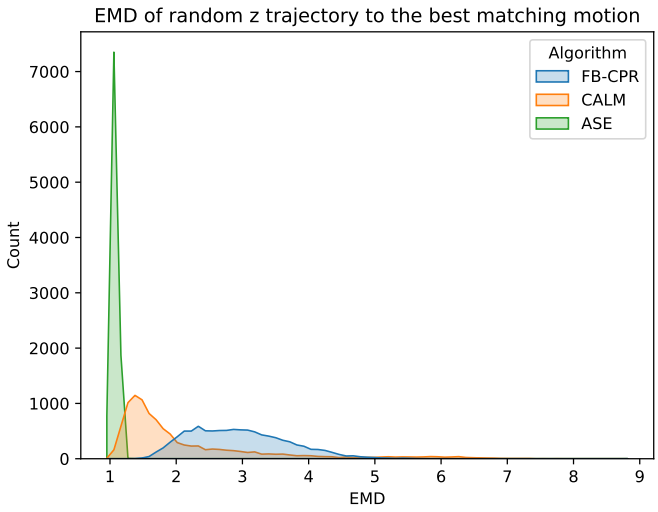

Figure 13: Histogram of the values of distance of trajectories generated from random z to the best matching motion from the training dataset.

In this section, we complement the quantitative analysis in Sect. 4 with a qualitative evaluation assessing whether FB-CPR is able to express more "human-like" behaviors, similar to what is done in (Hansen et al., 2024a). For this purpose, we enroll human raters to compare TD3 and FB-CPR policies over 45 reward and 50 goal tasks. Similar to the protocol in Sect. 4, for each single reward or goal task, we train three single-task TD3 agents with different random seeds. We then compare the performance of the TD3 agent with the best metric against the zero-shot policy of FB-CPR.

We generate videos of the two agents for each task. Each pair of matching videos is presented to 50 human raters, who fill the forms presented on Fig. 14. The position of the videos is randomized and the type of the agent on a video is not disclosed to the raters.

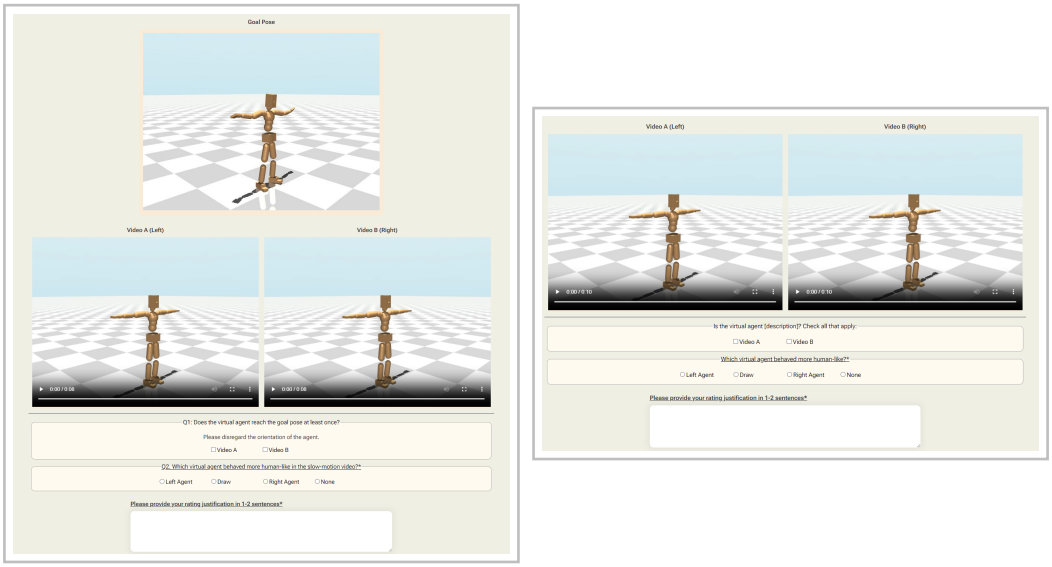

Figure 14: The online forms presented to the human raters to evaluate human-likeness for goal and reward tasks.

Task	TD3	ORACLE MPPI	Normalized	DIFFUSER	Normalized	ASE	Normalized	FB-CPR	Normalized
move-ego-0-2-raisearms-l-l	191.13	168.22	0.88	148.10 (0.47)	0.77 (0.00)	145.78 (7.59)	0.76 (0.04)	145.59 (4.38)	0.76 (0.02)
move-ego-0-2-raisearms-l-m	174.97	194.84	1.11	125.14 (2.16)	0.72 (0.01)	109.36 (30.34)	0.63 (0.17)	143.90 (7.09)	0.82 (0.04)
move-ego-0-2-raisearms-l-h	194.72	114.30	0.59	103.11 (1.22)	0.53 (0.01)	129.21 (31.41)	0.66 (0.16)	123.14 (15.90)	0.63 (0.08)
move-ego-0-2-raisearms-m-l	179.42	199.26	1.11	124.31 (4.28)	0.69 (0.02)	125.39 (5.79)	0.70 (0.03)	136.74 (2.40)	0.76 (0.01)
move-ego-0-2-raisearms-m-m	178.42	155.28	0.87	121.55 (3.97)	0.68 (0.02)	60.19 (24.89)	0.34 (0.14)	139.19 (18.63)	0.78 (0.10)
move-ego-0-2-raisearms-m-h	179.02	129.99	0.73	116.50 (3.88)	0.65 (0.02)	123.84 (6.10)	0.69 (0.03)	128.15 (0.86)	0.72 (0.00)
move-ego-0-2-raisearms-h-l	191.00	115.25	0.60	101.58 (2.72)	0.53 (0.01)	85.89 (7.09)	0.45 (0.04)	111.92 (1.20)	0.59 (0.01)
move-ego-0-2-raisearms-h-m	175.72	130.86	0.74	113.81 (3.34)	0.65 (0.02)	121.19 (4.20)	0.69 (0.02)	128.10 (0.78)	0.73 (0.00)
move-ego-0-2-raisearms-h-h	165.19	112.35	0.68	102.09 (3.56)	0.62 (0.02)	133.96 (14.35)	0.81 (0.09)	143.83 (14.21)	0.87 (0.09)
Average	181.06	146.70	0.81	117.36	0.65	114.98	0.64	133.40	0.74
Median	179.02	130.86	0.74	116.50	0.65	123.84	0.69	136.74	0.76

Table 25: Average return for each task in the composite reward evaluation. These tasks combine between locomotion and arm-raising behaviors

We gather two subjective metrics: *success*, and *human-likeness*. For success, we ask the rater to evaluate whether the presented behavior is actually achieving the desired objective. For goal-based task, the objective is directly illustrated as the target pose, while for reward functions it is a text formulated in natural language which replaces the [description] placeholder in the template shown in Fig. 14 (e.g., for the task "raisearms-l-h" we generate text "standing with left hand low (at hip height) and right hand high (above head)"). For human-likeness, the rater has to choose among four options where they can express preference for either of the two behaviors, or both (a draw), or none of them. We then compute success rate and average human-likeness by taking the ratio between the positive answer and the total number of replies. The FB-CPR is considered more human like than TD3 in the large majority of cases. FB-CPR is sometimes assessed as human-like by raters, even in tasks when they consider it failed completing the task. Interestingly, while the human-likeness of FB-CPR may come at the cost of lower reward scores, it does not affect the perceived success in accomplishing the assigned goal tasks and FB-CPR has better success rate than TD3 for those tasks.

More in detail, per-task success rate scores are presented in Fig. 15 and Fig. 16.

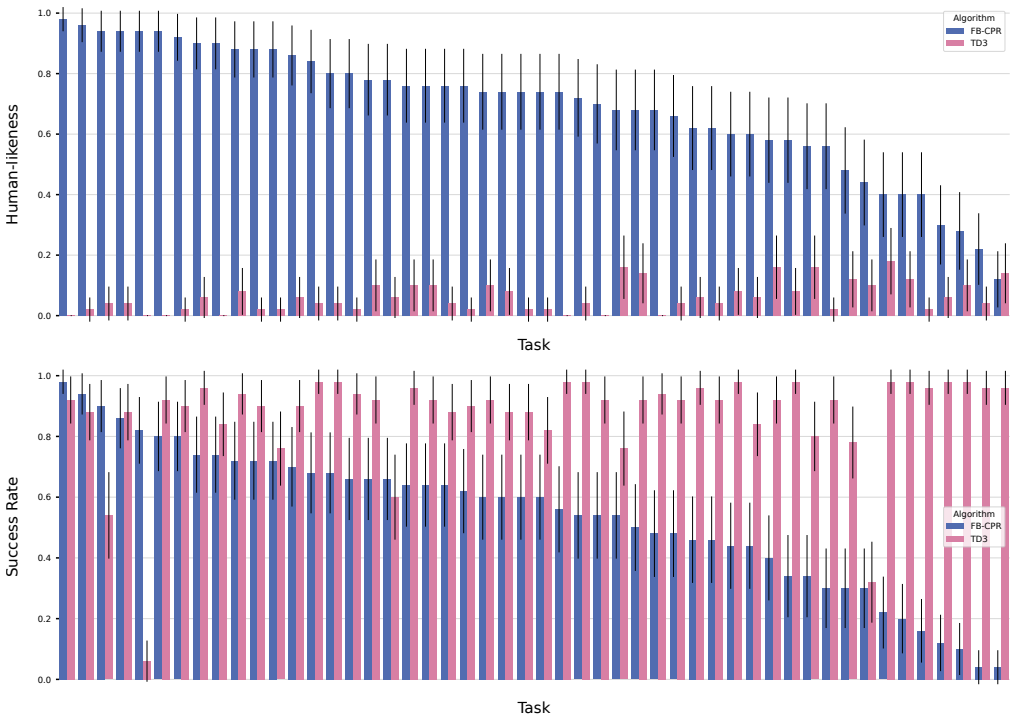

Figure 15: Human-likeness and success rate scores of algorithms per goal task sorted by FB-CPR performance.

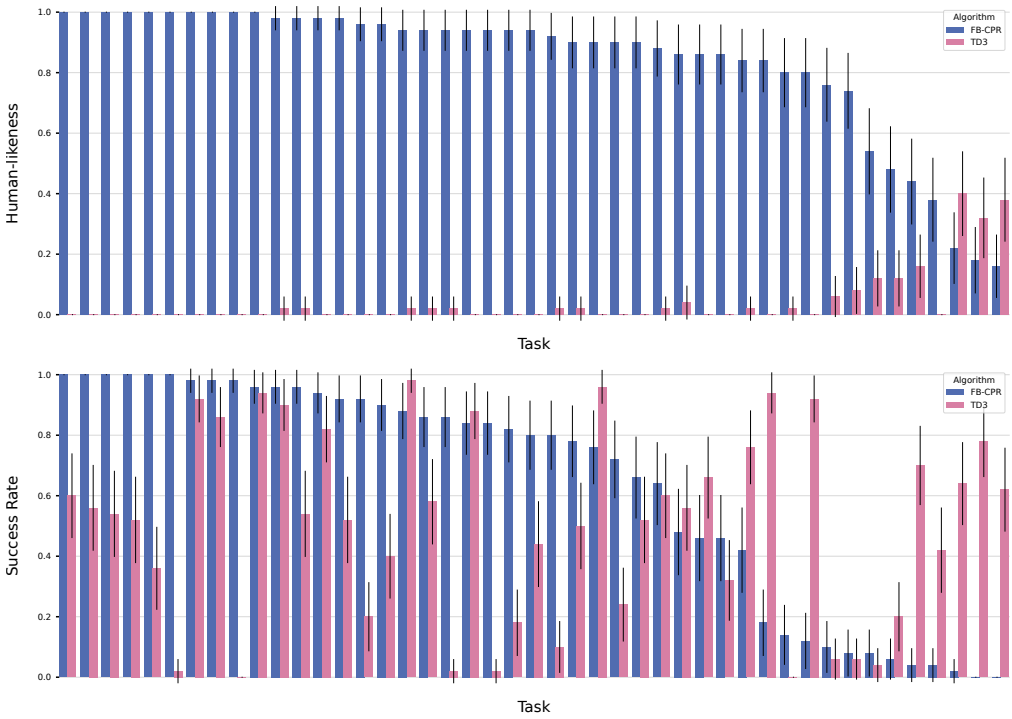

Figure 16: Human-likeness and success rate scores of algorithms per reward task sorted by FB-CPR performance.

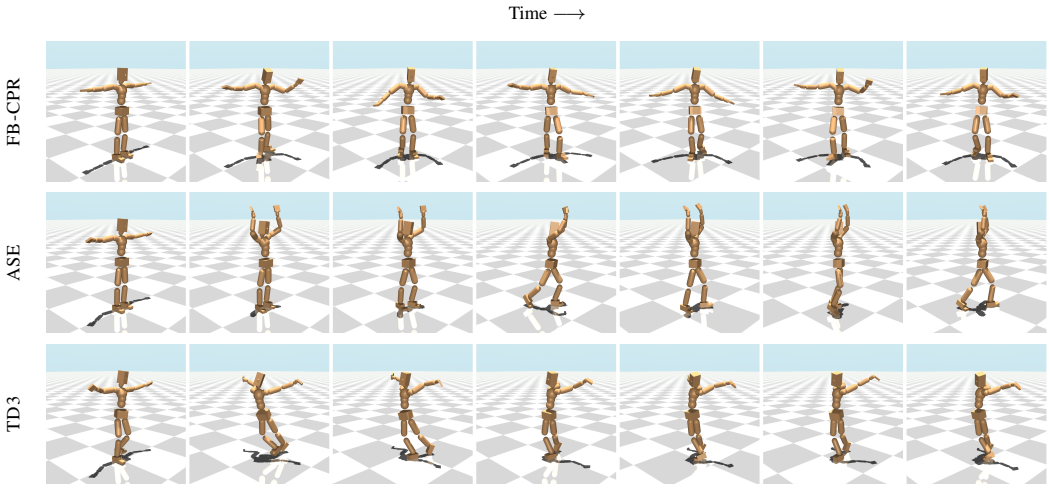

Figure 17: Example of combination of locomotion and arm raising tasks (`move-ego-0-2-raisearms-m-m`). Our FB-CPR (top) agent produces natural human motions while TD3 (bottom) learns high-performing but unnatural behaviors. ASE (middle) has a natural behavior but it is not correctly aligned with the tasks (arms are in the high position not medium).

D.4.2 Reward-based tasks

We provide a further investigation of the performance of our FB-CPR agent on tasks that are i) a combination of tasks used for the main evaluation; and ii) highly under-specified.

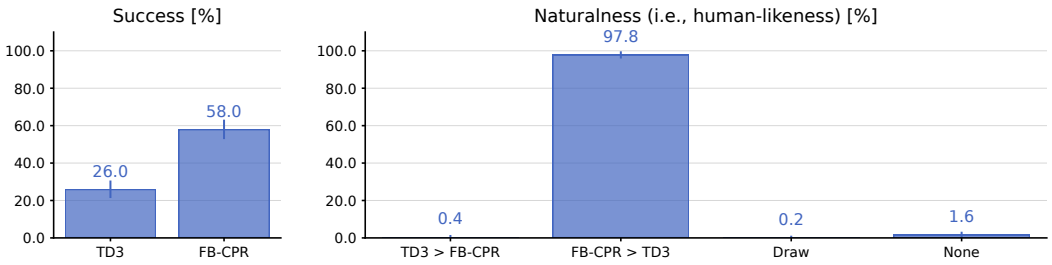

Figure 18: Human-evaluation on locomotion combined with arm raising. Left figure reports the percentage of times a behavior solved a reward-based task (tasks are independently evaluated). Right figure reports the score for human-likeness by direct comparison of the two algorithms.

The objective *i)* is to evaluate the ability of FB-CPR of composing behaviors. We thus created a new category of reward-based tasks by combining locomotion and arm-raising tasks. Specifically, we pair the medium-speed forward locomotion task (with an angle of zero and speed of 2) with all possible arm-raising tasks. Since these two types of tasks have conflicting objectives – locomotion requires movement, while arm-raising rewards stillness – we define a composite reward function that balances the two. This is achieved by taking a weighted average of the individual task rewards, where the weighting varies depending on the specific task combination. Tab. 25 reports the performance of the algorithms on these "combined" tasks. We can see that FB-CPR is able to achieve 74% of the performance of TD3 trained on each individual task. Despite the higher performance, even in this case, TD3 generates unnatural behaviors. The higher quality of FB-CPR is evident in Fig. 17 where we report a few frames of an episode for the task `move-ego-0-2-raisearms-m-m`. Similarly, almost the totality (about 98%) of human evaluators rated FB-CPR as more natural than TD3 on these tasks.

The objective of *ii)* is to evaluate the ability of our model to solve task with a human-like bias. To show this, we designed a few reward functions inspired by the way human person would describe a task.

Run. The simplest way to describe running is "move with high speed". Let v_x and v_y the horizontal velocities of the center of mass at the pelvis joint. Then, we define the reward for the task RUN_{eq} as

$$r(s') = \mathbb{I}(v_x^2 + v_y^2 > 2)$$

Walking with left hand up. This task has two component: walking requires moving with low speed; raising the hand means having the hand z-coordinate above a certain threshold. Then, we define the reward for the task $\text{WALK-LAM}_{\text{eq}}$ as

$$r(s') = \mathbb{I}\Big[1 < (v_x^2 + v_y^2) < 1.5\Big] \cdot \mathbb{I}\Big[z_{\text{left wrist}} > 1.2\Big]$$

Standing with right foot up. This is the most complex task. We define standing at being in upright position with the head z-coordinate above a certain threshold and zero velocity. Similar to before, we ask the right ankle to be above a certain threshold. Then, we define the reward for the tasks $\text{STAND-RTM}_{\text{eq}}$ ($\beta = 0.5$) and $\text{STAND-RTH}_{\text{eq}}$ ($\beta = 1.2$) as

$$r(s') = \mathbb{I}\Big[\text{up} > 0.9\Big] \cdot \mathbb{I}\Big[z_{\text{head}} > 1.4\Big] \cdot \exp\Big(-\sqrt{v_x^2 + v_y^2}\Big) \cdot \mathbb{I}\Big[z_{\text{right ankle}} > \beta\Big]$$

It is evident to any expert in Reinforcement Learning (RL) that the reward functions in question are not optimal for learning from scratch. These reward functions are too vague, and a traditional RL algorithm would likely derive a high-performing policy that deviates significantly from the natural "behavioral" biases. For instance, with TD3, we observe completely unnatural behaviors. In stark contrast, FB-CPR manages to address the tasks in a manner that closely resembles human behavior (refer to Fig. 19). Intriguingly, FB-CPR appears to identify the "simplest" policy necessary to solve a task. It effectively distinguishes between two different policies, $\text{STAND-RTM}_{\text{eq}}$ and $\text{STAND-RTH}_{\text{eq}}$, even though the policy designed for the higher task would suffice for the medium

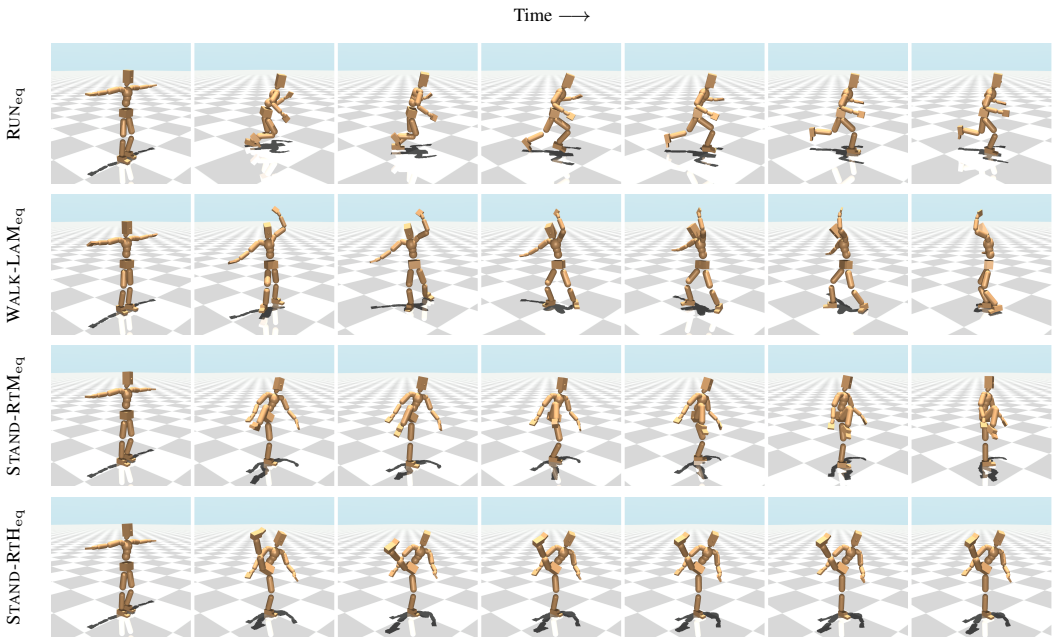

Figure 19: Example of behaviors inferred by FB-CPR from under-specified reward equations.

task, provided that the foot remains above a certain threshold. It is also evident the data bias. For example, we do not specify the direction of movement in run, just the high speed. FB-CPR recovers a perfect forward movement probably because the majority of run motions in $\mathcal{M}$ show this behavior. ASE is not able to solve all the tasks.

E ABLATIONS ON BIPEDAL WALKER

Method	Data	Reward *Return*	Demonstration *Return*	Goal *Proximity*
FB	RND	0.52 ± 0.02	0.43 ± 0.02	127.38 ± 20.51
FB	RND+$\mathcal{M}_{\text{TRAIN}}$	0.60 ± 0.03	0.56 ± 0.03	211.46 ± 17.78
FB+AWAC	$\mathcal{M}_{\text{TRAIN}}$	0.51 ± 0.02	0.54 ± 0.02	$\mathit{279.90} \pm \mathit{44.07}$
FB+AWAC	RND+$\mathcal{M}_{\text{TRAIN}}$	0.42 ± 0.03	0.43 ± 0.05	249.72 ± 23.92
FB Online	None	0.19 ± 0.03	0.19 ± 0.02	120.51 ± 10.83
FB-CPR	$\mathcal{M}_{\text{TRAIN}}$	$\mathit{0.71} \pm \mathit{0.02}$	$\mathit{0.75} \pm \mathit{0.01}$	$\mathbf{297.17} \pm \mathbf{52.14}$
FB-MPR	$\mathcal{M}_{\text{TRAIN}}$	$\mathbf{0.77} \pm \mathbf{0.02}$	$\mathbf{0.78} \pm \mathbf{0.01}$	258.66 ± 43.89

Table 26: Mean and standard deviation of performance with different prompts. Averaged over 10 random seeds. Higher is better. Normalized returns are normalized w.r.t expert TD3 policy in the same, rewarded task. RND data is generated by RND policy (Burda et al., 2019), while $\mathcal{M}_{\text{TRAIN}}$ data was generated by rolling out TD3 policies trained for each task separately.

We conduct an ablation study in the Walker domain of `dm_control` (Tunyasuvunakool et al., 2020) to better understand the value of combining FB with a conditional policy regularization and online training.

Tasks. For this environment only a handful of tasks have been considered in the literature (Laskin et al., 2021). In order to have a more significant analysis, we have developed a broader set of tasks. We consider three categories of tasks: **run**, **spin**, **crawl**. In each category, we parameterize *speed* (or angular momentum for spin) and *direction*. For instance, `walker_crawl-{bw}-{1.5}` refers to a task where the agent receives positive reward by remaining below a certain height while moving backward at speed 1.5. By combining category, speed, and direction, we define 90 tasks. We also create a set of 147 poses by performing a grid sweep over different joint positions and by training TD3 on each pose to prune unstable poses where TD3 does not reach a satisfactory performance.

Data. We select a subset of 48 reward-based tasks and for each of them we a TD3 policy to obtain 50 *expert* trajectories that we add to dataset $\mathcal{M}^{\text{demo}}_{\text{TRAIN}}$. We also run TD3 policies for a subset of 122 goals, while using the same 122 states as initial states, thus leading to a total of 14884 goal-based trajectories that are added to $\mathcal{M}^{\text{goal}}_{\text{TRAIN}}$. We then build $\mathcal{M}_{\text{TRAIN}} = \mathcal{M}^{\text{demo}}_{\text{TRAIN}} \cup \mathcal{M}^{\text{goal}}_{\text{TRAIN}}$, which contains demonstrations for a mix of reward-based and goal-reaching policies. For algorithms trained offline, we use either data generated by random network distillation (RND) (Burda et al., 2019)[14] or combining RND with $\mathcal{M}_{\text{TRAIN}}$. The $\mathcal{M}_{\text{TRAIN}}$ dataset contains 17,284 rollouts and 1,333,717 transitions[15], while the "RND" dataset contains 5000 episodes of 100 transitions for a total of 5,000,000 transitions.

Evaluation. For reward-based evaluation, we use the 42 tasks that were not used to build the demonstration dataset. For imitation learning, we consider the same 42 tasks and only 1 demonstration is provided. For goal-based evaluation, we use the 25 goals not considered for data generation.

Baselines. For ablation, we compare FB-CPR to the original FB algorithm (Touati et al., 2023) trained offline, offline FB with advantage-weighted actor critic (AWAC) (Nair et al., 2020), FB trained online, and FB-CPR with an unconditional discriminator (*i.e* discriminator depends solely on the state), that we refer to as FB-MPR (FB with marginal policy regularization).

Results. Table 26 shows the results for each evaluation category averaged over 10 seeds. For reward-based and imitation learning evaluation, we compute the ratio between each algorithm and the TD3/expert's performance for each task and then average it. For goal-reaching evaluation, we report the average proximity. We first notice that training FB online without access to any demonstration or unsupervised dataset leads to the worst performance among all algorithms. This suggests that FB representations collapse due to the lack of useful samples and, in turn, the lack of a good representation prevents the algorithm from performing a good exploration. Offline FB with only RND data achieves a good performance coherently with previous results reported in the literature.

[14] For walker, RND is successful in generating a dataset with good coverage given the low dimensionality of the state-action space. In humanoid, this would not be possible.

[15] Notice that goal-based trajectories have different lengths as episodes are truncated upon reaching the goal.

This confirms that once provided with a dataset with good coverage, the unsupervised RL training of FB is capable of learning a wide range of policies, including some with good performance on downstream tasks. Adding demonstration samples to RND further improves the performance of FB by 15% for reward-based tasks, 30% for imitation learning, and by 60% for goal-reaching. This shows that a carefully curated mix of covering samples and demonstrations can bias FB offline training towards learning behaviors that are closer to the data and improve the downstream performance. Nonetheless, the gap to FB-CPR remains significant, suggesting that regularizing the policy learning more explicitly is beneficial. Interestingly, behavior cloning regularization used in FB-AWAC does not significantly improve the performance of FB. When trained on $\mathcal{M}_{\text{TRAIN}}$, FB-AWAC significantly improves in goal-based problems, but in reward and imitation learning it is only able to match the performance of FB with RND. Mixing the two datasets only marginally improves the goal-based performance, while degrading other metrics. Overall FB with online training with a policy regularization emerges as the best strategy across all tasks. Interestingly, the version with unconditional discriminator achieves better performance for reward and demonstration tasks, while it is significantly worse for goal reaching problems, where FB-CPR is best. We conjecture that this result is due to the fact that the dataset $\mathcal{M}$ is well curated, since trajectories are generated by optimal policies and they cover close regions of the state space, whereas in the humanoid case, $\mathcal{M}$ is made of real data where different motions can be very distinct from each other and are very heterogeneous in nature and length. While in the former case just reaching similar states as in $\mathcal{M}$ is sufficient to have a good regularization, in the latter a stronger adherence to the motions is needed.

F Ablations on AntMaze

We conduct an ablation study in the antmaze domains from the recently introduced goal-conditioned RL benchmark (Park et al., 2024a) to better understand the value of combining FB with a conditional policy regularization and online training. Antmaze domains involve controlling a quadrupedal Ant agent with 8 degrees of freedom.

Data. We use *stitch datasets* for antmaze domains provided in Park et al. (2024a), which consist of short goal-reaching demonstrations trajectories. These datasets are designed to challenge agent's stitching ability over subgoals to complete the downstream tasks.

Evaluation. We use the same evaluation protocol employed in Park et al. (2024a). Each domain has 5 downstream tasks. The aim of these tasks is to control the agent to reach a target (x, y) location in the given maze. The task is specified by the full state, but only the

$$(x, y)$$

coordinates are set to the target goal, while the remaining state components are randomly generated. For each goal, we evaluate the agent using 50 episodes.

Results. We present a comparison of three methods in Table 27: online FB trained solely on environment interactions, offline FB with advantage weighting (AWAC) using the offline stitch datasets, and online FB-CPR that utilizes stitch datasets for policy regularization. We report both success rate and proximity (averaged distance to the goal) averaged across 3 models trained with different random seeds. Online FB fails to reach any test goals, achieving zero success rate due to the lack of exploration. In contrast, FB-AWAC achieves decent performance, which is indeed competitive with the non-hierarchical offline goal-conditioned RL algorithms reported in Park et al. (2024a). Finally, FB-CPR achieves the strongest performance and it outperforms the other FB-variants by a significant margin, both in success rate and proximity.

G Understanding the Behavioral Latent Space

In this section, we summarize results from a qualitative investigation aimed at better understanding the structure of the latent space learned by FB-CPR. We recall that the latent space Z works at the same time as a state embedding through $B(s)$, a trajectory embedding through ER_{FB}, and a policy embedding through π_z.

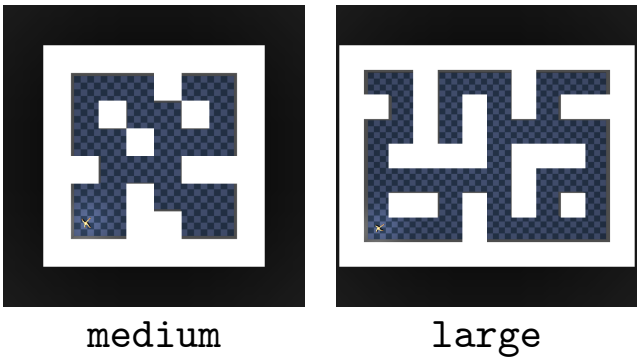

Figure 20: Layout of antmaze-medium and antmaze-large domains from (Park et al., 2024a)

Algorithm	Antmaze-medium		Antmaze-large	
	Proximity (↓)	Success (↑)	Proximity (↓)	Success (↑)
(online) FB	19.71 (0.11)	0 (0)	25.74 (0.05)	0 (0)
(offline) FB-AWAC	6.70 (0.4)	0.67 (0.08)	18.00 (1.54)	0.28 (0.05)
(online) FB-CPR	3.19 (0.13)	0.90 (0.1)	7.97 (0.39)	0.53 (0.08)

Table 27: Performance of different algorithms in Antmaze domains (medium and large mazes). We report mean and standard deviation of the performance over three random seeds.

G.1 Dimensionality Reduction of the Behavioral Latent Space

We investigate the structure of the latent space learned through FB-CPR by performing dimensionality reduction via UMAP (McInnes et al., 2018) on the embeddings z coming from two sources: 1) motion embeddings using $\mathrm{ER}_{\mathrm{FB}}$ and 2) reward embeddings computed via weighted regression. In order to see meaningful structure in the latent space we decide to classify various motions into five categories: jumping, running, walking, crawling, and motions containing headstands or cartwheels.

Given these categories we construct a dataset of motions by first choosing a single representative motion for each category and subsequently searching for other motions that are sufficiently close to the reference motion as measured be the Earth Mover's Distance (EMD). We chose all motions where the EMD fell below some threshold that was chosen by visual inspection. With this dataset of motions $\tau_i = \{x_1, \dots, x_n\}$ of length n we embed the center most subsequence, i.e., $\tau_i^{\perp} = \{x_i : i \in [\lfloor n/2 \rfloor - 4, \lfloor n/2 \rfloor + 4]\}$ using $\mathrm{ER}_{\mathrm{FB}}$. The center subsequence was chosen as it was most representative of the category whereas other locations usually had more "set up" in preparation for the motion, e.g., walking before performing a headstand.

Reward embeddings were chosen from Appendix C.3.1 to be representative of the motion category. Specifically, we use the following reward functions for each class:

1. Jumping: `smpl_jump-2`
2. Running: `smpl_move-ego-90-4`
3. Walking: `smpl_move-ego-90-2`
4. Crawling: `smpl_crawl-0.5-2-d`
5. Headstand: `smpl_headstand`

Figure 21 depicts both motion and reward embeddings along with illustrative visualizations for each class of behaviors. Interestingly, the motions involving similar activities are accurately clustered in similar regions through the embedding process. Furthermore, even the reward tasks are embedded within the clusters of motions they are closely connected to. This reveals that the training of FB-CPR leads to learning representations that effectively align motions and rewards in the same latent space.

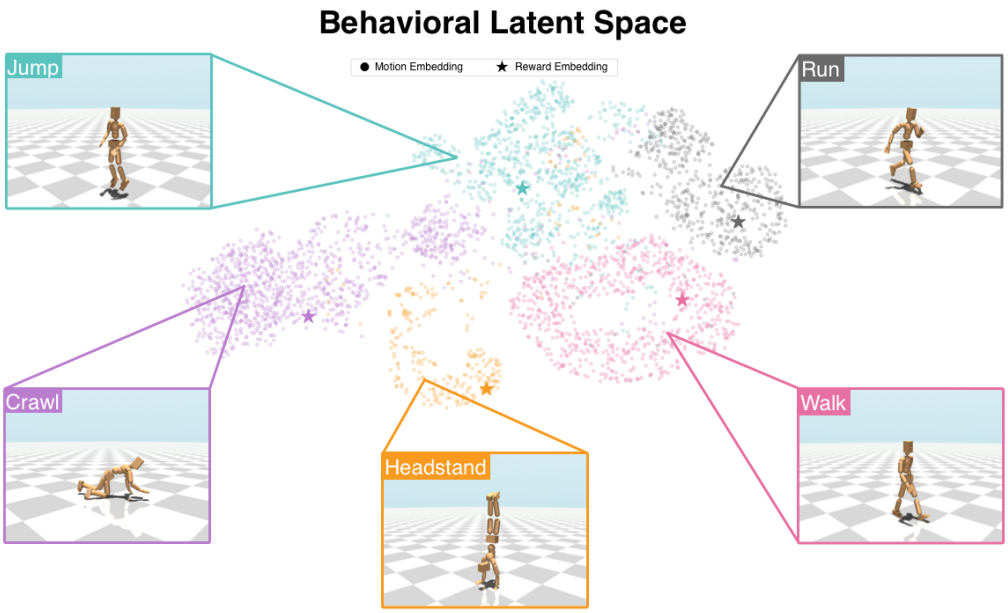

Figure 21: UMAP (McInnes et al., 2018) plot of the latent space of FB-CPR with both motion embeddings (circle) and reward embeddings (star). We can see that reward functions are projected to clusters that correspond with motions of the same class of behaviors.

G.2 Behavior Interpolation

While the analysis in App. G.1 shows that the latent space effectively clusters behaviors that are semantically similar, we would like to further understand whether it also supports meaningful interpolation between any two points. We have first selected a few reward functions that are underspecified enough that can be combined together (e.g., "run" and "raise left hand" tasks could be composed into "run with left hand up"). We make this choice to investigate whether interpolating between the behaviors associated to each reward function would produce a resulting behavior that is the result of the composition of the two original behaviors. More precisely, given the reward functions r_1 and r_2, we first perform inference to compute z_1 and z_2 and we then define $z_\alpha = \alpha z_1 + (1-\alpha) z_2$ and we let vary α in $[0, 1]$. Refer to the supplmentary material for videos illustrating the behaviors that we obtained through this protocol for a few pairs of reward functions. In general, not only we observed a smooth variation of the behavior as α changes, but the interpolated policies often combine the two original tasks, obtaining more complex behaviors such as running with left hand up or moving and spinning at the same time.

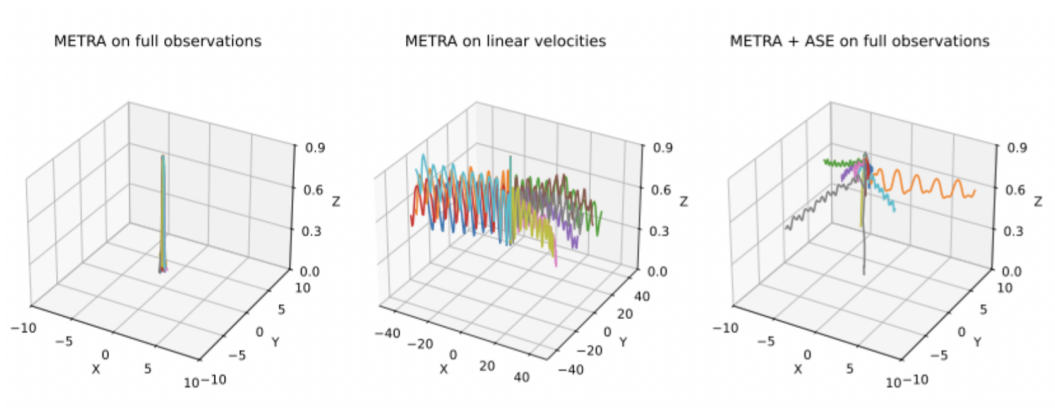

Figure 22: Rollouts of policies learned by different variants of METRA on Humanoid. Each line corresponds to a trajectory in (x, y, z) space generated by a policy π_z with z uniformly sampled from the unit sphere. *(left)* The original METRA algorithm trained from scratch (no unlabeled data) with representation ϕ taking as input the full observation vector. *(middle)* The original METRA algorithm trained from scratch (no unlabeled data) with representation ϕ taking as input only the linear velocities of the robot's pelvis along the x,y,z axes. *(right)* The ASE algorithm trained within the same setting as in Table 1 but with METRA replacing DIAYN as the skill discovery component.

Algorithm	Reward (↑)	Goal		Tracking - EMD (↓)		Tracking - Success (↑)	
		Proximity (↑)	Success (↑)	Train	Test	Train	Test
METRA	6.37 (1.04)	0 (0)	0 (0)	9.92 (0.13)	9.95 (0.18)	0 (0)	0 (0)
METRA-ASE	37.98 (6.61)	0.30 (0.01)	0.24 (0.05)	2.11 (0.07)	2.12 (0.05)	0.54 (0.04)	0.56 (0.06)
DIAYN-ASE	105.73 (3.82)	0.46 (0.37)	0.22 (0.37)	2.00 (0.02)	1.99 (0.02)	0.37 (0.02)	0.40 (0.03)

Table 28: Performance of METRA (Park et al., 2024c) and ASE (Peng et al., 2022) with METRA replacing DIAYN as the skill discovery component in the same setting as Table 1. We also include the original ASE algorithm from such table (called DIAYN-ASE) to ease comparison.

H Comparison to Unsupervised Skill Discovery Methods

In FB-CPR, we leverage unlabeled datasets to scale unsupervised RL to high-dimensional problems like Humanoid control. The main conjecture is that unlabeled datasets provide a good inductive bias towards the manifold of behaviors of interest (e.g., those that are human-like), and that this bias is crucial to avoid the "curse of dimensionality" suffered when learning over the (probably intractable) space of all expressible behaviors. On the other hand, there is a vast literature on Unsupervised Skill Discovery (USD) which focuses on learning over such full space of behaviors while providing inductive biases through notions of, e.g., curiosity (e.g., Pathak et al., 2017; Rajeswar et al., 2023), coverage (e.g., Burda et al., 2019; Liu & Abbeel, 2021), or diversity (e.g., Gregor et al., 2016; Eysenbach et al., 2019; Sharma et al., 2020; Park et al., 2022; 2024c).

In this section, we compare to METRA (Park et al., 2024c), the current state-of-the-art USD method, and show that it fails on our high-dimensional Humanoid control problem unless given extra inductive biases through unlabeled data or by restricting the set of variables on which to focus the discovery of new behaviors. Given that METRA remains, to our knowledge, the only USD method to discover useful behaviors in high-dimensional problems like humanoid and quadruped control, we conjecture that this "negative" result also applies to all existing USD methods.

Implementation and parameters. We implemented METRA following the original code of Park et al. (2024c), with the only difference that we replaced SAC with TD3 as RL optimizer since we used the latter for all algorithms considered in this paper. We also follow Park et al. (2024c) to tune the hyperparameters related to the representation learning component, while for TD3 we use the same parameters and network architectures we found to work well across all baselines tested in this paper. We found the dimension d of the latent space to be the most important parameter, and we found $d = 16$ to work best after searching over 2,4,8,16,32,64,128,256. All parameters are summarized in the following table.

Table 29: Hyperparameters used for METRA pretraining.

Hyperparameter	Value
General training parameters	See Tab. 3
General prioritization parameters	See Tab. 4
z update frequency during rollouts	once every 150 steps
z dimension d	16
actor network	third column of Tab. 6, output dim = action dim
critic networks	second column of Tab. 6, output dim 1
ϕ encoder network	fourth column of Tab. 5, output dim 16, 2 hidden layers
Learning rate for actor	10^{-4}
Learning rate for critic	10^{-4}
Learning rate for ϕ	10^{-6}
Constraint slack ϵ	10^{-3}
Initial Lagrange multiplier λ	30
z distribution ν	uniform on unit sphere
Probability of relabeling zs	0.8
Polyak coefficient for target network update	0.005
Actor penalty coefficient	0.5
Critic penalty coefficient	0.5

Inference methods. For goal-based inference, we follow the zero-shot scheme proposed by Park et al. (2024c): when given a goal state g to reach from state s, we set $z = (\phi(g) - \phi(s))/\|\phi(g) - \phi(s)\|_2$. Similarly, for tracking we set $z_t = (\phi(g_{t+1}) - \phi(s_t))/\|\phi(g_{t+1}) - \phi(s_t)\|_2$ at each step t of the episode, where g_{t+1} is the next state in the trajectory to be tracked, while s_t is current agent state. Finally, for reward inference, given a dataset of transitions (s, s', r) sampled from the train buffer and labeled with the corresponding reward r, we infer z through linear regression on top of features $\phi(s') - \phi(s)$. This is motivated by the fact that METRA's actor is pretrained to maximize a self-supervised reward function given by $r(s, s', z) := (\phi(s') - \phi(s))^T z$. Notice, however, that we do not expect this to work well since such a reward, up to discounting, yields a telescopic sum which eventually makes the agent care only about the reward received at the end of an episode instead of the cumulative sum. Thus we report its performance for completeness.

Results. We test METRA in the same setting as Table 1. The results are reported in the first row of Table 28, where we find that METRA achieves near zero performance in all tasks. After a deeper investigation, we found that in all runs, and with all hyperparameters we tested, the agent simply learned to fall on the floor and remain still in different positions, as shown in Figure 22 (left). Interestingly, this happens despite all the objectives, and in particular the "diversity loss" for representation learning, are well optimized during pre-training. This is due to the fact that, from the agent perspective, lying still on the floor in different positions can be regarded as displaying diverse behaviors, and no extra inductive bias would push the agent to learn more complicated skills (e.g., locomotion ones). On the other hand, we believe that METRA manages to learn few of such skills in the Humanoid experiments of Park et al. (2024c) given that it is pretrained on pixel-based observations (instead of proprioception) with a color map on the ground and very small dimension of the latent space ($d = 2$). This may provide an implicit inductive bias towards locomotion behaviors that make the robot move around the x,y coordinates, which are likely to be the observation variables that can be maximally spread out by the agent's controls. On the other hand, we do not have any such bias in our setup, where each joint has roughly the same "controllability" and the agent thus learns the simplest way to display diverse behaviors.

To verify this last conjecture, we retrained METRA with the same parameters except that we make the representation ϕ only a function of the linear velocities of the robot's pelvis along the three x,y,z directions. Intuitively, this should provide an inductive bias that makes the agent focus on controlling those variables alone, thus learning locomotion behaviors to move around the x,y,z space. This is confirmed in Figure 22 (middle), where we see that the learned skills do not collapse anymore but rather move around different directions of the space.

METRA with ASE regularization. Finally, we tried to combine METRA with the same policy regularization on top of unlabeled data as used by ASE. As we recall that ASE (Peng et al., 2022) combines a USD algorithm (DIAYN) with an unconditional policy regularization term, we simply replace DIAYN with METRA and keep all other components the same. The results are shown in Table 28, where we see that the ASE regularization improves the performance of METRA significantly on goal reaching and tracking. Moreover, METRA-ASE achieves competitive performance w.r.t. the original DIAYN-based ASE, improving its success rate in those tasks. Both DIAYN-ASE

and METRA-ASE perform, however, significantly worse than FB-CPR. Finally, we note from Figure 22 (right) that METRA-ASE learns to navigate along different directions, though less far than plain METRA trained only on the pelvis' velocities. This is likely due to the regularization w.r.t. unlabeled data, which makes the agent focus on human-like behaviors, thus avoiding over-actuated movements that would be otherwise learned when naively trying to maximize controls of a subset of the observation variables.